THE UNIVERSITY OF QUEENSLAND

AUSTRALIA

Fluid Dynamics Studies Related to Bottom Blown Copper Smelting Furnace

Lang SHUI
Master of Engineering

A thesis submitted for the degree of Doctor of Philosophy at

The University of Queensland in 2016

School of Chemical Engineering

Abstract

The bottom blown copper smelting furnace is a novel technology developed by Dongying Fangyuan Nonferrous Metals Co. Ltd. China. Since it started in 2008, many advantages have been reported from industrial practice, such as high volume specific smelting capacity, low copper loss, autogenous smelting, adaptive to feeds, low temperature operation and so on. Most of those features are relevant to the fluid dynamics of the molten bath in the furnace. However, the detailed behaviour of molten bath in the bottom blown reactor still is not comprehensively understood.

To understand the behaviour of molten bath in this newly established furnace, a 1/12 lab scale cold model was constructed according to the principles of similarity. In this physical model, water was used to simulate the liquid matte, compressed air was used to simulate oxygen enriched air blowing and its flowrate was adjusted accordingly. Silicone oils with different viscosities were used to simulate the molten slag layer of various viscosities. In the present study, several features of the bottom blown bath behaviour were investigated by using this physical model.

The mixing behaviour in the single phase bath with single lance blowing was investigated in the first stage. Mixing time was used as the index of mass transfer efficiency in this cold model and was measured to examine the characteristics of the fluid dynamics in the bath. It was found that there is an effective stirring range within an area adjacent to the blowing lance, in which mixing time changes little with horizontal or vertical distance, while out of the range mixing time increases with increasing horizontal distance and the increment is much greater on the surface of the bath. Mixing time was found to decrease with increasing bath height and gas flowrate within the effective stirring range. However, the effective stirring range can be reduced with increasing the bath height. An empirical prediction of mixing time from gas flowrate and bath height was then established for horizontal bottom blown furnace with single phase bath.

$$\tau = 37.5Q^{-0.39}H^{-1.08}$$

In addition to single phase mixing behaviour study, multiphase bath mixing behaviour was also studied to further investigate the mass transfer in the presence of top layer. Single lance blowing was used and experimental variables including water height, gas flowrate, oil layer height and oil

viscosity were adjusted to investigate the impact of each on mixing. It was found that the mixing time decreases with water height and gas flowrate in a greater rate than that of single phase system, while it is increasing with oil layer height and oil viscosity, where the rate with oil layer height is much greater. An overall empirical relationship with these variables was developed as following, and it showed a good prediction of mixing time under different conditions.

$$\tau = 0.21 H^{-1.53} Q^{-1.73} h^{2.21} \nu_s{}^{0.24}$$

The correlation was then generalised to a model-independent format for wider use:

$$\frac{\tau}{R^{\frac{1}{2}} g^{-\frac{1}{2}}} = 182 \left(\frac{H}{R}\right)^{-1.53} \left(\frac{Q}{R^{\frac{5}{2}} g^{\frac{1}{2}}}\right)^{-1.73} \left(\frac{h}{R}\right)^{2.21} \left(\frac{\nu_s}{R^{\frac{3}{2}} g^{\frac{1}{2}}}\right)^{0.24}$$

Three different types of surface waves were studied in the single phase bath with single lance blowing. The 1st asymmetric standing wave was found the most significant type among the three because it leads the entire bath to swing laterally. The 1st asymmetric standing wave was found to take place only at certain combination of bath height and gas flowrate, which is summarised in two sub-boundaries in terms of bath depth, gas flowrate and blowing lance angle.

Sub-boundary 1

$$\frac{H}{D} = 0.036 Fr_{mD}^{-0.1} \alpha^{0.084}$$

Sub-boundary 2

$$\frac{H}{D} = 0.63 We^{0.44} \alpha^{-0.39}$$

The measured amplitudes at several conditions show that tapping end amplitude increases with flowrate and bath height, and when the 1st symmetric standing wave is taking place, the amplitude is remarkably increased. The frequency of the 1st asymmetric standing wave does not change with flowrate or blowing angle, but slightly increases with bath height.

The longitudinal wave exists on bath surface when the combination of bath height and gas flowrate is out of the critical occurrence boundary. To study the behaviour of the longitudinal wave, the model dynamic condition was constructed closer to industrial practice. Nine lances were used for blowing and silicone oil was applied on water surface to investigate the behaviour of longitudinal wave. It was found that the amplitude trend of longitudinal wave along the furnace length is dependent on the combination of gas flowrate and bath level, and three typical trends were observed.

At the gas flowrate corresponding to industrial flowrate, the amplitude of wave increases with water level, but remains almost stable with oil level. Higher viscosity oil layer leads to lower amplitude of wave, while lower viscosity oil leads to rising of amplitude near tapping end. The amplitude of wave at the edge of tapping end is found always higher than the centre. The frequency of longitudinal wave is not affected by the water level, oil level or oil viscosity.

All these features are linked to the industrial operation of this novel copper smelting furnace. The investigation in this study provides guidelines and useful information for understanding and further improvement of bottom blown copper smelting technology in the future.

Declaration by author

This thesis is composed of my original work, and contains no material previously published or written by another person except where due reference has been made in the text. I have clearly stated the contribution by others to jointly-authored works that I have included in my thesis.

I have clearly stated the contribution of others to my thesis as a whole, including statistical assistance, survey design, data analysis, significant technical procedures, professional editorial advice, and any other original research work used or reported in my thesis. The content of my thesis is the result of work I have carried out since the commencement of my research higher degree candidature and does not include a substantial part of work that has been submitted to qualify for the award of any other degree or diploma in any university or other tertiary institution. I have clearly stated which parts of my thesis, if any, have been submitted to qualify for another award.

I acknowledge that an electronic copy of my thesis must be lodged with the University Library and, subject to the policy and procedures of The University of Queensland, the thesis be made available for research and study in accordance with the Copyright Act 1968 unless a period of embargo has been approved by the Dean of the Graduate School.

I acknowledge that copyright of all material contained in my thesis resides with the copyright holder(s) of that material. Where appropriate I have obtained copyright permission from the copyright holder to reproduce material in this thesis.

Publications during candidature

Journal papers:

1. Lang Shui, Zhixiang Cui, Xiaodong Ma, M. Akbar Rhamdhani, Anh Nguyen, and Baojun Zhao, "Mixing Phenomena in a Bottom Blown Copper Smelter: A Water Model Study", Metallurgical and Materials Transactions B, Vol. 46B, 2015, pp. 1218-1225.
2. Lang Shui, Zhixiang Cui, Xiaodong Ma, M. Akbar Rhamdhani, Anh V. Nguyen, and Baojun Zhao, "Understanding of Bath Surface Wave in Bottom Blown Copper Smelting Furnace", Metallurgical and Materials Transactions B, In Press, DOI: 10.1007/s11663-015-0466-z

Conference papers:

1. Shui L., Cui Z., Ma X., Rhamdhani A., Nguyen A. and Zhao B., "Understanding of Bath Surface Waves in Bottom Blown Copper Smelting Furnace", *Proceedings of High Temperature Processing Symposium*, Editors Geoffrey Brooks and M. Akbar Rhamdhani, publisher Swinburne University of Technology, Melbourne, Australia, ISBN 978-0-9875930-3-0, 2015, pp. 121-124.
2. Shui L., Cui Z., Ma X., Rhamdhani A., Nguyen A. and Zhao B., "Flow Dynamic Study in Bottom Blown Copper Smelting Furnace", Proceedings of High Temperature Processing Symposium, Editors M. Akbar Rhamdhani and Geoffrey Brooks, publisher Swinburne University of Technology, Melbourne, Australia, ISBN 978-0-9875930-2-3, 2014, pp. 82-89.

Publications included in this thesis

Lang Shui, Zhixiang Cui, Xiaodong Ma, M. Akbar Rhamdhani, Anh Nguyen, and Baojun Zhao, "Mixing Phenomena in a Bottom Blown Copper Smelter: A Water Model Study", Metallurgical and Materials Transactions B, Vol. 46B, 2015, pp. 1218-1225. – Incorporated as chapter 5

Contributor	Statement of contribution
Author Lang Shui (Candidate)	Designed experiments (80%) Wrote the paper (70%)
Author Zhixiang Cui	Provided the industrial data for experiment design
Author Xiaodong Ma	Designed experiments (10%) Edited paper (10%)
Author M. Akbar Rhamdhani and Anh Nguyen	Edited paper (10%)

Author Baojun Zhao	Designed experiments (10%) Edited paper (10%)

Lang Shui, Zhixiang Cui, Xiaodong Ma, M. Akbar Rhamdhani, Anh V. Nguyen, and Baojun Zhao, "Understanding of Bath Surface Wave in Bottom Blown Copper Smelting Furnace", Metallurgical and Materials Transactions B, In Press, DOI: 10.1007/s11663-015-0466-z. – Incorporated as chapter 7

Contributor	Statement of contribution
Author Lang Shui (Candidate)	Designed experiments (80%) Wrote the paper (70%)
Author Zhixiang Cui	Provided the industrial data for experiment design
Author Xiaodong Ma	Designed experiments (20%) Edited paper (10%)
Author M. Akbar Rhamdhani and Anh Nguyen	Edited paper (10%)
Author Baojun Zhao	Edited paper (10%)

Contributions by others to the thesis

During the research project, there were some important contributions made by other researchers who were working together with me. I would like to acknowledge their contributions:

Prof Baojun Zhao contributed in proposing the issue of fluid mechanics study in this newly established copper smelting technology, designing of cold model experiment, interpreting experimental result and critically reviewing the drafted papers and thesis chapters.

Dr Xiaodong Ma contributed in experiment design, experimental work, data analysis, discussion of experimental plans and paper editing.

Mr Zhixiang Cui contributed in carrying out industrial operational trials and providing updated industrial data for experimental design.

Mr Xu Jiang contributed in carrying out part of experimental work in chapter 6 and providing useful data for analysis.

Prof Anh V. Nguyen and Dr M. Akbar Rhamdhani contributed in reviewing and editing the drafted papers and providing methodologies for progressing of this project.

Ms Jie Yu provided helpful assistance in designing of the experimental physical model and regular maintenance of it.

Statement of parts of the thesis submitted to qualify for the award of another degree

None

Acknowledgements

I would like to thank my principle supervisor Prof Baojun Zhao who proposed this project and enabled it to come true. During my candidature, his knowledge and expertise guided my study and helped me keep making progress in this field. I also wish to thank my associated supervisors Prof Anh V. Nguyen and Dr M. Akbar Rhamdhani for their valuable advice on experimental methodology and comments on those drafted papers.

I wish to thank Dongying Fangyuan Nonferrous Metals Co., Ltd. and The University of Queensland for their financial support of this research through "Fangyuan Fellowship" program.

I would like to thank Dr Xiaodong Ma and Mr Xu Jiang in our research group. Dr Xiaodong Ma shared his knowledge as well as experience and helped me in each step of my candidature, like experiment designing, results discussion, data analysis, paper editing and so on. Mr Xu Jiang helped me carry out a part of my experimental work which enables me to have sufficient time to process the previous data.

I would like to thank Ms Jie Yu who works as lab technician in our group. She assisted me to design the physical model for experiment, and kept good communication with the mechanical workshop for manufacture and any modification of it. She is also helpful in experimental setup maintaining, device purchase, repairing and so on, which provides me good lab condition for study. I also wish to thank the other members of our group. It was good experience sharing knowledge and working together.

Finally, I would like to thank my wife Chunmao Yuan for supporting and encouraging me during my pursuing of PhD. Her accompanying helped me overcome the frustration and difficulties in my candidature.

Keywords

bottom blown furnace, copper smelting, cold model, fluid mechanics, transport phenomena, mass transfer, mixing time, surface wave

Australian and New Zealand Standard Research Classifications (ANZSRC)

ANZSRC code: 091407, Pyrometallurgy, 100%

Fields of Research (FoR) Classification

FoR code: 0914, Resources Engineering and Extractive Metallurgy, 100%

Table of Contents

List of Figures

List of Tables

1 Introduction

1.1 Background

Copper is one of the first metals utilised by humankind. It has been one of the essential materials used by humans since the Bronze Age. Copper mining sites and smelting sites of ancient civilisations in different eras are dispersed all over the world. Since 17^{th}-19^{th} century, the copper industry in Europe has developed substantially, and modern copper smelting technology has been established. Later, the Bessemer converter and copper electrolysis were invented, which contributed to the production of high purity copper and accelerated the development of the copper industry. Subsequently, copper industry in USA, Chile, Russia, Canada, Australia, Japan, China, and African countries advanced rapidly. During the past year, copper dominance has been challenged first by aluminium for radiators then by fibre optics in telecommunications, but so far, the third world continues to have a steady demand for copper for industrial and residential uses[1].

In natural land, copper mostly exists in copper sulphide and copper iron sulphide minerals, such as chalcopyrite, chalcocite, bornite, cubanite and enargite. The rest part of copper is present in oxidised minerals such as oxides, carbonates, hydroxyl-silicates and sulphates. Typical copper ores usually contain only 0.5%-2% Cu. These ores are mined and concentrated to about 30% Cu before sent to extraction. The other source of copper production includes scrap copper and copper alloys from recycled wastes. In 2003, worldwide total copper and alloy yield was about 19.5million tonnes, in which 75-80% were produced from ores, while 20%-25% from scrap melt. Products of copper can be divided into two categories: (1) Wires and cables and (2) Other copper products and alloy products, where wires and cables consume approximately 2/3 of worldwide refined copper yield[2-3].Generally, there are two means to produce copper metal, pyro-extraction and hydro-extraction, of which pyro-extraction is more widely spread over the world.

Modern copper pyro-extraction mainly consists of flash smelting and bath smelting, where bath smelting of copper accounts for a big part of total copper yield. Compared to flash smelting, it holds advantages such as adaptive to feeds, less dust generation and lower investment[4]. From the

perspective of gas injection regime, copper bath smelting can be categorised into three general types: 1. Top submerged blowing; 2. Top suspended blowing; 3. Submerged side blowing. In 2008, Dongying Fangyuan Nonferrous Metals Co. Ltd. in Shandong Province of China commenced industrial production of a novel copper bath smelting technology: the bottom blown copper smelting technology. The flowsheet of bottom blown copper smelting is shown in Figure 1-1. The bottom blown technology has been widely applied in steelmaking convertor, refinery and lead smelting furnace throughout decades, but it was firstly put into practice for copper metallurgy by Fangyuan. The main facility of this process is one bottom blown Φ4.4 m ×16.5m smelting furnace which is horizontal, cylinder-shaped, rotatable and with chrome-magnesite brick lining. Instead of supplying oxygen with tuyeres like submerged side blowing smelting, bottom blown furnace is equipped with nine oxygen lances which are aligned in two rows: lower row contains four lances, which are 7 º offset from vertical line; upper row contains five lances, which are 22 º offset from vertical line, making angles between these two rows 15 º. The structure of the furnace is shown in Figure 1-2. Oxygen enriched air is blown into molten bath via these lances at the pressure of 0.4-0.5 Mpa[5-6].

Reports from industrial operations showed that the volume specific capacity of this reactor is higher than other current copper smelters[7]. Besides, it is autothermal smelting, which means that the heat generated by chemical reactions is sufficient to keep the bath temperature constant. Some other advantages such as low copper loss, adaptive to various feeds, low dust generation, and low temperature operation were also reported [5]. However, the mechanism of chemical reactions in the molten bath still remains little known. Fluid dynamics of molten bath are intimately related to the mixing, heat and mass transfer, chemical reactions and phase separations inside the furnace. Therefore, the author conducted fundamental studies of fluid dynamics in this furnace, which is aimed to extend the understanding of the furnace and to provide guidelines for the industrial operation and improvement of technology in future.

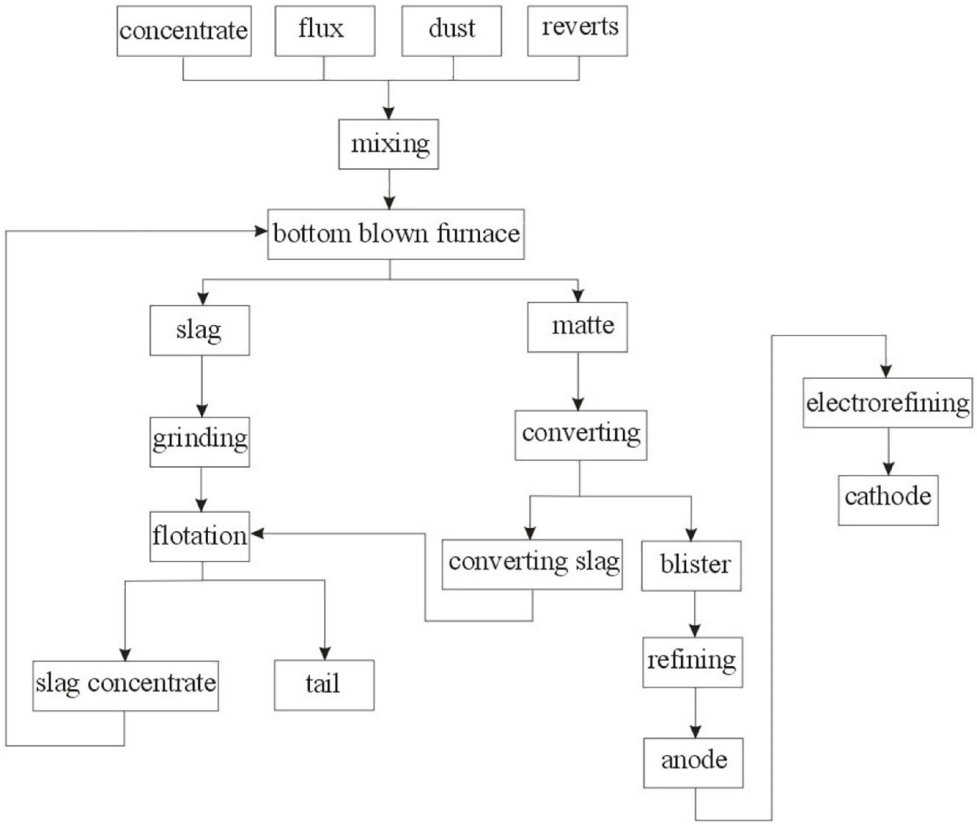

Figure 1-1 Flowsheet of Fangyuan plant

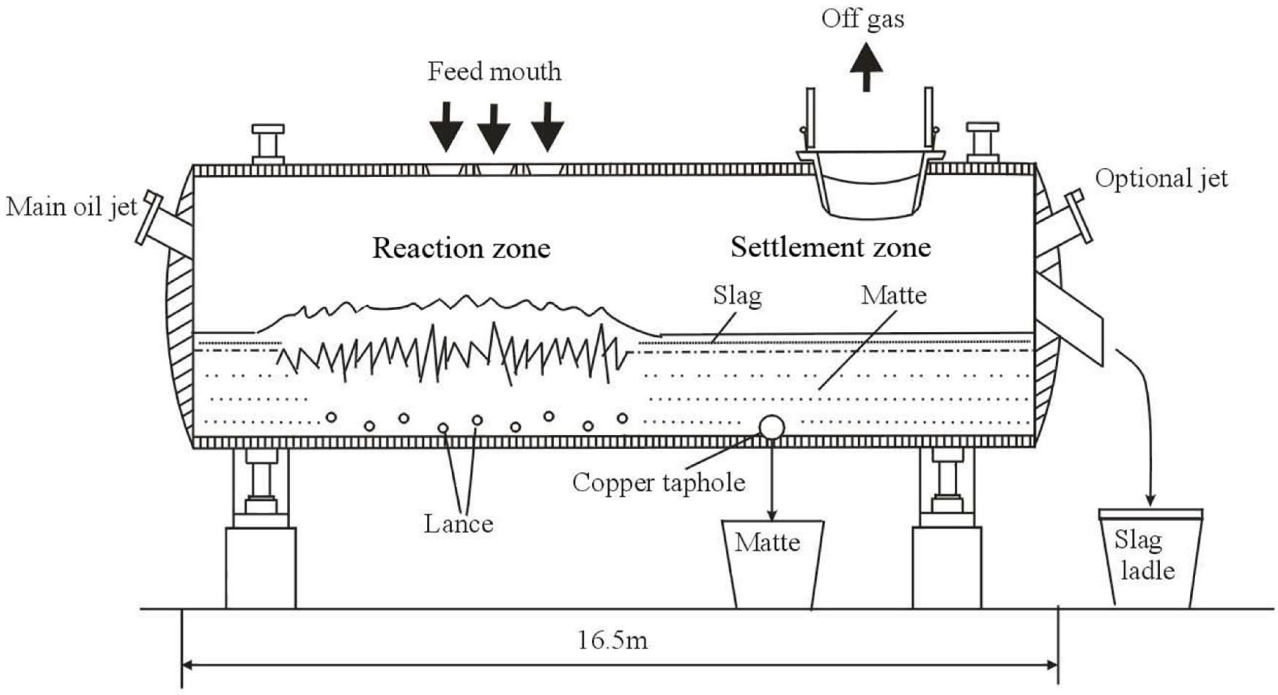

Figure 1-2 Schematic diagram of Fangyuan bottom blown copper smelting furnace

1.2 Research objectives

(1) To establish the methodology of cold model study on the bottom blown copper smelting furnace.

Due to extreme conditions such as high temperature, toxic gas or heavy dust in plants, it is usually difficult to observe or directly investigate the behaviour of the molten bath in metallurgical reactors. As a result, it is necessary to establish the methodology of cold model study in the laboratory. The design of lab-scale cold model must follow a group of principles that guarantee the information obtained in model is indicative to the prototype, which is the basis of further experimental work. Moreover, the methodology developed in this study is also helpful to the projects related to the bottom blown copper smelting furnace in future. Therefore, the methodology of cold model study should be considered in the first step.

(2) To investigate the effect of operational factors on the mixing of bath in the bottom blown furnace, and develop the theory of mixing

The mass transfer in metallurgical bath is highly related to the reaction efficiency, which is eventually related to the yield of the plant. The mixing phenomenon is a widely used index to evaluate the level of mass transfer in bath. To investigate the mixing phenomenon, firstly, a single phase bath is used to collect data under the simplest condition, and then a multiphase bath is used to investigate the effect of operational factors on the mixing of the bath.

(3) To investigate the formation of standing wave on bath surface and its effect on smelting operation.

The standing wave is created by gas bottom injection and causes different types of deformation of bath surface. The deformation is related to splash, refractory wearing, slag tapping of the furnace. Such behaviour of the bath could affect the operation in field and the furnace life. Therefore, it is significant to obtain more information of the standing wave on the bath surface for the better understanding of the furnace.

(4) To investigate the longitudinal wave transmitting on bath surface and its effect on smelting operation.

The longitudinal wave is the wave transmitting from the reaction zone to the settlement zone. This wave is related to the settlement of matte droplets in the slag layer and is relevant to the slag tapping. Therefore, to understand the behaviour of this type of wave is helpful to understand the mechanism of the settling of matte droplets and the tapping of slag.

1.3 References

[1] Z. Qiu: *Ye Jin Xue [Metallurgy]*, NEU Press, Shenyang, China, 2001

[2] R. R. Moskalyk and A. M. Alfantazi: *Minerals Engineering*, 2003, No. 16, vol. 16, pp. 893-919.

[3] J. M. Toguri, N. J. Themelis and P. H. Jennings: *Canadian Metallurgical Quarterly*, 1964, vol. 3, No. 3, pp. 197-220.

[4] Mark E. Schlesinger: *Extractive Metallurgy of Copper*, 5th ed, Elsevier, Saint Louis, MO, USA, 2011.

[5] Z. Cui, D. Shen, Z. Wang, W. Li, and R. Bian: *You Se Jin Shu [Nonferrous Metals]*, 2010, No.3, pp. 17-20.

[6] B. Zhao, Z. Cui, and Z. Wang: *Int. Symp. High-Temp. Metall. Process., 4th,* 2013, pp. 1-10.

[7] X. Hao, Z. Lu, and K. Wei et al: *Proc. Copper 2013—Cobre 2013 Int. Conf.*, 2013, pp.1035-1045.

2 Literature review

2.1 Copper bath smelting technologies

The general methodology of copper bath smelting is to blow oxygen or oxygen-enriched air into the molten matte and slag bath in the furnace via tuyeres that are opened on the side wall and submerged under the bath surface, or via lances that stretch from the roof into the molten bath. In the smelting process, feeds that are not completely dried are charged into the intensively gas stirred molten bath, and intensive gas-liquid-solid triple phase reactions are taking place. From the perspective of injection regime, copper bath smelting technologies can be categorised into three general types: 1. Submerged side blowing, including Noranda, Teniente, Vanyukov and Baiyin smelting; 2. Top submerged blowing, including Ausmelt and Isasmelt; 3. Top suspended blowing, such as Mitsubishi smelting; 4. Newly established bottom lance blowing: the Fangyuan copper smelting furnace.

2.1.1 Submerged tuyere smelting: Noranda, Teniente, Vanyukov and Baiyin

Noranda and Teniente smelting use large 4-5 m diameter × 14- 26 m long horizontal cylindrical furnaces, which are lined with refractory and rotatable in a certain angle. Smelting process is continuous, so molten matte and slag are always present in the furnace. The slag layer, due to its lower density and immiscibility, is floating on matte bath and oxygen for concentrate oxidation is blown into the molten matte layer via submerged tuyeres that are opened on the side wall[1].

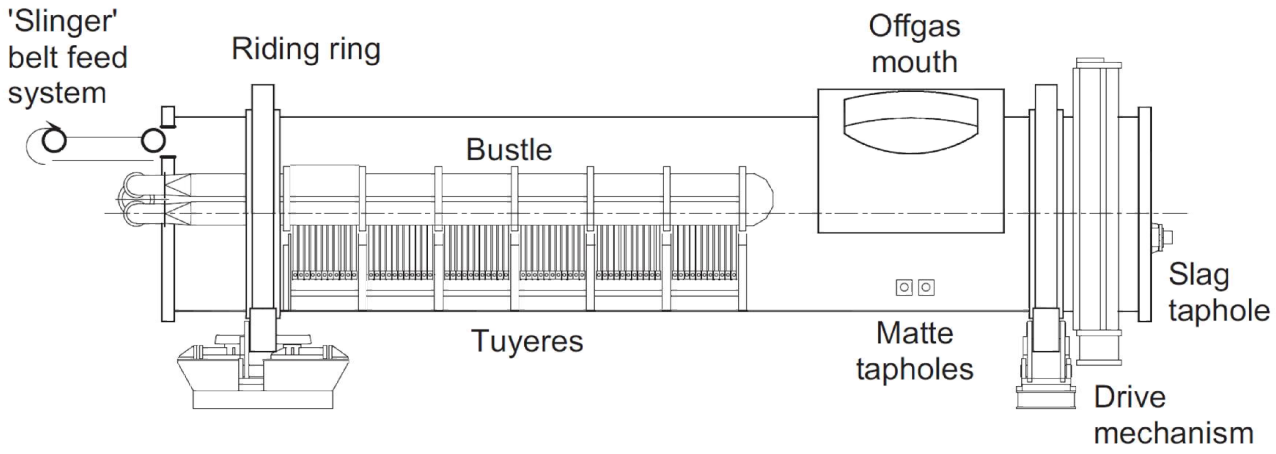

Figure 2-1 Schematic diagram of Noranda furnace [1]

The furnace can be roughly separated into two zones: the reaction zone and the settlement zone. About 54-66 tuyeres are lined at the side of furnace. Major reactions are occurring in the zone with tuyeres, so it is named the reaction zone. The other section of furnace has no tuyeres on the side wall but matte and slag tapholes, where reactions are less intensive for matte to settle and separate with slag, so it is named the settlement zone. During smelting, sulphide concentrate is blown into the matte layer or thrown by slinger belt onto the slag surface, and then the particles of concentrate sink into the matte layer and are oxidised by oxygen blown in via tuyeres. Iron oxides generated from the oxidation keep on reacting with SiO_2 flux charged from top feed mouth and form slag which then rises to the bath top and becomes the slag layer. SO_2 from the oxidation rises through the bath and leaves the furnace along with N_2 and CO_2 via offgas mouth above the settlement zone. Typical operational parameters of Noranda smelting are shown in Table 2-1.

Table 2-1 Operating details of two typical Noranda smelting furnaces

	Noranda, Canada	Altonorte, Chile
Inner length × diameter, m	20.58 × 4.35	25.55 × 4.45
Slag layer thickness, m	0.3-0.6	0.5
Matte layer thickness, m	0.9-1.15	1.2
Active tuyeres	44	47
New concentrate dry basis, t/day	1900-2200	3000
Silica flux, t/day	200-300	200
Slag concentrate, t/day	80-260	250
Recycle dust, t/day	50-75 +converter dust	40
Reverts, t/day	140-440	120-140
Other, t/day	0-64 liquid converter slag	Solid converter slag
Flowrate per tuyere, Nm^3/min	18.4-27.3	20-22
Oxygen-enrichment, %	38-42	37-40
Matte, t/day	700-900 (71-72%Cu,3-5%Fe)	1350 (74%Cu, 3.5%Fe)
Slag, t/day	1300-1500 (3-4% Cu)	1350 (6% Cu)
Matte/slag/offgas temperature, ºC	1210/1230/1300	1230/1220/1200

Teniente smelting has the similar furnace structure with Noranda, but it blows dry concentrate into

the furnace through four or six dedicated tuyeres. Rest feeds such as flux, recycle materials and moist concentrate are charged on to matte/slag surface via feed mouth. As show in Figure 2-2, the geometry of furnace is close to Noranda smelter except that the matte tapping hole is located at the end wall of reaction zone. Several dedicated tuyere to blow dry concentrate are set among normal tuyeres. The operational parameters of several typical Teniente smelters are shown in Table 2-2.

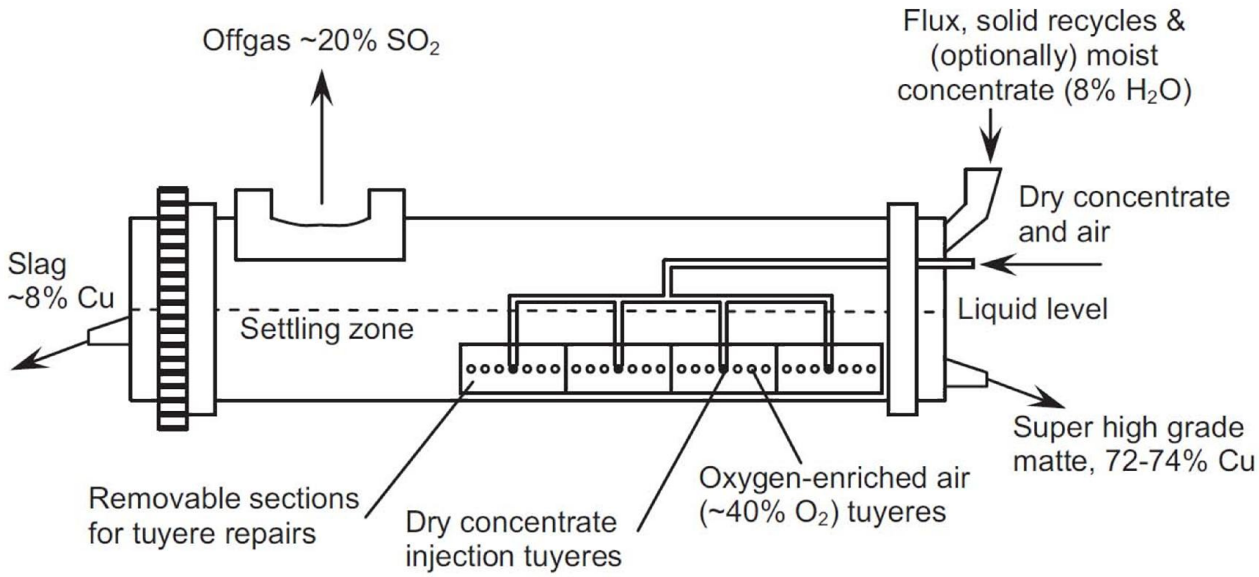

Figure 2-2 Schematic diagram of Teniente furnace [1]

Vanyukov smelting was developed in the former Soviet Union and is still being used in Russia and Kazakhstan nowadays. The furnace is rectangular instead of cylindrical, and unlike rotatable Noranda and Teniente furnace, it is operated in stationery. One typical feature of Vanyukov smelting is its slag layer depth is much higher than matte, usually 1.8 m slag and 0.8 m matte. Feeds are charged into slag layer from top feed mouth. Oxygen-enriched air is blown into slag layer, and the slag layer is intensively stirred and emulsified, where major chemical reactions are taking place. Its operating temperature normally reaches 1300-1350ºC, higher than Noranda and Teniente smelting. During smelting, feeds charged from top are dissolved in the gas stirred slag layer, and oxidation and slag formation are quickly taking place under such dynamic condition. Matte droplets generated by reactions settle down due to gravity, where these droplets collide and grow into larger ones, and then form matte layer below. Molten slag is flowing above matte towards slag tapping hole. As the smelting temperature is relative high, the viscosity of slag is decreasing, which leads to smaller amount of copper droplets entrained in slag. Besides, the dynamic condition in smelting provides condition for the Fe_3O_4 reduction in slag, which is also beneficial for the settling of matte droplets.

As a result, the copper content in slag can reach to as low as 1-2%.

Table 2-2 Operating details of two typical Teniente smelting furnaces

	Caletones, Chile	Chuquicamata, Chile
Inner length × diameter, m	21.1 × 4.2	22 × 5
Slag layer thickness, m	0.45-0.75	0.9-1.0
Matte layer thickness, m	0.9-1.2	1.0-1.2
Active tuyeres	43	49
New concentrate dry basis, t/day	2100	2200-2500
Silica flux, t/day	160-220	150-200
Slag concentrate, t/day	-	-
Recycle dust, t/day	-	0-50
Reverts, t/day	264-300	400-600
Other, t/day	0-75	-
Flowrate per tuyere, Nm^3/min	20-27	18-22
Oxygen-enrichment, %	35-38	39-42
Matte, t/day	801-909 (72-74%Cu)	990-1150(72-74%Cu)
Slag, t/day	1600-1900(6-10%Cu)	1550-1800(6-10%Cu)
Matte/slag/offgas temperature, ℃	1220/1240/1250	1220/1240/1250

On the other hand, as the furnace body of Vanyukov is stationery, it is not possible to lift up tuyere above slag surface for maintenance or emergency. Therefore, the operation of Vanyukov furnace is unstable from time to time, which is a disadvantage of this technology.

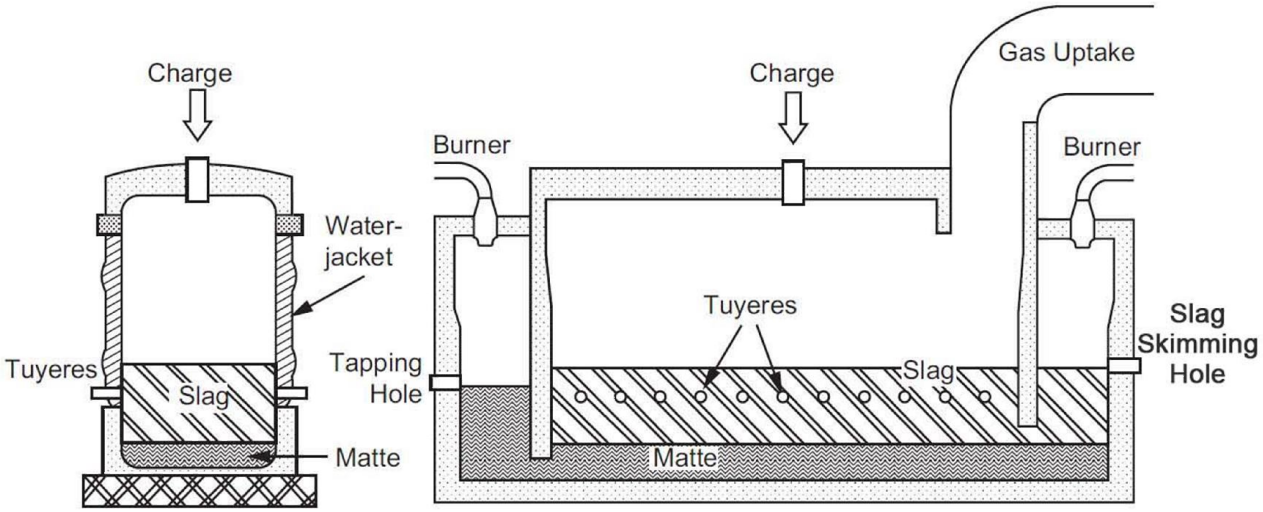

Figure 2-3 Schematic diagram of Vanyukov furnace [1]

Baiyin smelting was developed by Baiyin Nonferrous Metals Corporation in China in 1970s, and has been put into commercial operation in 1990. Nowadays, the Baiyin smelting technology is capable to produce blister copper 100kt/a. The fundamentals of Baiyin smelting are similar to the Noranda and Teniente technologies above, but there are some specific improvements. The shape of Baiyin smelting furnace is rectangular, and it is also stationery as Vanyukov smelting. The Baiyin smelting furnace uses submerged tuyeres to blow oxygen-enriched air into molten matte, but tuyeres are set in a line on walls of both sides of the furnace as in Figure 2-4. Additionally, a separation dam is added inside the furnace to separate the smelting zone and settlement zone. It is found that this dam solves the contradiction of smelting and settlement. On one hand, it intensifies agitation in smelting zone which increases chances that matte droplets collide with each other to form bigger droplets and settle down to the matte layer, on the other hand, it reduces agitation in the settlement zone for relatively smaller droplets to settle down by gravity. A hole is opened at the bottom of the dam to enable molten bath flows from the reaction zone to the settlement zone. Improved Bayin furnaces increase the height of the separating dam and completely separates the reaction zone and settlement zone into two independent chambers, which enhances the function of each chamber. Baiyin smelting uses wet concentrate and is adaptable to various concentrate. Humidity of concentrate is 6%-8%, concentrate with smaller amount of larger particles can also be charged directly, which reduces the cost of concentrate pre-treatment and dehydration. The matte grade of Baiyin smelting is about 50%, which is relatively low compared to other smelting technologies, so the promotion of matte grade is desirable in future. Baiyin smelting has relatively

simple structure and auxiliary devices, and its operation is steady and simple. It is also a competitive copper smelting technology[2].

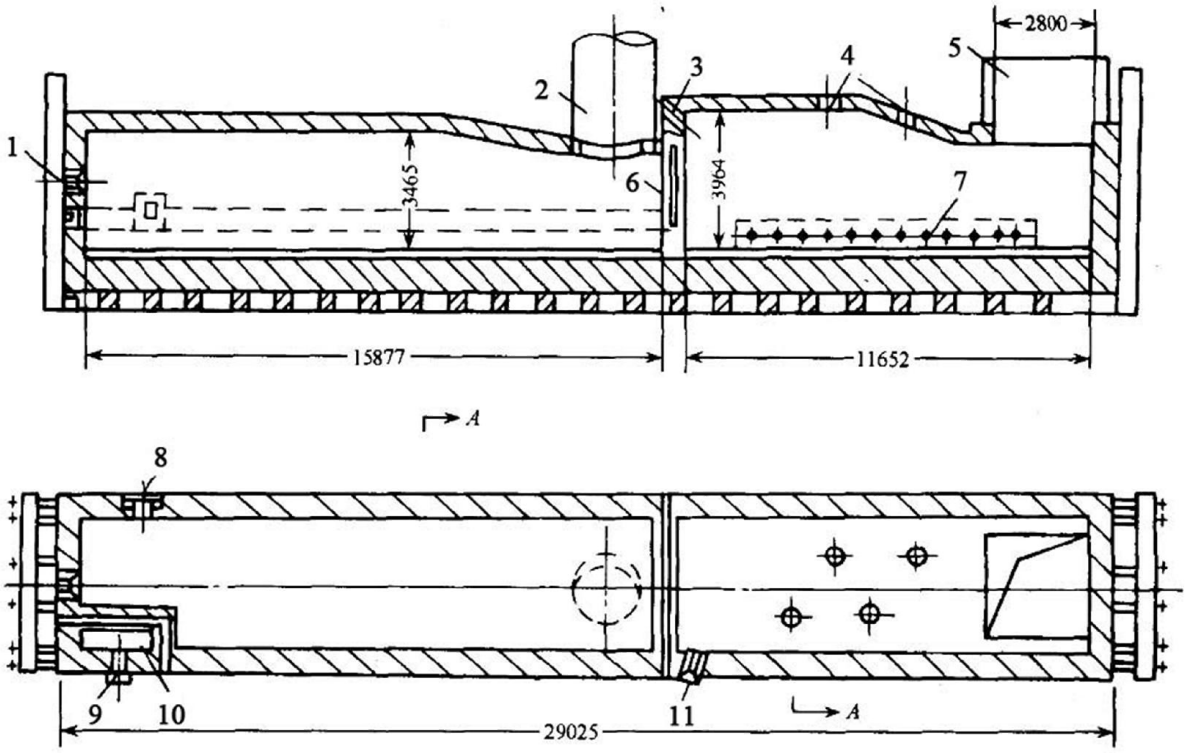

1.burning mouth 2.offgas mouth of settling section 3.mid burning mouth 4.feed mouth
5.offgas mouth of smelting section 6.separation dam 7.tuyeres 8.slag mouth 9.matte

(a)

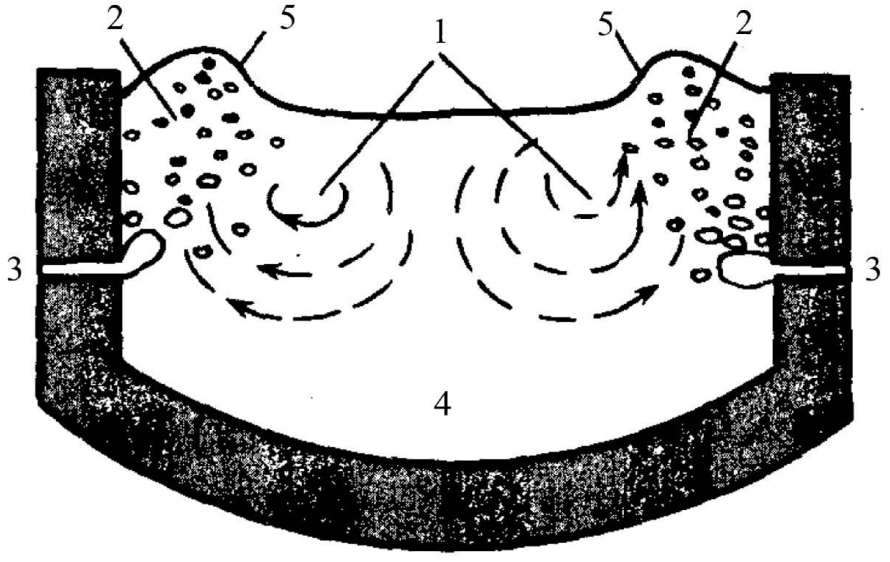

1. turbulence zone 2. gas-liquid mixing zone 3. tuyeres
4. matte 5. concentrate

(b)

Figure 2-4 (a) Schematic diagram of Baiyin furnace (b)Tuyere configuration and the bath flow scheme in Baiyin furnace [2]

All these four technologies mentioned above are continuous, tuyere submerged, bath smelting. Concentrate is charged from the top of the bath some with dried concentrate blown in via dedicated tuyeres as complement. The submergence of tuyeres enables the injected gas to stir molten slag and matte intensively, which results in rapid melting and oxidation of feeds. Consequently, the intensive stirring enhances mass and heat transfer, leading to high smelting rate and thermal efficiency. In addition, as major chemical reactions are taking place in bath, a relatively smaller amount of dust is generated compared to flash smelting. Besides, the molten bath is able to consume different types of copper ores as well as scrap and revert, so these furnaces are adaptive to extensive range of feeds.

2.1.2 Top submerged lance smelting: Ausmelt and Isasmelt

In 1970s, researchers at the Australian Commonwealth Scientific and Industrial Research Organisation (CSIRO) studied the use of top-lancing technology for injecting coal into tin slag to improve reduction kinetics. Later this research was applied in various pyro-metallurgical processes, such as smelting and converting copper sulphide concentrate. Nowadays, this technology was well established and known as Top Submerged Lance (TSL) technology, and licensed by two separate organisations, Isasmelt and Ausmelt.

The shape of Isasmelt and Ausmelt furnace is a vertical cylinder with spherical bottom, as shown in Figure 2-5. It is usually 3.5-5 m in diameter and 12-16 m in height, and the molten bath depth is about 1.2 m. It is lined with chrome-magnesite refractory, and sometimes backed with copper water-cooling blocks. Isasmelt and Ausmelt employs a specially designed lance, with outside diameter 0.3-0.5 m, stretching from the furnace roof to 0.3 m below the slag layer surface to blow oxygen and air into the bath. The lance of Ausmelt contains four annular pipes, of which the most inside one blows dry coal powders with air, the second inside layer blows oxygen, the third blows air and the outside one is designed to blow air to protect the wall of the third annular pipe and burn sulphur and other combustible compositions in offgas, so the outside pipe does not penetrate into the molten bath. The structure of the Isasmelt lance is alike but without the outside pipe.

During smelting, moist solid feeds are charged into furnace from top, and oxygen is blown via the lance into the bath. As intensive chemical reactions are taking place in the bath, large amount of

SO_2 offgas generated is drawn from the top mouth through a vertical flue and matte/slag mixing is tapped periodically (Isasmelt) or continuously (Ausmelt) into a fuel-fired (Isasmelt only) or electrical settling furnace for separation. Most of energy for smelting comes from oxidising the concentrate charge. Additional energy is provided by combusting fuels like oil, gas, or coal fines blown through the vertical lance and coal fines in the solid charge. Operational details of typical Isasmelt and Ausmelt are shown in Table 2-3 and Table 2-4. It is found that this smelting technology cannot reach autothermal smelting and fuel is always necessary to keep the furnace temperature constant.

Table 2-3 Operating details of typical Isasmelt furnaces

	Mount Isa, Australia	Kunming, China	Miami, USA
Inner diameter, m	3.75	4.4	3.75
Molten bath depth, m	1-2	1-2	1-2
Number of tapholes	2	2	2
Concentrate process capacity, t/a	1,000,000	800,000	750,000
Cu content in concentrate, %	22-26	18-22	25-29
Solid fuel	Coal or coke breeze	Coal	-
Nominal bore of lance, mm	450	350	400
Oxygen-enrichment, %	60-65	45-50	45-50
Hydrocarbon fuel in lance	Natural gas	Diesel	Natural gas
Matte grade, %	60-63	52-55	55-60
Matte-slag mixture temperature, ℃	1190	1180	1185

One typical advantage of TSL technology is that the furnace structure is relatively simple, which leads to less construction investment. Meanwhile, the same as submerged tuyere smelting, major chemical reactions of TSL furnaces are taking place in bath, which enables the furnace to consume a wide range of feeds and generates less dust. However, there are some shortcomings of TSL technology, including: (1) the furnace is not able to reach autogenous smelting, so a large amount of fuel, such as coal, diesel or natural gas, is consumed to keep the furnace temperature constant, which increases cost; (2) the furnace produces mixture of matte and slag which requires a further separation process that consumes fuel or electricity as well.

Table 2-4 Operating details of typical Ausmelt furnaces

	Zhong Tiao Shan, China	Tongling, China	RCC, Russia
Inner diameter, m	4.4	4.4	5
Molten bath depth, m	~1.2	~1.5	~1.5
Number of tapholes	Weir	Weir	Weir
Concentrate process capacity, t/a	200,000	700,000	550,000
Cu content in concentrate, %	17-22	25	14-23
Solid fuel	-	-	-
Nominal bore of lance, mm	~300	~400	~500
Oxygen-enrichment, %	40	40	60
Hydrocarbon fuel in lance	Coal	Coal	Natural gas
Matte grade, %	60	50	40
Matte-slag mixture temperature, ℃	1200-1300	1180	1180

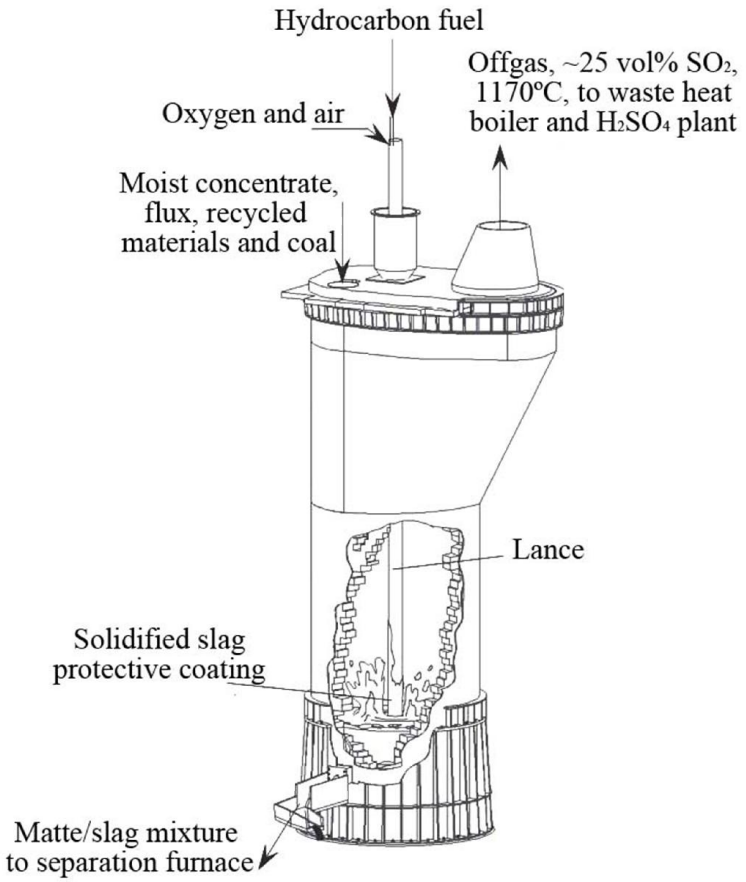

Figure 2-5 Cutaway view of Isasmelt furnace [1]

2.1.3 Top suspended smelting: Mitsubishi smelting

The Mitsubishi process organises smelting, slag-cleaning and converting three furnaces together, to operate the entire process continuously. The typical Mitsubishi process is shown in Figure 2-6. In the current study, only smelting furnace is discussed. Smelting furnace applies top lances to blow oxygen enriched air, dried concentrate, flux and recycles into the bath. Each lance consists of two concentric pipes. The inner pipe is 5 cm in diameter, and is used to blow dried feeds with air. The outer annular pipe with diameter 10 cm is used to blow oxygen enriched air. The outer pipe extends to about 0.7 m above molten bath, and the inner pipe is just to the furnace roof. The feeds meet oxidising gas at the exit of inner pipe, and the mixture then jets onto molten bath surface to form matte-slag-gas foam where chemical reactions are taking place. Usually, lances tips are slowly corrupted, so the height and position of lances need adjustment in time. The furnace employs nine lances which are lined in two rows to blow feeds and oxygen enriched air. These reactions continuously occur and the mixture of matte and slag flows down a sloped launder via a siphon hole to a slag cleaning furnace. Waste gas from oxidation is drawn up from the top of the furnace.

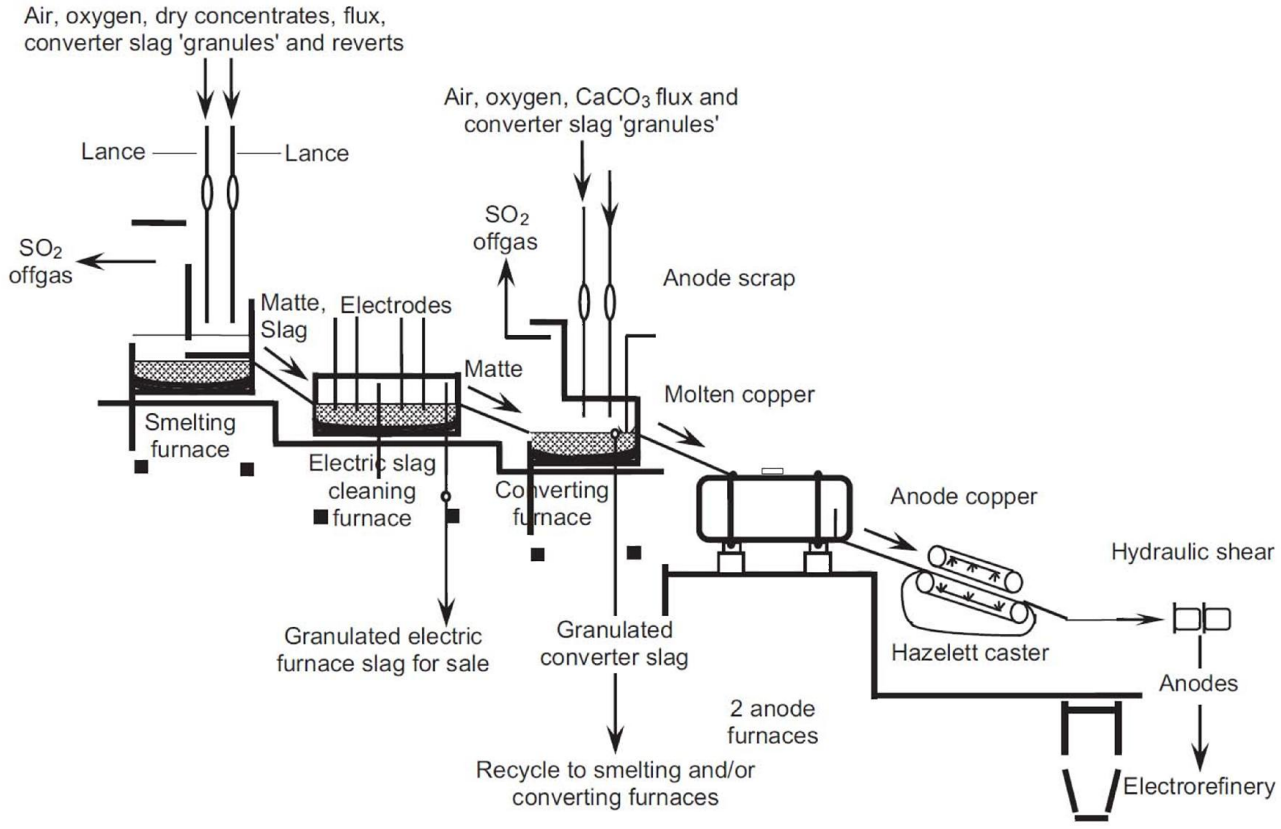

Figure 2-6 Typical Mitsubishi process flowsheet [1]

Industrial evidence indicates that the smelting furnace contains mainly matte with a gas/slag/matte emulsion beneath the lances. Away from the lances, SO_2/N_2 gas disengages from the foam, and matte and slag start to separate. The matte layer is 1.2-1.5m deep, while the slag layer is 0.05 thick with some matte droplets entrained.

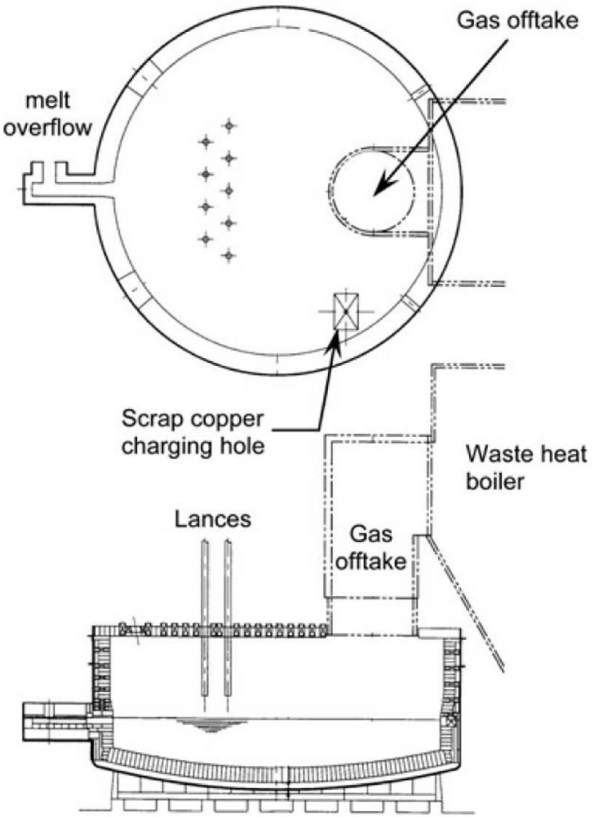

Figure 2-7 Schematic diagram of Mitsubishi smelting furnace [1]

The continuous operation of Mitsubishi smelting increases production rate and reduces energy consumption. Meanwhile, bath smelting reduces dust generation, which reduces environmental cost. The Mitsubishi smelting furnace also taps matte and slag together like Isasmelt or Ausmelt, but slag cleaning furnace is well interconnected, so the entire process is operated continuously. On the other hand, the connection of smelting, slag cleaning and converting of Mitsubishi process requires stable control and coordination of these three furnaces, as entire production could be affected if one part is not well coordinated. Moreover, Mitsubishi smelting furnace blows fine particles of feeds via inner pipe of lance. This requires pre-treatment of concentrate and other feeds.

2.1.4 Summary

This section reviews the main technologies of copper bath smelting around the world. It is found that each technology has its advantages as well as shortcomings, and thus all of them coexist in

copper smelting industry nowadays. Among those, Noranda, Teniente, Isasmelt, Ausmelt and Mitsubishi smelting are more widely spread.

Table 2-5 Operating details of typical Mitsubishi smelting furnaces

	Mitsubishi, Naoshima, Japan	PT smelting Co. Gresik, Indonesia	LG Nikko Onsan, Korea
Inner diameter × height, m	10 × 4	10.1 × 4	10 × 4
Slag layer thickness, m	0.1	0.1	0.1
Matte layer thickness, m	1.4	1.4	1.4
Number of lances	9	9	9
Lance rotations per min	7.7	6.5	7.8
New concentrate, t/day	2300	2000-2300	2109
Silica flux, t/day	340	300-400	386
Limestone flux, t/day	42	35	52
converting furnace slag, t/day	240	160-180	96
Smelting furnace dust, t/day	67	60	60
Converting furnace dust, t/day	61	60	60
Other, t/day	5	40	14
Blowing flowrate, Nm^3/min	540	600-650	600
Oxygen-enrichment, %	56	50-55	45-55
Hydrocarbon fuel (coal), t/day	63	90	140
Liquid temperature, ºC	1225-1240	1240	1240

Noranda and Teniente smelting furnaces account for about 15% of world copper smelting. One of the features of Noranda and Teniente smelting is its horizontal cylindrical furnace, in which both of the reaction zone and the settlement zone are present. Therefore, the smelting and separation of matte and slag are continuously occurring inside the furnace, and thus no separation furnace is needed, which reduces production steps. Furthermore, the energy consumption of Noranda and Teniente smelting is considerably low. Noranda smelting continuously feeds the moist concentrate (~8% moisture) through end wall onto the slag bath surface. The use of moist concentrate reduces the processing of concentrate pre-treatment but requires more heat in smelting, so fuel is needed from time to time in smelting to remain the stable furnace temperature. However, as technology is

improved, the energy efficiency of Noranda smelting is promoted. The fuel rate is less than 3% per ton concentrate. Besides, Noranda furnace is also adaptive to different types of fuels. Gaseous, liquid or solid fuels such as natural gas, diesel, heavy oil, coal or metallurgical coke can be used. Instead, Teniente smelting feeds dry concentrate through dedicated tuyeres into molten matte. Dried concentrate brings no moisture into furnaces so it consumes less energy generated by chemical reactions. Therefore, most Teniente furnaces are running in autothermal smelting, which means the heat from chemical reactions is sufficient to keep the furnace temperature constant and no fuel is needed. This reduces much energy consumption.

Isasmelt and Ausmelt share the similar vertical cylindrical furnace shape, and entail the central annular cross-section lance. The construction of Isasmelt and Ausmelt is relatively simple, and the smelting rate is considerably high. Therefore, the two smelting technologies are also widely spread. Isasmelt and Ausmelt feed moist concentrate (~8% moisture) into furnace. Despite of higher oxygen enrichment than Noranda and Teniente, the smelting cannot achieve autothermal operation. Instead, hydrocarbon fuel is added. Isasmelt and Ausmelt furnaces are designed to use natural gas, oil, or coal. On the other hand, a cool lance tip is important for reducing lance wear. As a result, coal is often added to the feed as partial substitution for flammable fuel oil and natural gas to avoid lance tip overheated. The principal product of Isasmelt and Ausmelt is the mixture of matte and slag, and a special separation unit such as rotation holding furnace or electrical furnace should be arranged for separation.

The Mitsubishi smelting furnace blows fine dried concentrate via top suspended lances into bath, and emulsion of matte, slag and gas is created on bath surface, where main chemical reactions are taking place. Under such intensive condition, the outside pipe of lance is burning back about 0.4 m per day, and it is slipped downward periodically to maintain the specific tip position. Despite the use of dried concentrate, the Mitsubishi smelting furnace does not achieve autothermal operation. Hydrocarbon fuel (mainly coal) is needed to keep the smelting temperature constant. The fuel rate of the Mitsubishi smelting furnace is 3-6% per ton concentrate.

Table 2-6 shows the typical operational parameters comparison of various smelting technologies. It

is found that the novel Fangyuan bottom blown furnace possesses some special advantages[3-11] as follows:

Table 2-6 Typical operational parameters comparison of smelting technologies

	Location	Concentrate Cu content, %	Slag Cu content, %	Matte grade, %	Oxygen enrichment, %	Operating temperature, ºC	Area capacity, t/(d·m^2)	Volume capacity, t/(d·m^3)
Noranda	Horne	~28	3-4	71-72	38-42	1230±20	43.2	12.0
	Daye	~21	5.76	68-70	38-42	1220±20	47.2	14.9
	Altonorte	37	6	74	38-42	1230±20	46.0	12.8
Teniente	Caletones	26-28	6-10	72-74	35-38	1220-1250	41.1	12.2
	Chuquicamata	30-33	6-10	72-74	39-42	1220-1250	39.1	9.8
Vanyukov	Norilsk	19-23	1-2	55-74	60-70	1300-1350	-	-
Baiyin	Baiyin	16-17	~1	30-50	21-47	1200-1250	-	-
Isasmelt	Mt Isa	22-26	Mixture	60-63	60-65	1180-1190	248.1	20.7
	Miami	25-29	Mixture	55-60	45-50	1180-1190	186.1	14.3
Ausmelt	Zhong Tiao Shan	17-22	Mixture	60	40	1180	36.0	4.0
	Tongling,	25	Mixture	50	40	1180	126.1	11.5
Mitsubishi	Naoshima	34	Mixture	~68	55	1220	29.2	7.3
Fangyuan	Dongying	~20	2-3	72-73	72-75	1150-1170	61.2	21.2

(1) Adaptive to feeds

The bottom blown furnace is adaptive to feeds. It uses moist concentrate as Noranda smelting, which reduces the cost of concentrate pre-treatment. Besides, it is capable to process the concentrate with Cu content as low as 20% and dimension < 20 mm. This tolerance to feeds is beneficial for spreading.

(2) High matte grade

The matte grade produced by the bottom blown furnace is 72-73%, close to Noranda and Teniente smelting but higher than other technologies. High grade of matte reduces the cost of following converting process, which is desirable in smelting furnace.

(3) Low temperature and autothermal smelting

The smelting temperature of bottom blown furnace is in the range of 1150-1170 ºC, lower than other smelting furnaces. The advantages of low temperature smelting include: 1) autothermal smelting. As operational temperature is lower, the energy required to sustain the temperature is less than other smelting furnace. The energy created by the oxidation of concentrate is sufficient to supply the required amount of energy. Therefore, the autothermal smelting condition is easier to achieve. 2) low consumption of refractory. As the operational temperature is lower, the erosion of refractory is slower. It is reported that there was no significant erosion of refractory after one and half years operation. 3) relatively higher viscosities of matte and slag allow higher pressure of gas injecting. 4) low temperature is beneficial to produce higher grade of matte at a given oxygen partial pressure. This is because at a lower temperature there is less Cu_2O dissolved into slag. In addition, at a lower temperature more Fe_3O_4 is generated, which reduces Fe in matte, and the matte grade is accordingly increased. Thirdly, the oxidation of $CuFeS_2$ is an exothermic reaction. A lower temperature helps the oxidation of Fe and S in matte, which increase the Cu content in matte.

(4) Low Cu content in slag

As the smelting temperature range is below the liquidus temperature of slag, droplets of spinel are present in liquid slag, which increases the apparent viscosity of slag. The high viscosity slag is detrimental for matte droplets to settle down. However, the surface wave generated by bottom gas injection is helping the matte droplet settling, and it is also beneficial for the tapping of slag. As a result, though the slag viscosity is relatively high, the copper content in smelting slag is considerably low. This is beneficial because low Cu in slag reduces the cost of slag cleaning process. Additionally, bottom blown furnace taps slag and matte separately, like Noranda and Teniente smelting. The matte is transported to converting furnace directly after tapping, which increases the production rate.

(5) High oxygen enrichment and long lance life

The oxygen enrichment of Fangyuan bottom blown furnace is 72-75%, much higher than other copper smelting furnaces. High oxygen enrichment enables the fast and intensive oxidizing reaction to take place, which increases production rate. Current industrial report shows that the oxidising reactions are so intensive that the furnace is able to allow even higher oxygen enrichment, or pure oxygen. Due to the oxygen supply limit in plant, further study is needed to evaluate the application of higher enrichment. In most present copper smelting furnaces, the oxygen enrichment is limited

by lance tip or tuyeres wearing. To solve this problem, in Fangyuan bottom blown furnace, the blowing lances are designed as double layered: the inner channel for oxygen and outer annular channel for compressed air. The fast flowing compressed air in outer annular channel reduces heat accumulation at lance tip protecting the lance from overheated. Furthermore, a protective accretion is formed at the tip of lance due to lower temperature there, which prevents lance tip from directly contacting with molten bath and enables the lance life to be over 10 months.

(6) High smelting rate

The area smelting capacity and volume smelting capacity of various smelting furnaces are shown in Table 2-6. The area capacity and volume capacity are usually used as index of processing rate to evaluate productivity of metallurgical reactors. The area capacity shows the quantity of concentrate processed by smelting furnace in unit bath surface per day, where the Noranda, Teniente and Fangyuan smelting use the bath surface area of the reaction zone to exclude the calm settlement zone in furnace. Likewise, the volume capacity shows the quantity of concentrate processed in unit volume of furnace per day, where the reaction zone volume is used for calculation of Noranda, Teniente and Fangyuan smelting as well. It is shown that the bottom blown furnace has the highest area capacity among the horizontal cylindrical furnaces. The Isasmelt and Ausmelt also have the high area capacity because of the relatively small bath surface area. The volume capacity shows the smelting rate per spatial volume. It is found that the Fangyuan bottom blown furnace has the highest value of volume capacity, even higher than the Isasmelt furnaces. Both area capacity and volume capacity show the high smelting rate of the bottom blown furnace. This is one of the significant features of the bottom blown furnace.

2.2 Bottom blown technology in metallurgy

Bottom blown technology was firstly developed and put into industrial production in 1950s-1960s. Nowadays it has become an essential technology widely used in metallurgy, such as steelmaking converters, steel refinery ladles and some nonferrous smelting furnaces.

In 1950, the first argon bottom blown agitation steelmaking ladle was set up for steel refinery in France. Argon injected from the bottom of the bath forms bubbles rising in the bath. During this process, inclusions such as entrained slag particles or other impurities are captured by bubbles and

rise to slag layer, meanwhile decarburisation, dephosphorisation or desulphurisation reaction are accelerated on the gas-liquid two phase interface. In addition, continuous bubble rising motion drives entire bath to flow in circulation, which enhances mass transfer in the bath. These thermodynamic and kinetic conditions created by bottom blowing are beneficial to accelerate chemical reactions in the metallurgical bath, thus this technology has been investigated, optimised and improved through decades[12-13].

In 1968, the first bottom blown oxygen converter was set up and put into industrial production in Germany. In practice, it was found that the liquid metal bath is more intensively agitated compared to previous top blown technology, which leads to faster decarburisation. Meanwhile, the carbon-oxygen reaction tend to be equilibrium as well. Faster chemical reactions enables the smelting rate to increase, so production rate is consequently increased. Besides, later researches reported that an ideal agitation rate can be acquired at a relatively lower blowing rate compared to the top blowing, which reduces energy consumption in industrial operation. Due to metallurgical advantages created by bottom blowing, the bottom blown steelmaking converter was developed and spread quickly around the world. It almost replaced open-hearth steelmaking process recently. Similar as the bottom blown ladle refinery process, bottom blown oxygen converter has also been investigated and optimised by researchers from different countries[14-15].

Bottom blown technology has also been applied in nonferrous metallurgy. In 2002, Yu Guang Corporation from Henan Province of China built up a bottom blown lead smelting furnace. Compared to previous well establish steelmaking oxygen converter or argon bottom blown refinery ladle, it is the first time using a bottom blown furnace to smelt metal ore[16]. The structure of the bottom blown furnace is shown in Figure 2-8. It is a horizontal cylindrical vessel, with oxygen lances set at bottom. Lead concentrate is charged from the top of the furnace, while industrial oxygen is blown via lances at the bottom [17]. Intensive chemical reactions are occurring in the bath, and primary liquid lead, slag and SO_2 are produced. As shown in Figure 2-9. Primary lead is drained by siphonic effect at one end of the furnace and sent to electrolytic refinery, while slag is tapped at the other end to the lead recovery process. Waste gas containing mostly SO_2 is exhaled from the top of the furnace via waste heat recovery devices and de-dusting devices to the acid

making plant [18-20].

As bath smelting is agitated by the oxygen-enriched air from bottom, metallurgical reactions in bath are enhanced, so the entire smelting efficiency is promoted[21-22]. Major advantages of Yu Guang's technology include: the furnace has good adaptability with feeds, the smelting process is relatively short, the oxygen enriched air blowing intensifies smelting, and SO_2 content in waste gas can reach 20% which is convenient for acid making and reduces environmental issues. This technology accounts for 50% lead production in China in 2008, and yield reaches 1.24 million ton/annual. By using this technology, SO_2 emission can be reduced by 800,000 ton/annual and coke can be saved up to 150,000-200,000 ton/annual.

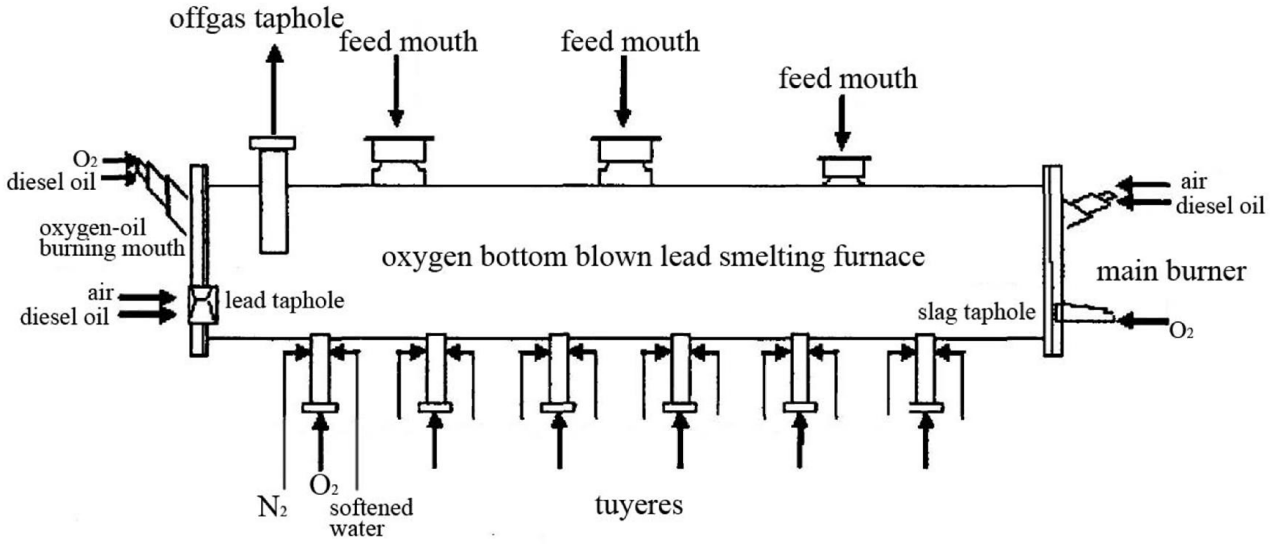

Figure 2-8 Schematic diagram of Yu Guang bottom blown lead smelting furnace

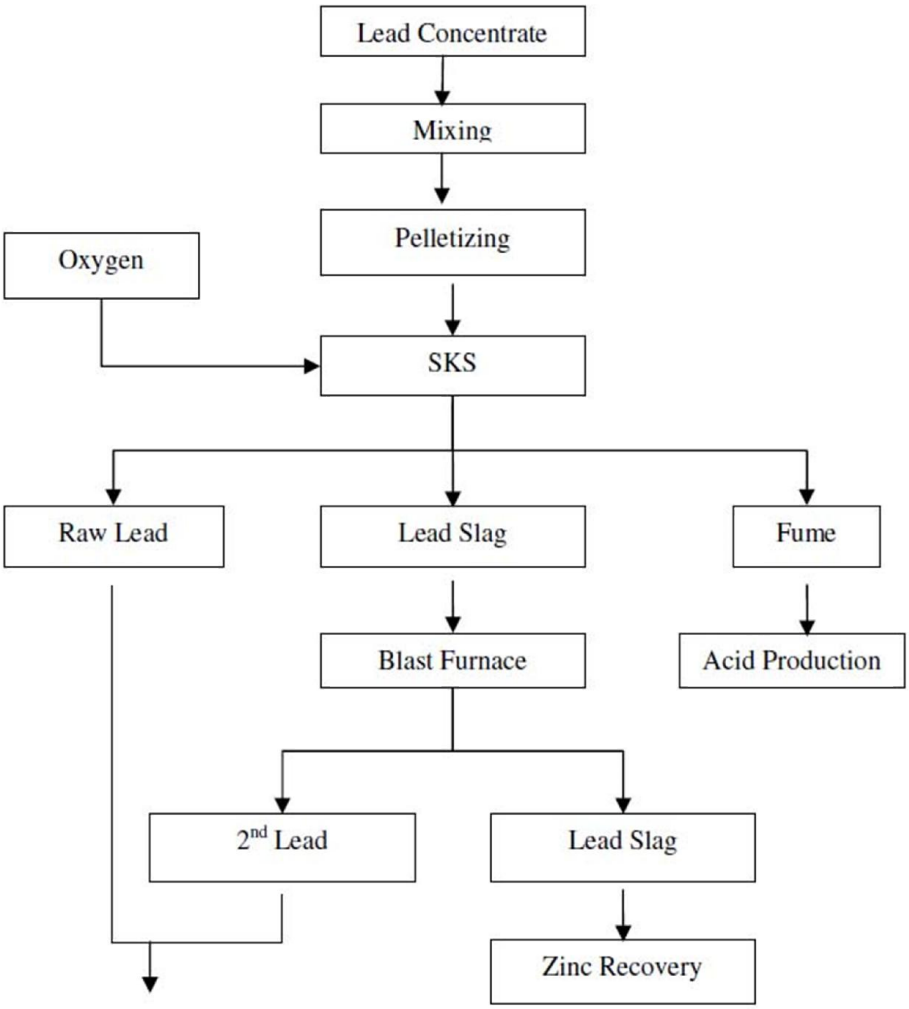

Figure 2-9 Yu Guang lead smelting process

2.3 Submerged combustion technology

Submerged combustion is a new method of reprocessing metallurgical (blast furnace) slag into materials for the construction industry. In literature, the melt aggregating by submerged combustion were developed and tested. One major feature of this technology is the multi-jet gas-air burners that are submerged into the melt. This feature provides melt bubbling and helps to achieve maximum heat transfer from combustion product to the melt, which enhances mixing and increases chemical reaction rate [23]. The process of submerged combustion is shown in Figure 2-10. Pioro *et al*[24] carried out a series of experiments to investigate features of this submerged combustion furnace.

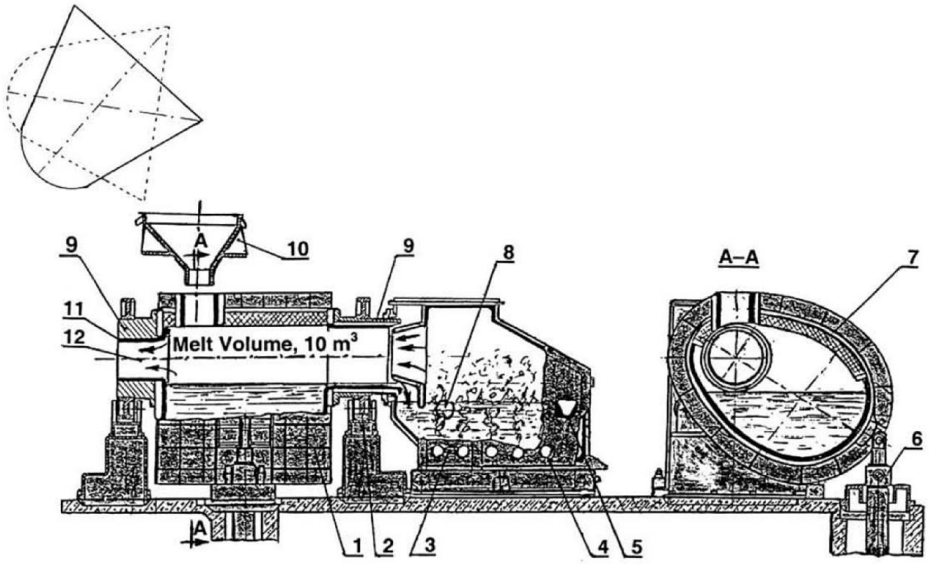

(1) slag receiver, (2) supporting rollers, (3) converter, (4) openings for lances, (5) tap-hole, (6) hydraulic jack, (7) refractory, (8) charge loading, (9) receiver trunnions, (10) interim funnel, (11) melt lining, (12) flue gases.

Figure 2-10 Submerged combustion furnace for metallurgical slag reprocessing [24]

Rue [25-27] investigated submerged combustion in glassmaking industry, and developed submerged combustion melting (SCM). It is an advanced, high-temperature melting technology in which fuel and oxidant are charged directly into a bath of material being melted. Combustion gases bubble through the melt, providing high heat transfer and turbulence, which leads to high mass transfer efficiency and homogeneous product composition, as shown in Figure 2-11. Raw materials which need little or no crushing and are charged from top of bath, and product melt is drained from a tap near bottom of furnace.

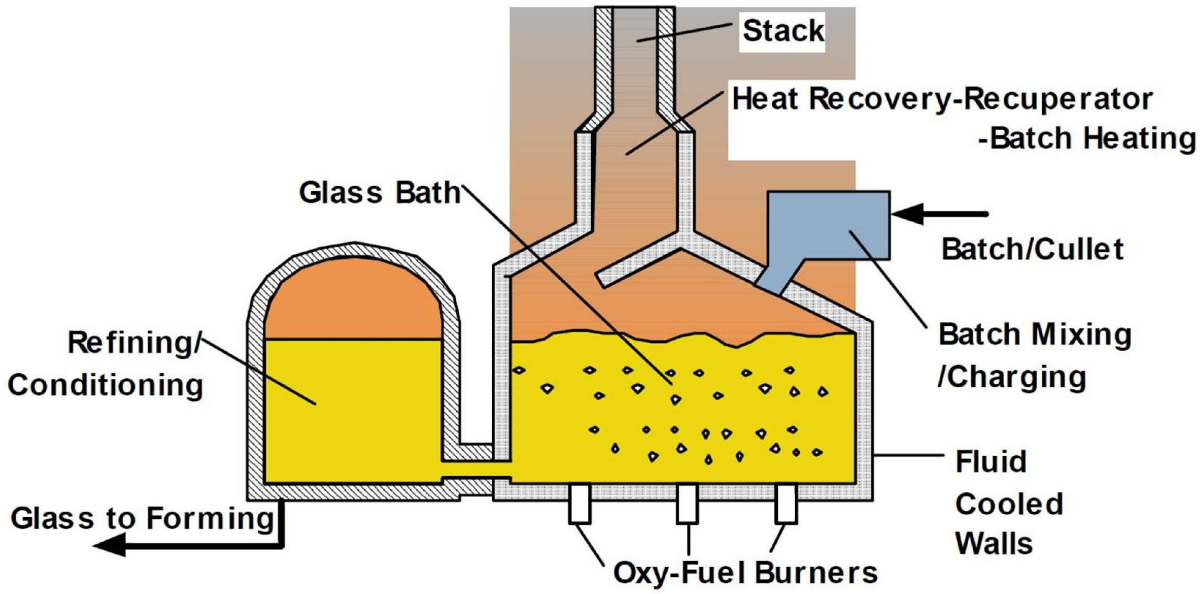

Figure 2-11 Submerged combustion glass smelting furnace [26]

The major feature of submerged combustion smelting is the multi-jet gas-air burners that are submerged into the melt, which is similar to copper bath smelting containers. Though the geometric shape of this furnace is different from copper smelting furnaces, the basic physical mechanisms are analogical. Therefore, the studying of the mechanism in copper smelting furnaces can follow the same methodology used in the studying of submerged combustion.

2.4 Mixing time and stirring energy investigation in metallurgical vessels

2.4.1 Mixing time and stirring energy investigation in single phase bath

Physical modelling is an essential method in metallurgy. Due to complication of metallurgical process, such as high temperature or toxic gas, it is usually difficult to observe metallurgical reaction directly. Therefore, modelling is widely used to understand chemical or physical phenomena in smelting, and it is also useful to investigate metallurgical processes and operations. Much work about modelling in metallurgy has been done in recent decades, including steelmaking converter, ladle argon blowing, and tundish argon blowing[28].

Mixing time measurement is a common quantitative approach to investigate the mass transfer ability of metallurgical vessel in physical modelling. Mixing time is defined as the time needed for the molten bath composition to reach homogenous, and it represents the efficiency of bath agitation. It has been widely used as an index to evaluate metallurgical container designing as well as blowing tuyere configuration.

In 1975, Nakanishi *et al*[29] built up a model ladle 0.465m in height and 0.42m in diameter for mixing effect investigation. Mixing time under different conditions was measured for evaluation. In experiment, argon gas was used for stirring, and was injected through a porous plug located at the bottom of ladle. Sulphuric acid was used as the tracer which was charged at the bottom of the ladle. A pH probe served as a detector, which recorded pH value continuously.

In this research, Nakanishi firstly plotted mixing time data against global rates of specific energy dissipation rate for an RH vacuum degassing unit, an induction stirred ASEA-SKF system.

$$\varepsilon = \frac{0.0285QT}{W_g} log\left(1 + \frac{Z}{148}\right) \quad (2.1)$$

Where, ε --- stirring energy dissipation, W/t

Q--- gas flowrate, L/min

T --- bath temperature, K

W_g --- weight of bath, t

Z --- bath depth, cm

Gas flowrate was correlated into stirring energy dissipation ε so the relationship between mixing time and ε was proposed. According to Nakanishi's report, the empirical equation acquired in the model ladle experiment is

$$\tau = 800\varepsilon^{-0.4} \quad (2.2)$$

where τ is the time in seconds required to attain complete mixing and ε is the stirring energy dissipation in W/t.

Haida *et al*[30] found that in industrial experiments using copper powder as tracer, mixing time can be expressed in following equation

$$\tau = 12.68 \times 10^3 \varepsilon^{-0.4} \quad (2.3)$$

This equation is quite similar to Nakanishi's except the constant. The same as Eq. (2.2), the vessel's geometry features do not appear in the equation, which implies that shape and size of the vessel have little or negligible influence on mixing effect. Nakanishi [31] later found that in steelmaking bottom blown reactors, Eq. (2.3) performed well when dealing with single tuyere blowing, but needed to be modified coming to multiple tuyere blowing. Therefore, Eq. (2.3), was modified to

$$\tau = 12.68 \times 10^3 \varepsilon^{-0.4} N^{\frac{1}{3}} \quad (2.4)$$

where N represents the number of tuyeres. This equation shows that for the same energy input, increasing in the number of tuyeres leads to increasing in total mixing time. Furthermore, a point was suggested that mixing in metallurgical reactors is caused primarily by turbulent diffusion rather than by bulk recirculation. It was believed that the time required to attain complete mixing in such systems could be predicted reasonably well by postulating a non-convecting melt and using turbulent diffusivities, where the result is only slightly greater than those deduced from turbulence

flow calculations.

Szekely *et al*[32] predicted mixing time and turbulent diffusivity in a pilot scale container and then industrial size argon stirred ladles. In their report, mixing time and diffusivities by theoretical calculation via Eq. (2.2) were found to be in good consistence with industrial scale experiments, but not well agreed with results in pilot scale experiments.

Haida *et al*[30] did water model experiments to measure mixing time in argon stirred ladle with and without top slag layer. The results suggested that the exponent on ε without a top slag layer was approximately -0.31, while with a simulated slag layer was approximately -0.42. Though difference between these results and Nakanishi's is slight, Haida noted the relationship Eq. (2.3) may not agree with mixing time measured in water model. Haida suggested the difference may be caused by 3 reasons: (1) the definition of ε (2) the definition of complete mixing (3) geometry of the vessel. Haida also found that mixing time measured in industrial torpedo cars using copper tracer tended to be higher than results calculated by Eq. (2.3).

Asai *et al*[33] attempted to classify mixing into bulk convection and eddy diffusion. They proposed Eq. (2.5) for convection controlled mixing

$$\tau \propto \frac{L_c}{U} \tag{2.5}$$

and Eq. (2.6) for turbulent diffusion controlled mixing

$$\tau \propto \frac{L_c^2}{D_E} \tag{2.6}$$

These authors carried out experiments in different size vessels, and an empirical correlation was proposed

$$\tau = 274.3\varepsilon^{-0.33}R^{1.36}L^{-1} \tag{2.7}$$

Eq. (2.7) is the first time considered possible influence of vessel geometry and gas injection configuration on mixing time. For later researchers, geometry and injection configuration become experimental conditions that must be taken into consideration. In terms of these two mechanisms in mixing, these authors found that mixing in gas stirred ladles at a high gas flowrate regime appears to be largely caused by eddy diffusion rather than by bulk recirculation of the melt.

Sinha and McNallan[34] found different exponents on ε at the same physical condition compared to previous researchers. They further noticed that the position where the tracer is charged, and where mixing time is being monitored could significantly affect time required to attain complete mixing. Besides, turbulent diffusivities are used to explain faster rate of homogenisation near bath surface.

Sahai and Guthrie did a series of research to investigate features of turbulence in ladles in 1980s. They studied hydrodynamics in steel refinery ladle. An effective viscosity model for asymmetrically gas stirred ladles was proposed in 1982[35]. This model describes re-circulatory flows and related hydrodynamic phenomena taking place during the central injection of gas into the cylindrical steel refinery ladle. The same year, a hydrodynamic model with general applicability was proposed for prediction of plume hydrodynamics and liquid stirring in gas stirred ladles [36]. This model is based on the phenomenon that an incoming gas envelope breaks into an array of large spherical cap bubbles which rise through the melt in a dispersed manner transferring energy to re-circulating bulk of liquid. This analysis is considered appropriate for vessels with aspect ratios similar to those considered in their research. Later, they improved their investigation into two phase flowing system and built up similar turbulent flow model with central gas injection in cylindrical vessels [37]. In addition, they also tested the effectiveness of model in prediction flow fields in laboratory, pilot and industrial scale systems.

Mazumdar and Guthrie [38] studied hydrodynamic modelling of gas injection in ladle metallurgy operations in 1985. Predictions for flow fields generated in a 150 t steelmaking ladle with or without tapered side walls, and with or without surface baffles around the rising plume were considered. They also employed a 3/10 scaled water model of a 150 t steelmaking ladle to test adequacy of a generalised two dimensional computational scheme which predicts flow motion created by fully submerged and partially submerged gas injection lances. The turbulence models and grid configurations were evaluated. On the basis of studies conducted with a reduced scale water model, it was demonstrated quantitative agreement could be achieved between predicted and observed flow fields. This justifies the adequate nature of their theoretical approach which is based on numerical solution of differential equations describing such phenomena.

In 1986, Maumdar and Guthrie [39] studied mixing models for gas stirred metallurgical reactors. They firstly summarised previous researchers' work on mixing time and stirring energy, and then promoted their own mixing time equation by hydrodynamic deduction.

$$\varepsilon = \frac{\rho_L g \beta Q L}{\rho_L \pi R^2 L} = \frac{4gQ}{\pi D^2} \tag{2.8}$$

$$\tau_m = 37\varepsilon^{-\frac{1}{3}} R^{\frac{5}{3}} L^{-1} \tag{2.9}$$

where, ε --- specific input energy rate, watt/kg

ρ_L --- liquid density, kg/m^3

g --- Gravity constant, 9.8m/s^2

b--- fractional depth of lance submergence

Q --- gas flowrate, m^3/s

L --- liquid depth, m

R --- vessel radius, m

D --- vessel diameter, m

τ_m --- mixing time, second

They finally conducted experiments in two different cylindrical tanks, in which water was agitated by air injected through a central vertical lance. A conductivity cell made from a pair of stainless steel electrodes was employed to record changes in the local concentration of a pulse tracer addition of 1 N hydrochloric acid. This addition was made to the bath at a point just over the eye of the surface bubble plume. Change in local ion concentration around the monitoring cell was measured through changes in the water's electrical conductivity, and recorded via strip chart recorder. The recording of the tracer response was carried out until the concentration was considered to have reached the homogeneously mixed value. The analogue response curves obtained in this were then used to deduce "mixing time". It was defined as the time require for the concentration variation at the monitoring point to fall below 5 per cent of the well mixed or homogeneous value. At least five measurements were made for each operating condition, and average mixing time was thereby determined. Variations between these measurements and their associated average were within ±10%. The results showed that it was quantitatively demonstrated that addition dispersion in a typical gas stirred operation could be characterised solely neither by bulk convection nor by turbulent diffusion

phenomena. An empirical correlation for estimating mixing times during central injection into cylindrical vessels ($0.5 \leq L/D \leq 2.0$) was given.

In 1988, Mazumdar *et al*[40] did further study on mixing effect of gas stirring steelmaking ladles. They investigated the relationship between mixing time and stirring energy with presence of a top slag layer. By hydrodynamic analysis and high speed camera observation in oil-water dual phase modelling system, final conclusion was drawn that overlying oil phase dissipates a part of the input stirring energy, which in turn, causes the velocity of liquid recirculation and the level of turbulence in the bath to decrease significantly. In this research, three modes of energy dissipation were discussed: slag droplet creation, slag droplet suspension, and slag /metal interface distortion. It was shown experimentally that the third mode, i.e. deformation of the overlying oil phase into the lower aqueous phase around the perimeter of the surfacing plume, was primarily responsible for the energy deficit in the recirculating liquid [41]. On this basis, several physical models and mathematical models were developed for detailed hydrodynamics in steelmaking ladles [42-44].

Iguchi and his co-workers did much work to study bottom blown steelmaking ladles and converters. In his reports, swirling motion in metallurgical cylindrical vessel was observed, including its condition of occurrence, velocity and turbulence distribution, effect on mixing, application in metallurgy, optimisation and so on[45-46]. For convenience of research, physical models such as Figure 2-12 were built up. Aqueous KCl solution with a concentration of 1 kmol/m^3 was used as tracer. The volumetric concentration of the tracer in bath was adjusted to be 0.1%. The cylindrical vessel was made of transparent acrylic resin. The electrical conductivity of liquid in the bath was measured using a sensor shown in Figure 2-13. The mixing time measurement was carried out by the electrical conductivity meter and a pen recorder. The time gap between each measuring is 0.25 s and measurements were repeated ten times at each measuring position. Likewise, the mixing time was defined as a period for an instantaneous tracer concentration to settle within ±5% deviation around the final constant tracer concentration in the bath [47-48].

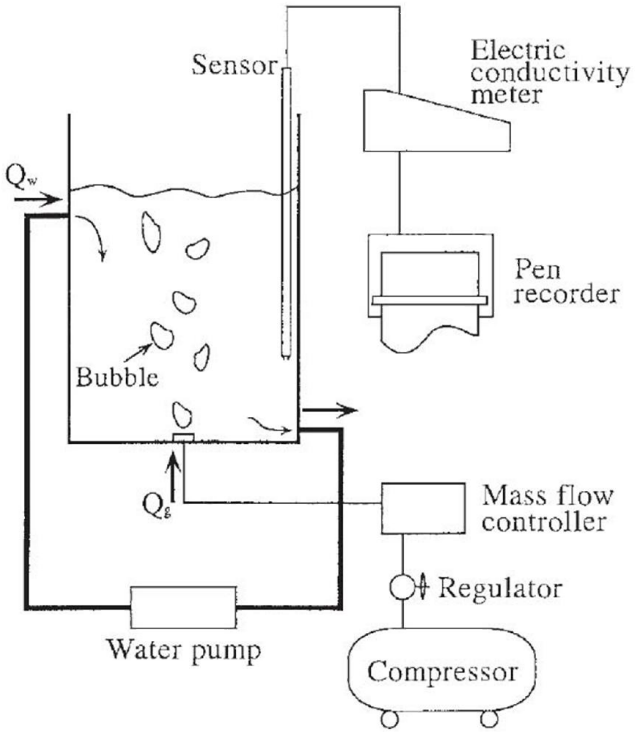

Figure 2-12 Experimental apparatus in Iguchi's research [45-48]

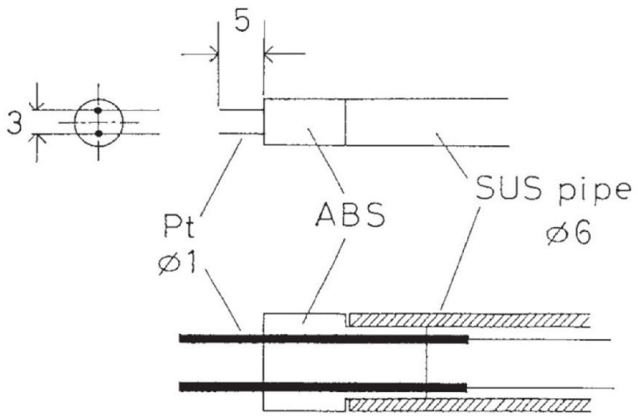

Figure 2-13 Conductivity electrode in Iguchi's research [45-48]

In order to study fluid flow phenomena in liquids of varying kinematic viscosities, Iguchi built up another physical model[49-51]. Transparent oily liquids such as silicone oil were usually used to simulate slag. However, it is difficult to measure the mixing time in oily liquid baths by making use of the conventional electrical conductivity sensor, because aqueous KCl solution is insoluble in oily liquid baths. Accordingly, Iguchi developed a new method for determining the mixing time in an oily liquid bath. Fine $CaCO_3$ powder was used as a tracer. This method was based on the measurement of a temporal change in the transmittance of a laser beam crossing through a

transparent vessel containing oily liquid. The output voltage of the sensor, which was uniquely related to the change in the transmittance, approached a constant value as mixing proceeded, and accordingly, the mixing time could be determined in the same manner as for the conventional electrical conductivity method. This model is convenient for different kinematic viscosities change in this experiment [52-53].

2.4.2 Mixing time and stirring energy investigation in multiphase bath

In most metallurgical containers, there is always a slag layer with substantial thickness existing on liquid metal. The slag layer is a solution of several metal oxides, which is usually lighter and immiscible to metal phase, so it is floating on the surface of molten metal. The slag layer thickness is usually thin in steelmaking ladles, around 1/10 of the molten metal layer. Whereas in the bottom blown copper smelting furnace, the height of slag layer can reach about 1/3 of the matte layer, which necessarily impacts the flow of the matte phase. Therefore, it is significant to study the mixing behaviour with the top immiscible phase.

In literature, most researchers carried out their mixing time investigation experiment in slag-free cold models. Many studies correlated measured mixing time against experimental variables such as bath level, container dimension, flowrate, and nozzle configuration, and proposed empirical or semi-empirical equations to predict mixing. However, only a few studies took the overlying slag layer into consideration [54-63].

Kim and Fruehan[57] carried out experimental study in a 1/7.2 scaled model of a 200 ton steelmaking ladle. A secondary phase - oil was applied onto the water bath surface and mixing time in the presence of oil layer was monitored. It was reported that the presence of second phase, *i. e.* oil, increases the mixing time significantly, indicating its resistance to the recirculatory velocity of fluid near the surface. It was also found in the experiment that there were three regimes of oil layer behaviour depending on the gas flowrate. Regime I is that the oil layer is very calm, no oil droplets are driven into the water and the interface between oil and water phases is close to planar surface except for the very weak wave motion of the interface near the edge of plume eye. Regime II of oil layer behaviour is that the oil layer near the edge of plume eye continuously forms oil ligaments and

then breaks up into droplets which are entrained into the water. Regime III is that the entire oil layer breaks down into oil droplets without forming oil ligaments near the edge of plume eye right after injection and the oil droplets penetrate deep into the water bath. This study described the basic behaviour of upper immiscible layer in mass transfer.

Han[63] conducted both experiments and numerical simulation to investigate the characteristics of the flow in a model of gas stirred ladle with an oil layer. It was found that the plume eye size increased with increasing gas flowrate and decreased with increasing oil layer thickness. Moreover, from the results of numerical simulation, the flow pattern of oil free bath showed that bubbles rising eventually made a recirculation loop at the central area of the bath, which forms uniformly distributed velocity field in the bath. This type of flow pattern was regarded as a good flow pattern for the mixing. On the contrary, the flow pattern in the presence of oil layer was found to form distorted and localised recirculating loop near the side wall below the oil layer, which eventually extended the mixing time in bath.

Yonezawa and Schwerdtfeger[64-67] conducted several studies using a mercury bath with a silicone oil layer and large scale water models to investigate features of the spout height in the presence of slag layer. These authors also carried out industrial experiments on a 350 t steel ladle to validate results. It was reported that in these studies the spout height were fluctuating strongly, and long-term average values were collected and used to correlate empirical relationships with operational parameters. The empirical relationship can be used to predict the maximum spout height in industrial steelmaking ladles. Yonezawa *et al*. [67-68] also studied the area of the plume eye in the slag layer and reported correlated the dimensionless area of the plume eye in terms of the gas flowrate and bath height. Model-independent empirical equations were also proposed to show the area of the spout eye with the parameters such as the metal phase level, the slag phase level and the gas flowrate.

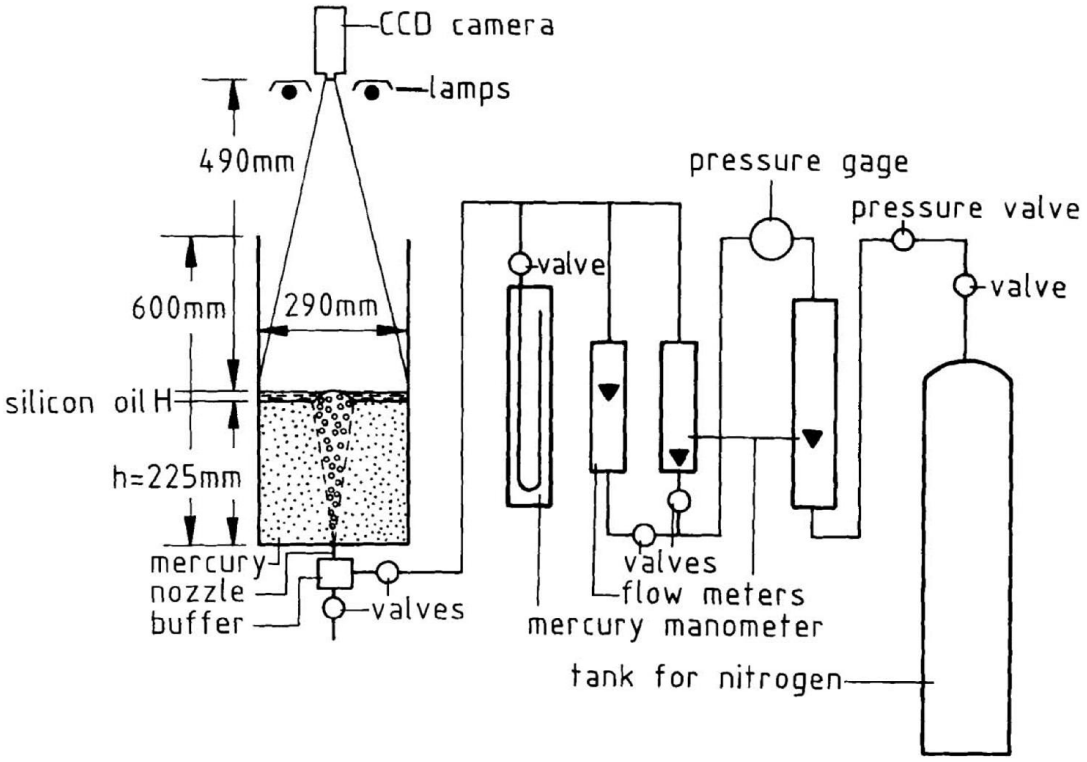

Figure 2-14 Yonezawa's experimental setup using mercury bath and silicone oil top layer[64]

Krishnapisharody and Irons[62] focused on the size of the plume eye in the slag layer, and obtained the same tendency of plume eye size with gas flowrate and oil layer thickness. These authors further found that the eye size increased with increasing lower phase depth, and less dense upper phase resulted into smaller eye size. A mechanistic model regarding dimensionless eye size was expressed in terms of density ratio and Froude number based plume velocity to predict the eye size change. This model is based on the force analysis of spout region and employs the plume velocity to express the Froude number, so it shows better prediction of the plume eye area.

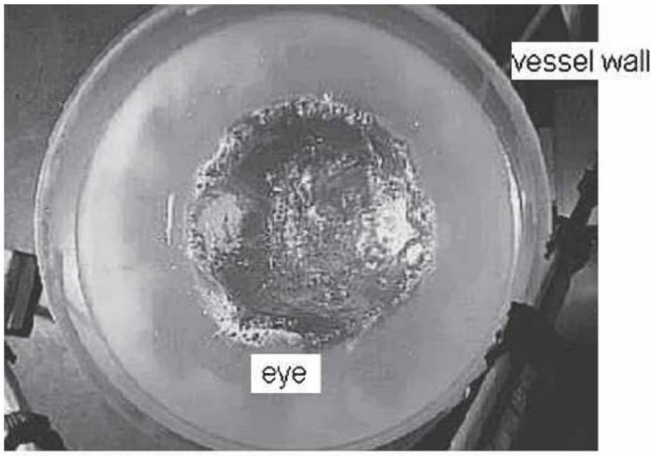

Figure 2-15 Plume eye formation in Krishnapisharody's cold model[62]

Mazumdar *et al*.[59,61] also studied the behaviour of the upper slag layer in steelmaking ladles using an oil-water system, and noticed the interaction mechanism between oil phase and water phase on the interface. These authors focused on the formation of plume eye in the oil layer and its consumption of input stirring energy, and pointed out the significant relationship between the plume eye area and input energy.

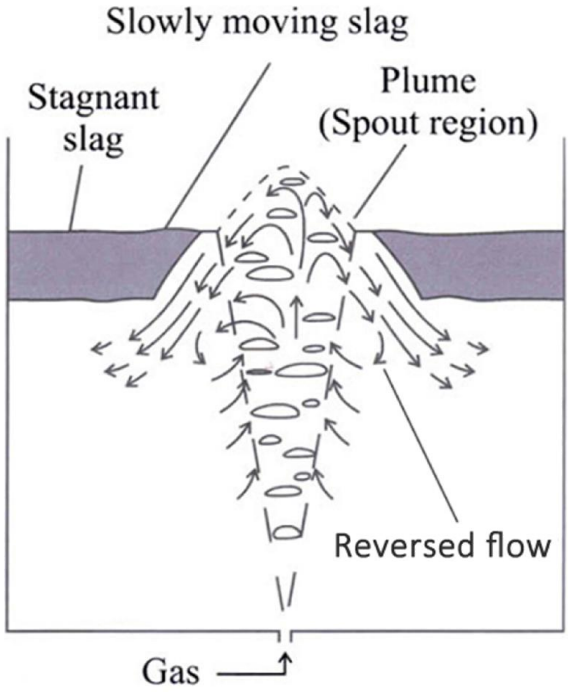

Figure 2-16 Reversed flow formation at the plume zone[60]

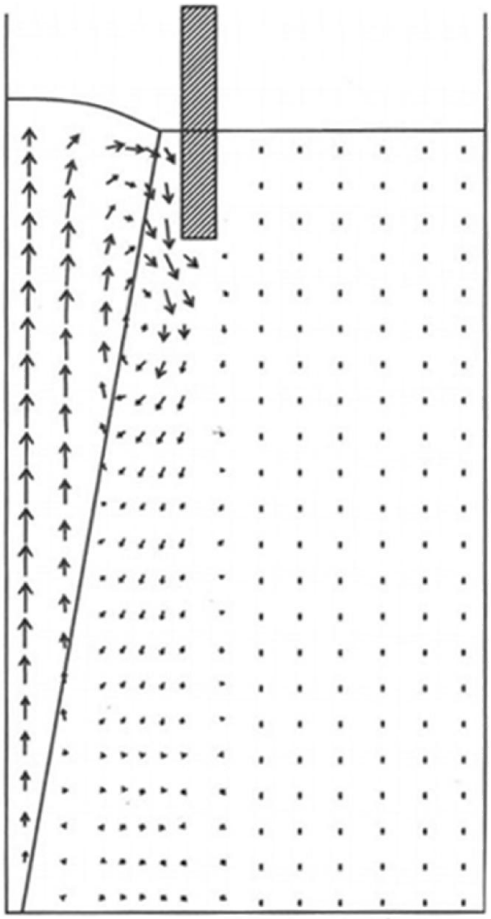

Figure 2-17 Analogue of formation of reversed flow using a baffle at the plume zone[60]

Mazumdar and Guthrie[60] then studied the energy dissipation phenomena in slag covered steel bath by using physical and mathematical model. These authors divided the stirring energy consumption into five parts: turbulence, bubble, wall friction, plume eye formation and slag metal interface. In this approach, the mixing in lower phase is linked with the spout height formation and features of the slag layer. It was found that a reversal of flow of metal phase is formed at the plume zone due to the presence of the thick oil layer. Upper oil layer is actually providing a barrier and tends to constrict the surface plume near the spout. Adjacent to the spout, the oil layer prevents the radial surface flows as shown in Figure 2-16, and it redirects the bulk liquid from the spout region at a downward angle which thus creates the fast recirculating reversed flow. This reversal of flow was believed to be the primary reason for the input energy consumption. The authors also proposed a mechanism to explain the formation of the reversed flow. As shown in Figure 2-17, a baffle is set at the spout region of a gas stirred slag free ladle. The baffle performs like the upper slag layer and provides a barrier to prevent the bulk radial surface flow. The flow then is redirected downward and

forms the fast recirculating reversed flow with rising plume. The mechanism of stirring energy consumption in the presence of upper layer was found the same in the presence of the baffle. It was also found under that low gas flowrate and a thin slag layer condition, bubble slippage and wall friction dissipate nearly 70 pct to 80 pct of the input energy. Energy dissipation at the free surface, most by forming a plume eye, is accounting for 6 pct to 9 pct of input. Slag layer dissipate about 10 pct of input energy. It was demonstrated that the thickness of the upper phase rather than the physical property of the upper phase is more important to the mixing phenomena in the lower phase.

Amaro-Villeda[69] applied Mazumdar's model to study the mixing time in a model of steel ladles with different bottom nozzle configurations. Under the system of multiple injection ladles, the mixing phenomena was getting complicated. It was found the mixing time was increasing with increasing slag thickness due to higher energy dissipation in the thicker slag layer. Mixing time was also increasing with decreasing gas flowrate or increasing number of blowing nozzles. The authors developed a practical approach to measure the average recirculation velocity in the ladle, which could be used to estimate the stirring energy consumed by the top slag layer. The exposed surface of lower phase was found decreased by increasing slag viscosity and increased by increasing flowrate. The exposed surface is also largely influenced by the configuration of nozzles.

The above studies provided basic methodology to study the mixing behaviour of slag covered metallurgical baths. However, most of these studies focused on the formation of the plume eye in the slag layer and its effect on bath recirculation but did not give explicit mixing time correlations with operational variables. Limited reports were found to address this topic.

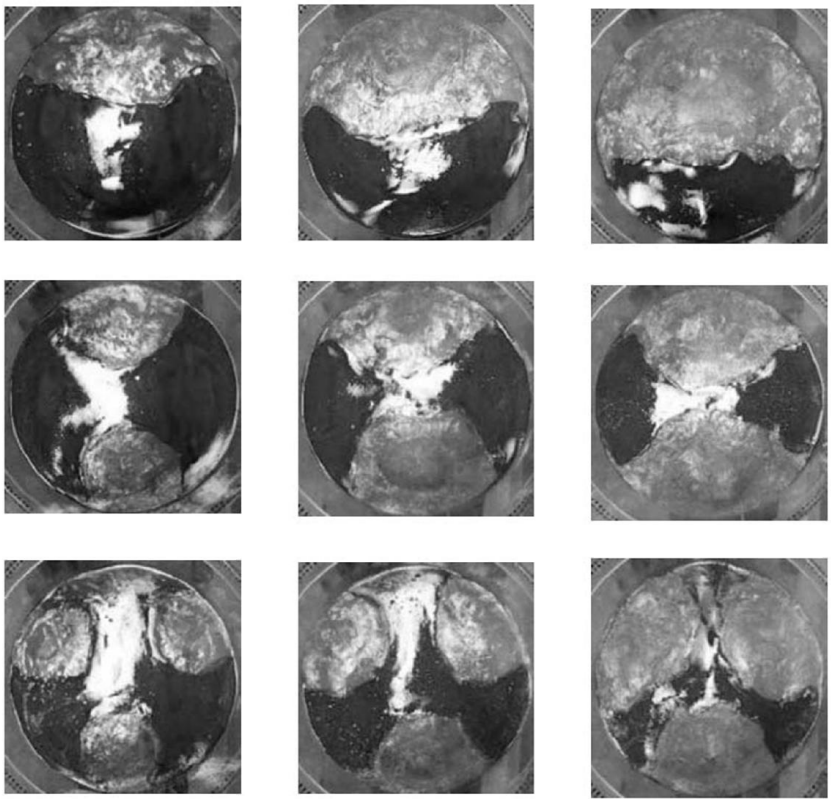

Figure 2-18 The shapes of plume eye in Amaro-Villeda's experiment[69]

Patil[70] investigated experimental mixing phenomena in water models of slag covered, gas stirred ladles, and then developed explicit empirical correlations for estimating mixing times. Besides, under their experimental conditions, the gas flowrate was relatively low to keep the slag layer almost intact, and slag layer was only 1-13% of the bulk depth, which enabled the authors to develop mixing time correlations on the basis of slag free models. The explicit empirical mixing time correlation with a top layer was given:

$$\tau_{95\%,Axisym,slag} = 120\left(\frac{\Delta L}{L}\right)^{0.3} Q^{-0.33} L^{-1.0} R^{2.33} \qquad (2.10)$$

where ΔL --- thickness of the upper phase, m

L --- depth of lower phase in the ladle, m

Q --- gas flowrate, m^3/s

R --- ladle radius, m

The relationship between slag covered and slag free system under such experimental condition was expressed:

$$\tau_{95\%,slag} = \tau_{95\%,no\ slag}\left[6\left(\frac{\Delta L}{L}\right)^{0.3} {\nu_s}^{0.033}\left(\frac{\Delta\rho}{\rho_L}\right)^{-0.044}\right] \qquad (2.11)$$

where ν_s --- kinematic viscosity of the upper phase, m^2/s

$\Delta\rho$ --- density differential between upper phase and bulk liquid, kg/m^3

ρ --- density of the bulk liquid, kg/m^3

Patil's explicit mixing time relationship with operational variables predicts mixing time under required dynamic condition very well, but the low flowrate and thin slag layer is only applicable to limited metallurgical containers. Furthermore, in most cases of literature that studies the effect of upper layer, the height of the overlying slag layer is limited to about 10% of the bulk height and the gas flowrate is constrained to a relatively low value to avoid large amount of entrainment between two phases, as the ladle metallurgy requires.

Khajavi and Barati[71] reported a study that investigated mixing time in thick slag covered metallurgical baths. The authors carried experimental studies in kerosene-water and silicone oil-water systems and used the effective bath height that combined both lower and upper layer height to correlate the relationship with mixing time. The experimental setup is shown in Figure 2-19. In their study, the oil height was varied from 3.3 to 16.4 cm while the water height was kept constant at 19.8 cm, which made the upper phase height 82% of the lower phase. Such thick slag layer condition was quite different from previous researchers. The mixing time can be predicted in terms of effective specific energy rate for blending $\dot{\varepsilon}_{blending}$ and the effective bath height h_{eff}:

$$\tau_m = 2.33 \dot{\varepsilon}_{blending}^{-0.34} h_{eff}^{-1.0} \tag{2.12}$$

where

$$\begin{cases} \dot{\varepsilon}_{blending} = 1.14 \exp(-3.16 \dfrac{h_s}{h_m}) \dot{\varepsilon}_m & \dfrac{h_s}{h_m} > 0.1 \\ \dot{\varepsilon}_{blending} = \dot{\varepsilon}_m & \dfrac{h_s}{h_m} \leq 0.1 \end{cases}$$

$\dot{\varepsilon}_m$ is the specific energy input rate, calculated by

$$\dot{\varepsilon}_m = \frac{Qg}{A} \tag{2.13}$$

h_{eff} is the effective bath height, calculated by

$$h_{eff} = h_m + \frac{\rho_s}{\rho_m} h_s \tag{2.14}$$

where, Q is the gas flowrate, g is the acceleration of gravity, and A is the cross section area of the container. h_s is the height of upper layer, h_m is the height of lower layer, ρ_s is the density of

upper layer and ρ_m is the density of lower layer. This study was addressing the mixing behaviour under the condition of a thick upper layer and great gas flowrate, where the mechanism was different from the steelmaking ladles. However, their results provide useful information for processes such as COREX and CRISP steelmaking technologies, and further studies under similar conditions can be expected in the future.

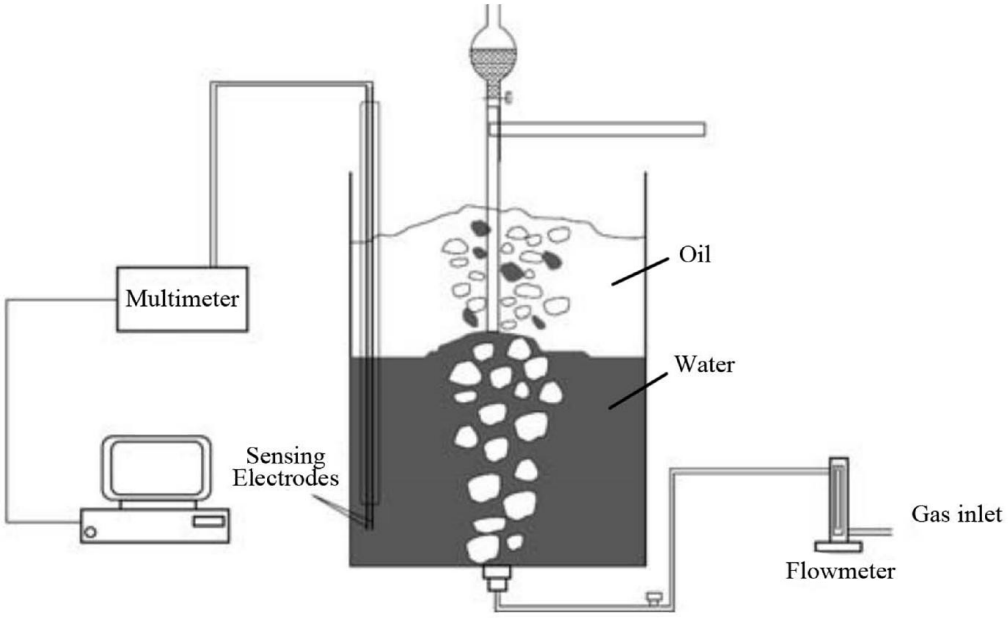

Figure 2-19 Khajavi's experimental setup with thick upper phase layer[71]

2.5 Surface wave studies in metallurgical bath

Gas injection into metallurgical baths usually leads to deformation of the bath surface. In some special cases, the deformation of the bath surface is able to develop into different types of surface waves. The surface waves on metallurgical bath are often linked to spitting, splashing and refractory abrasion in industrial practice. Therefore, many researchers have studied this phenomenon in literature.

2.5.1 Surface wave studies in vertical cylindrical container

One of the earliest reports of this phenomenon was given by Thomas[72], who studied the relationship between the bath sloshing motion and its influence on the ejection of molten metal in steelmaking converters. The author also noticed abrasion of the refractory material in presence of this phenomenon. Later researchers [73-75] found in water model that the sloshing of bath was created

by rotating of gas plume which only occurs when the gas flowrate is above a critical value. It was also found that this rotation wave is determined by gas flowrate, bath depth and nozzle configuration.

Schwarz [76-77] proposed a mechanism of the bath sloshing motion. According to this mechanism, the sloshing motion is occurring when the buoyancy force on bubbles which are displaced from the centre line as a result of the oscillation is sufficient to sustain the oscillation. A mathematical model of this mechanism was also developed to predict period and amplitude of the sloshing motion.

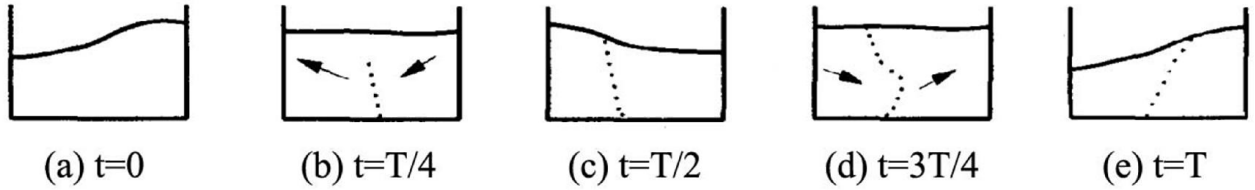

Figure 2-20 Schwarz's bath sloshing model in vertical cylindrical container[76-77]

Xie and Oeters[78-79] studied wave motion quantitatively in a water/air ladle model and Wood's metal /nitrogen ladle. These authors proposed a similar mechanism of the formation of wave as Schwarz. Furthermore, they also investigated the critical occurrence condition of this wave, and plotted the critical occurrence condition into bath height-gas flowrate figures, as shown in Figure 2-22. This occurrence condition map clearly shows the combination of bath height and gas flowrate that enables the wave to take place, which links this phenomenon with industrial operational parameters and makes the control of bath behaviour available. The authors further used the simple pendulum model to investigate features of the surface wave, by which the period and amplitude of the bath oscillation can be predicted.

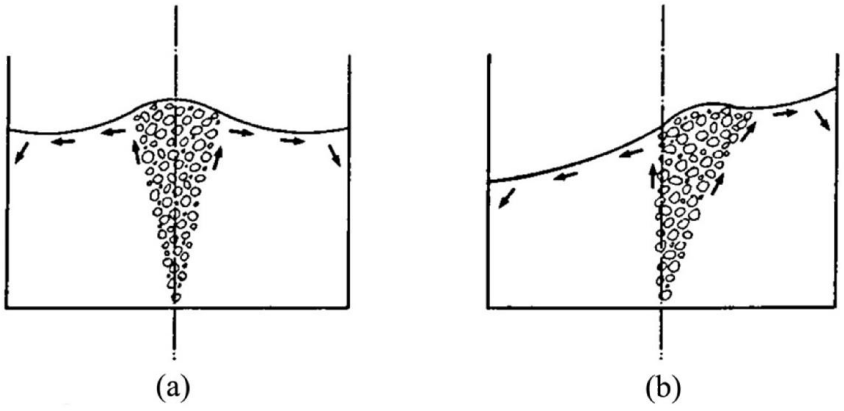

Figure 2-21 Xie and Oeters' bath sloshing model in vertical cylindrical container[78-79]

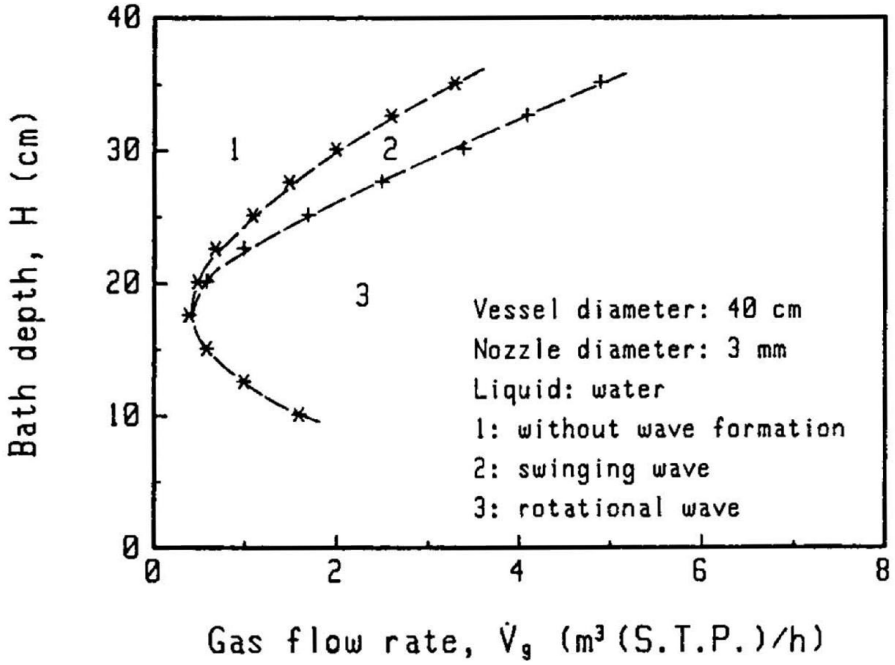

Figure 2-22 Typical bath sloshing critical occurrence boundary map plotted by Xie and Oeters[78-79]

Iguchi [80-81] classified the sloshing motion of bath in upright cylindrical containers into two kinds by the ratio of bath depth over diameter. The first kind of bath wave is when the bath depth H_L is smaller than the bath diameter D. The radial displacement of the blubbing jet is relatively small and the period of the bubbling jet is almost equal to the period of the rotary sloshing. This kind of wave motion is further divided into two categories as a function of bath depth: the shallow water type and the deep water type. The boundary dividing the two is $H_L/D = 0.3$. The Second kind of bath wave is that when the bath depth is larger than twice of the bath diameter, the radial displacement of bubbling jets becomes large and the bubbling jet approaches the side wall of the vessel. The swirl period becomes much longer than that of the first kind. In metallurgical baths, the first kind of bath wave is more common. These authors then proposed four sub-boundaries in terms of dimensionless bath height H_L/D and Weber number to describe the occurrence conditions of the first kind of bath wave on the basis of Xie and Oeters. These four sub-boundaries can be drawn in a H_L/D to We map as shown in Figure 2-24, which is similar to Xie and Oeters' maps.

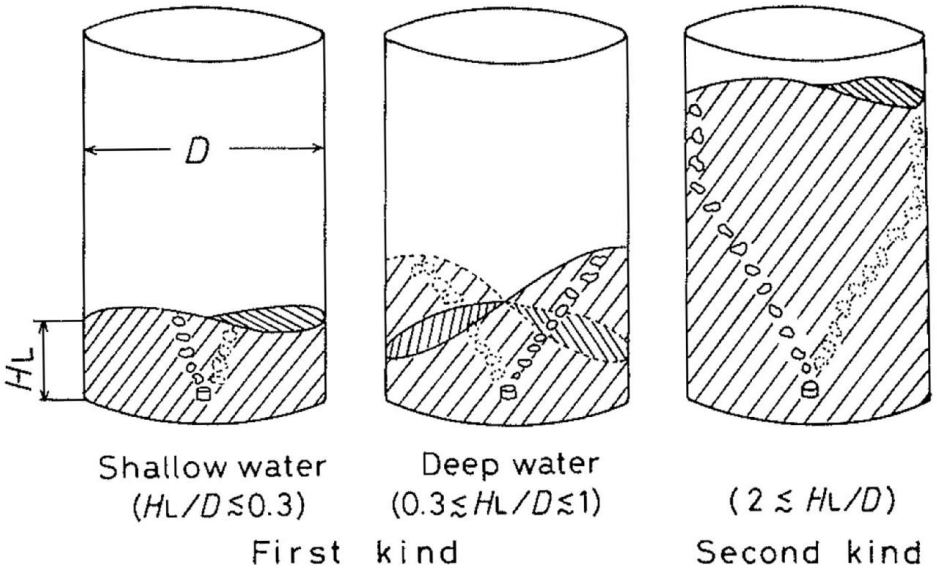

Figure 2-23 Iguchi's classification of bath motions in vertical cylindrical container[80]

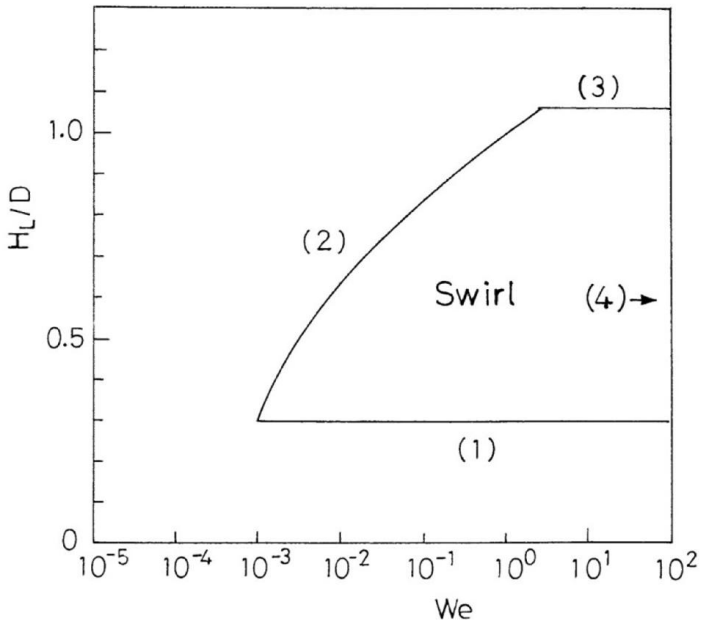

Figure 2-24 Schematic occurrence boundary lines of bath swirling proposed by Iguchi[81]

2.5.2 Surface wave studies in Peirce-Smith converter

Similar bath sloshing was also reported in horizontal cylindrical containers like copper Peirce-Smith converter. In such vessels, the geometry of bath is different from steelmaking ladles and the gas injection is not absolutely from bottom but with some offset angles, instead. Different geometries of container and offset of blowing angle made the bath motion appear differently from that in upright cylindrical containers. Kootz and Gille [82] found in their model of a Pierce-Smith converter that

there were 3 general types of surface motions. They were termed (1) the 1st asymmetric standing wave, (2) the 1st symmetric standing wave and (3) the 2nd asymmetric standing wave, as shown in Figure 2-25.

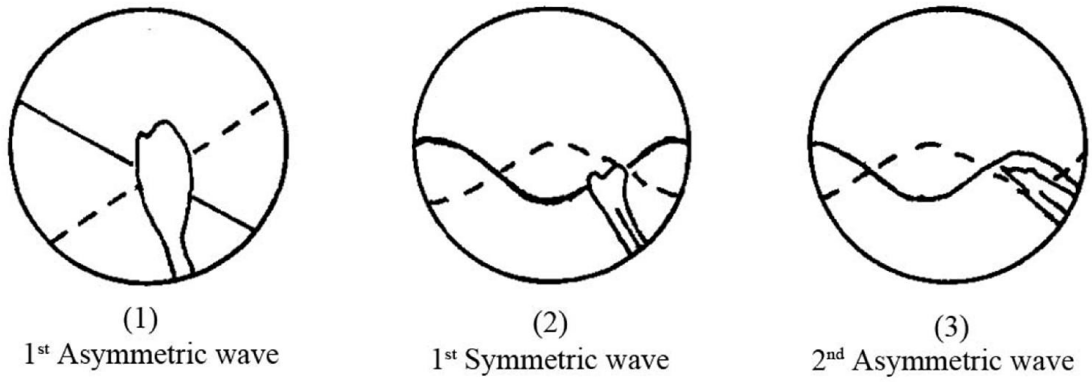

Figure 2-25 Definitions of the wave types in the PS converter model of Kootz and Gille[82]

Richards[83] studied slopping and splashing of copper Peirce-Smith converter in a 1/4th scaled sectional model with geometry Ø762 ×265 mm. It was found that a "standing wave" appears abruptly at a critical buoyancy power per unit mass. This standing wave was related to splashing and hence the limitation on converter capacity. The buoyant power level to form the standing wave was found a function of the tuyere diameter and was only slightly dependent on tuyere submergence. An empirical correlation was given using buoyant energy and gas flow per unit surface area.

Liow and Gray [84-86] continued this study in water models. The authors developed a fluid mechanical model of standing wave in a circular canal container on the basis of standing wave model in a rectangular container. The model was then used to predict the different types of standing waves that are able to take place in circular canal containers. Rosales[87] used the two dimensional Laplace equation to describe the formation of standing wave in circular canal container and proposed an approximate analytical solution to predict the types of standing waves that are able to occur in such container. The results of the two studies are similar. As shown in Figure 2-26, according to their prediction, the standing waves with certain vibration frequencies can be present in such circular canal container, each frequency is corresponding to a shape of standing wave. Liow and Gray then found that the occurrence of each standing wave is determined by the bath depth and the tuyere submergence .

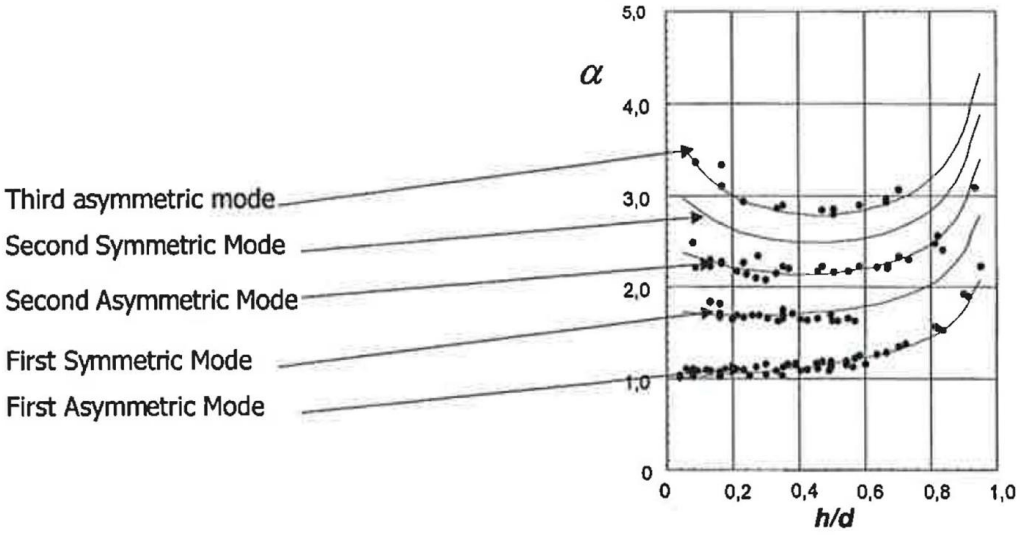

Figure 2-26 Rosales' prediction of standing wave types in PS converter (α represents dimensionless frequency of the wave)[87]

Researches related to bath sloshing have been done in upright cylindrical containers and Peirce-Smith converters, but little information was found in large horizontal channelled reactors such as the bottom blown copper smelting furnace. The geometry of this new furnace is far different from previous studies, so investigation to the bath surface wave needs to be carried out.

2.6 Summary

In general, bottom blown technology is widely applied in steelmaking and refining, and even in glassmaking industry, so technologies in these fields is relatively more mature than nonferrous industry. Regarding bottom blown steelmaking converters or steel refining ladles, researchers did much work to study its dynamic and kinetic process during smelting. Such concepts as mixing time, standing waves and empirical relationship are presented to investigate and optimise smelting. However, those researches are based on converters or ladles, which is approximately an upright cylindrical vessel or PS-converter shaped. Therefore, those empirical relationships or mixing rules are all based on this prerequisite. When it comes to Fangyuan's bottom blown copper smelting furnace, the results gained in those vessels need to be verified before applying into industry. Therefore, those empirical equations gained by experiments in those vessels should be reconsidered in this study.. Whereas methodologies presented by previous researchers are still helpful in the study of the Fangyuan bottom blown furnace, such as the mixing time measurement method, using of KCl solution as tracer, the categorising of surficial waves and so on.

As a result, due to the difference in furnace shape, gas flowrate etc., the flow field may follow a different rule in the Fangyuan bottom blown copper smelting furnace. To investigate these changes, a series of new experiments should be carried out in a more accurate model.

2.7 References

[1] Mark E. Schlesinger: *Extractive Metallurgy of Copper*, 5th ed, Elsevier, Saint Louis, MO, USA, 2011.

[2] Z. Zhu and J. He: *Xian Dai Tong Ye Jin Xue [Modern Copper Metallurgy]*, China Science Publishing, Beijing, China, 2001.

[3] Z. Cui, D. Shen, and Z. Wang: *You Se Jin Shu [Nonferrous Metals]*, 2010, No. 3, pp. 17-20.

[4] B. Zhao, Z. Cui, and Z. Wang: *Int. Symp. High-Temp. Metall. Process., 4th,* 2013, pp. 1-10.

[5] J. Yan: *Proc. Copper 2013—Cobre 2013 Int. Conf.*, 2013, pp.873-887.

[6] B. Li, J. Jiang, and K. Wei et al: *Proc. Copper 2013—Cobre 2013 Int. Conf.*, 2013, pp.889-896.

[7] L. Feng: *Proc. Copper 2013—Cobre 2013 Int. Conf.*, 2013, pp.897-909.

[8] Z. Cui, Z. Wang and B. Zhao: *Proc. Copper 2013—Cobre 2013 Int. Conf.*, 2013, pp.923-933.

[9 Z. Cui, Z. Wang and R. Li: *Proc. Copper 2013—Cobre 2013 Int. Conf.*, 2013, pp.935-943.

[10] Z. Cui, Z. Wang and R. Li: *Proc. Copper 2013—Cobre 2013 Int. Conf.*, 2013, pp.935-943.

[11] X. Hao, Z. Lu, and K. Wei et al: *Proc. Copper 2013—Cobre 2013 Int. Conf.*, 2013, pp.1035-1045.

[12] Z. Yu: *Lian Gang [Steelmaking]*, 2001, vol. 17, No.1, pp. 13-18.

[13] Z. Yu: *Lian Gang [Steelmaking]*, 2001, vol. 17, No.3, pp. 15-23.

[14] V. Singh, S. N. Lenka and S. K. Ajmani: *ISIJ Int.*, 2009, vol. 49, No. 12, pp. 1889-1894.

[15] V. Singh, J. Kumar and C. Bhanu: *ISIJ Int*, 2007, vol. 47, No. 11, pp. 1605-1612.

[16] P. C. Hayes, M. E. Schlesinger and H-U steil: *Lead-Zinc 2010 (The Minerals, metals & Materials Society, 2010)*, pp. 345-413.

[17] S. Yang, A. Jiang and Z. Shi: *Energy for Metallurgical Industry*, 2009, vol. 28, No. 6, pp. 50-53.

[18] S. Yang: *Master's thesis*, Central South University, China 2010.

[19] H. Wang, Z. Shi and H. Shen: *Journal of Central South University (Science and Technology)*, 2012, vol. 43, No. 7, pp. 2850-2854.

[20] H. Wang, Z. Shi and T. Chen: *You Se Jin Shu [Nonferrous Metals]*, 2011, No. 10, pp. 9-12.

[21] C. Li, J. Wang and Z. Wang: *Proceedings of copper 99-Cobre 99 international conference*, 1999, vol. VI, pp. 83-91.

[22]A. Jiang, S. Yang and C. Mei: *Journal of Central South University (Science and Technology)*, 2010, vol. 41, No. 3, pp. 1190-1195.

[23] N. Huda, J. Naser and G. A. Brooks: *Metall. Mater. Trans. B*, 2012, vol. 43 B, pp. 1054-1068.

[24] L. S. Pioro and I. L. Pioro: *Waste Management*, 2004, vol. 24, pp. 371-379.

[25] D. Rue, J. Wagner and G. Aronchik: *67th Conference on Glass Problems*, 2007, pp. 175-181.

[26] D. Rue: *Report by Gas Technology Institute*, 2008.

[27] D. Rue: *International Journal of Applied Glass Science*, 2011, vol. 2, No. 4, pp. 262-274.

[28] D. Mazumdar and J. W. Evans: *ISIJ Int.,* 2004, Vol. 44, No. 3, pp. 447-461.

[29] K. Nakanishi, T. Fujii and J. Szekely: *Ironmaking and Steelmaking*, 1975, No. 3, pp. 190-195.

[30] O. Haida, T. Emi, S. Yamada, and F. Sudo: *Proceedings, SCANINJECT II conference*, Lulea, Sweden, 1980, pp. 20:1-20:20.

[31] K. Nakanishi, K. Saito, T. Nozaki, Y. Kato, K. Suzuki, and T. Emi: *Proceedings, Steelmaking Conference*, 1982, pp. 101-08

[32] J. Szekely, T. Lehner, and C W. Chang: *Ironmaking and Steelmaking*, 1979, vol. 3, pp. 285-93

[33] S. Asai, T. Okamoto, J. He, and I. Muchi: *Trans. ISIJ*, 1983, vol. 23, pp.43-50

[34] U. P. Sinha and M. J. McNallan: *Metall. Mater. Trans. B*, 1985, vol. 16B, pp. 850-53

[35] Y. Sahai and R. I. L. Guthrie: *Metall. Mater. Trans. B*, 1982, vol. 13 B, pp. 125-127

[36] Y. Sahai and R. I. L. Guthrie: *Metall. Mater. Trans. B*, 1982, vol. 13 B, pp. 193-202

[37] Y. Sahai and R. I. L. Guthrie: *Metall. Mater. Trans. B*, 1982, vol. 13 B, pp. 203-211

[38] D. Mazumdar and R. I. L. Guthrie: *Metall. Mater. Trans. B*, 1985, vol. 16 B, pp. 83-90

[39] D. Mazumdar and R. I. L. Guthrie: *Metall. Mater. Trans. B*, 1986, vol. 17 B, pp. 725-733

[40] D. Mazumdar, H. Nakajima and R. I. L. Guthrie: *Metall. Mater. Trans. B*, 1988, vol. 19 B, pp. 507-511

[41] D. Mazumdar*: Metall. Mater. Trans. B*, 1989, vol. 20 B, pp. 967-969

[42] D. Mazumdar: *Metall. Mater. Trans. B*, 1990, vol. 21 B, pp. 925-928

[43] D. Mazumdar: *ISIJ Int.*, 1995, vol. 35, No. 1, pp. 1-20

[44] D. Mazumdar: *Metall. Mater. Trans. B*, 2000, vol. 27, No. 4, pp. 302-309

[45] M. Iguchi, T. Uemura and H. Yamaguchi: *ISIJ Int.*, 1994, vol. 34, No. 12, pp. 973-979

[46] M. Iguchi, S. Hosohara and T. Kondoh: *ISIJ Int.*, 1994, vol. 34, No. 4, pp. 330-337

[47] M. Iguchi, D. Iguchi and J. Yoshida: *Mater. Trans*, 2004, vol. 45, No. 5, pp. 1764-1768

[48] M. Iguchi, Y. Sasaki and N. Kawabata: *Mater. Trans*, 2004, vol. 45, No. 7, pp. 2369-2376

[49] M. Iguchi, T. Kondoh and Z. Morita: *Metall. Mater. Trans. B*, 1995, vol. 26 B, pp. 241-247

[50] M. Iguchi, T. Nakatani and H. Ueda: *Metall. Mater. Trans. B*, 1997, vol. 28 B, pp. 87-94

[51] M. Iguchi, T. Kondoh and K. Nakajima: *Metall. Mater. Trans. B*, 1997, vol. 28 B, pp. 605-612

[52] M. Iguchi, K. Nakamura and R. Tsujino: *Metall. Mater. Trans. B*, 1998, vol. 29 B, pp. 569-575.

[53] M. Iguchi, R. Tsujino and K. Nakamura: *Metall. Mater. Trans. B*, 1999, vol. 30 B, pp. 631-637.

[54] A. M. Amaro-Villeda, M. A. Ramirez-Argaez and A. N. Conejo: *ISIJ Int.*, 2014, Vol. 54, No. 1, pp. 1-8.

[55] L. T. Khajavi and M. Barati: *Metall. Trans. B*, 1982, vol.13B, pp. 193-202.

[56] J. Mandal, S. Patil, M. Madan and D. Mazumdar: *Metall. Trans. B*, 2005, Vol.36B, 479-487.

[57] S. H. Kim and R. J. Fruehan: *Metall. Trans. B*, 1987, Vol. 18B, 381-390.

[58] S. P. Patil, D. Satish, M. Peranandhanathan and D. Mazumdar: *ISIJ Int*., 2010, Vol. 50, No. 8, pp. 1117-1124.

[59] D. Mazumdar, H. Nakajima, and R. I. L. Guthrie: *Metall. Trans. B,* 1988*,* Vol. 19B, pp. 507-511.

[60] D. Mazumdar and R. I. L. Guthrie: *Metall. Trans. B*, 2010, Vol. 41B, pp. 976-989.

[61] D. Mazumdar and J. W. Evans: *Metall. Trans. B*, 2004, Vol. 35B, pp. 400-404.

[62] K. Krishnapisharody and G. A. Irons: *Metall. Trans. B*, 2006, Vol. 37B, pp. 763-772.

[63] J. W. Han, S. H. Heo, D. H. Kam, B. D. You, J. J. Pak and H. S. Song: *ISIJ Int.*, 2001, Vol. 41, No. 10, pp. 1165-1173.

[64] K. Yonezawa and K. Schwerdtfeger: *Metall. Mater. Trans. B*, 1999,vol. 30B, pp. 655-60

[65] K. Yonezawa and K. Schwerdtfeger: *Metall. Mater. Trans. B*, 2000, vol. 31B, pp. 461-68.

[66] K. Yonezawa and K. Schwerdtfeger: *Metall. Mater. Trans. B*, 1999,vol. 30B, pp. 411-18.

[67] K. Yonezawa and K. Schwerdtfeger: *ISIJ Int.*, 2004,vol. 44, pp. 217-19.

[68] Subagyo, G.A. Brooks, and G.A. Irons: *ISIJ Int.*, 2003,vol. 43, pp. 262-65.

[69] A. M. Amaro-Villeda, M. A. Ramirez-Argaez and A. N. Conejo: *ISIJ Int.*, 2014, Vol. 54, No. 1, pp. 1-8.

[70] S. P. Patil, D. Satish, M. Peranandhanathan and D. Mazumdar: *ISIJ Int.*, 2010, Vol. 50, No. 8, pp. 1117-1124.

[71] L. T. Khajavi and M. Barati: *Metall. Mater. Trans*. *B*, 2010, 41B, pp. 86-93.

[72] K. Thomas: *Stahl u. Eisen*, 1930, vol. 50, pp. 1665/674 and 1708/718.

[73] P. Leroy and G. Cohen de Lara: *Rev. Metall.,* 1958, vol. 55, pp. 75-97 and 186-200.

[74] A. Etienne: *Metal. Rep.,* 1975, No. 43, pp. 13-21.

[75] Y. Kato, K. Nakanishi, T. Nozaki, K. Suzuki and T. Emi: *Trans. ISIJ*, 1985, vol. 25, pp.

459-466.

[76] M.P. Schwarz: *Proc*. *Australas. Fluid Mech. Conf.*, *10th*, University of Melbourne, Melbourne, VIC, Australia, 1989, pp. 3.29-3.32.

[77] M. P. Schwarz: *Appl. Math. Modelling*, 1996, vol. 20, pp. 41-51.

[78] Y. Xie and F. Oeters: *Steel Res.*, 1992, vol.63, No. 6, 227-233.

[79] Y. Xie and F. Oeters: *Steel Res.*, 1992, vol.63, No. 7, 277-280.

[80] M. Iguchi, S. Hosohara, T. Koga, R. Yamaguchi and Z. Morita: *ISIJ Int.*, 1993, vol. 33, No. 10, pp. 1037-1044.

[81] M. Iguchi, D. Iguchi, Y. Sasaki, T. Kumagai and S. Yokoya: *ISIJ Int.*, 2004, vol. 44, No. 10, pp. 1623-1628.

[82] T. Kootz and G. Gille: *Stahl Eisen,* 1948, vol. 48, pp. 287-294.

[83] G.G. Richards, K.J. Legeard, A.A. Bustos, J.K. Brimacombe and D. Jorgensen: *Reinhardt Schuhmann Int. Symp. Innovative Technol. React. Des. Extr. Metall., Proc. Symp.,* D.R. Gaskell, ed., Colorado Springs, CO, TMS-AIME, Warrendale, PA, 1986, pp. 385-403.

[84] J. L. Liow and N. B. Gray: *Proc*. *Australas. Fluid Mech. Conf.*, *10th,* University of Melbourne, Melbourne, VIC, Australia, 1989, pp.14.33-14.36.

[85] J. L. Liow and N. B. Gray: *Metall. Trans. B,* 1990, vol. 21B, pp. 657-664.

[86] J. L. Liow and N. B. Gray: *Metall. Trans. B,* 1990, vol. 21B, pp. 987-996.

[87] M. Rosales, P. Ruz and R. Fuentes: *Proc. Copper 2003-Cobre 2003 Hermann Schwarze Symp.*, C. Diaz, C. Landolt and T. Utigard, ed., Santiago, Chile, Vol. IV, pp. 485-498.

3 Scope of research

The scope of the present study consists by series of published papers and papers to be submitted for publication:

1. Design and fabricate the specific lab-scale physical model of the Fangyuan bottom blown copper smelting furnace by following the principles of similarity. By using this physical model, to find out appropriate methodology to investigate the features of the new furnace.
2. The first part of the present study is to investigate the mixing behaviour of the newly established furnace.
    1) To study the mixing behaviour of single phase bath using single lance blowing(published). Mixing of reagents is one of the key factors that affect the productivity of the furnace. Due to the complication of physical and chemical condition in the mixing process, the first step to study this phenomenon is to understand the mixing in a single phase using a single lance.
    2) To investigate the mixing behaviour of multiphase bath on the base of single phase, still using single lance blowing(to be submitted for publication). The multiphase bath condition is closer to the industrial practice, which provides more information. The mixing behaviour with multi-lance blowing is not carried out in the present study as it is more complicated for this stage.
3. The second part of the present study is to investigate the surface wave generated by bottom blowing on the bath surface.
    1) To investigate the different types of standing waves that can be generated on bath surface (published). These standing waves have large amplitude and impose significant impact on bath flow, which is possibly related to the slag tapping, matte droplets settling and refractory wearing. Therefore, it is essential to understand the occurrence condition, shape, amplitude and frequency of these waves.
    2) To study the features of longitudinal wave on bath surface(to be submitted for publication). Though the longitudinal wave does not have as large amplitude as standing waves, it is constantly present on the bath surface transmitting from the reaction zone to the settling zone. This wave is also possibly related to the slag tapping, matte droplets settling and refractory wearing. This study is aimed to investigate the amplitude, frequency, transmission

features and how it is influenced by the smelting parameters.

4 Experimental methodology

4.1 Principles of similarity

The physical simulation methodology is based on principles of similarity, which are a series of fundamental rules to guide simulation experiments[1-2]. These principles provide methods to solve complex equation groups via experiments. In this study, the flow of the liquid matte in the furnace is a phenomenon that an incompressible liquid phase flows under the influence of gravity. In this case, the matte flow can be simplified as a viscous incompressible steady flow, where chemical reactions are ignored. As there are significant differences between the prototype and physical model, physical similarities must be satisfied between two physical bodies, that is to guarantee the similarity of geometry, kinetics and dynamics. Geometric similarity is to make sure angles of the model equal to corresponding angles of the prototype and lines of the model proportional to corresponding lines of the prototype. Dynamic similarity is to guarantee that forces at corresponding positions of the two systems are at a fixed proportion, especially inertial force, viscous force and gravity, because the interaction of these forces dominate the flow motion in the vessel. Kinematic similarity is to guarantee that the motions of corresponding particles of the model and the prototype have proportional velocity[3-6].

In practice, it is usually difficult to satisfy all the conditions, so the approximate modelling is needed in order to conduct the experiment. The approximate modelling requires to analyse which of the similarity conditions is the primary or predominating, and which of them is secondary. To build up an approximate model, primary conditions should be guaranteed as precise as possible, while secondary conditions can be satisfied approximately, or even negligible. By this means the experimental results obtained in the model is indicative to the prototype. For metallurgical baths, temperature is considerably high, and the temperature field as well as material concentration field is unsteady, with large amount of gas bubbles existing in bath. Therefore, it is impossible to guarantee the physical properties of fluid in the model the same with the prototype. As a result, it is essential to analyse the flow of the molten bath in metallurgical containers and find out the primary condition that influences the process more significantly.

Particularly, in this study, the temperature of the prototype is around 1200ºC, while the simulation experiments are designed to conduct at room temperature. Despite the huge temperature gap, it is feasible to simulate the flow of the molten bath under room temperature because the motion of the bath only involves geometric, dynamic and kinematic quantities, including length, density, viscosity etc., but free of temperature. Therefore, it is possible to build up a room temperature model to study the flow of the high temperature matte and slag bath.

The chemical reactions that are taking place in the molten bath of the prototype are another factor difficult to simulate in the model study. In the molten bath, the major chemical reaction of smelting can be expressed by the following formula[7]:

$$FeCuS_2(s) + O_2(g) \rightarrow Cu - Fe - S(s) + SO_2(g)$$

This reaction is taking place in the molten bath where oxygen-enriched air is constantly blown from the bottom and a large amount of offgas is continuously generated. The offgas, then, rises in the molten bath in the form of bubbles and gets exhaled via offgas duct once reaching the bath surface. It means that the chemical reaction of smelting generates offgas bubbles while absorbing oxygen bubbles, so the flow of the molten bath is not significantly affected due to sudden change of gas volume. Therefore, to make the lab-scale simulation experiment feasible, it is reasonable to simply ignore the chemical reactions when studying the flow of the bath. Taking this rule into account, the selection range of liquid and gas in lab-scale model is widened, for example, it is fine to use the liquid and gas that are not reacting with each other to simulate the liquid bath and injected gas.

4.2 Dimensionless number analysis

To establish a metallurgical physical model, usually there are five kinds of similarity to be considered: geometric similarity, kinematic similarity, dynamic similarity, thermal similarity and chemical similarity. In most cases, it is difficult to guarantee all the similarity at the same time. In this research, the goal is to simulate the flow of the liquid matte inside the furnace, so the thermal similarity and chemical similarity are not considered. Besides, if both the geometric similarity and dynamic similarity are guaranteed, the kinematic similarity is accordingly satisfied. Therefore, the key factors to be considered to develop a cold model of the Fangyuan bottom blown furnace are geometric and dynamic similarity.

4.2.1 Geometric similarity

Similarity ratio is the ratio of characteristic length of model over prototype.

$$\lambda = \frac{l_m}{l_p} \tag{4.1}$$

Where: λ—geometric similarity ratio

l_m—characteristic length of model

l_p ---- characteristic length of prototype

Geometric similarity requires the three dimensions of the model to be the same ratio λ with those of the prototype. It is the first step to scale down the prototype to the laboratory model.

Table 4-1 Dimensionless numbers related to water model experiment

Dimensionless numbers	Symbol	Definition	Physical meaning
Reynolds	*Re*	$\frac{\rho u L}{\mu}$	Inertial force/viscous force
Froude	*Fr*	$\frac{u^2}{Lg}$	Inertial force/gravity
Modified Froude	*Fr'*	$\frac{\rho_g u^2}{(\rho_l - \rho_g) g L}$	Inertial force/buoyance
Weber	*We*	$\frac{\rho u^2 L}{\sigma}$	Inertial force/surface tension
Eötvös	*Eo*	$\frac{g \Delta \rho d_b^2}{\sigma}$	Gravity/surface tension
Morton	*Mo*	$\frac{g \mu^4 \Delta \rho}{\rho^2 \sigma^3}$	Viscous resistance/surface tension
Schmidt	*Sc*	$\frac{\mu}{\rho D}$	Dynamic viscosity/diffusion coefficient
Grashof	*Gr*	$\frac{g L^3 \beta \Delta T}{v^2}$	Buoyance/viscous resistance
Tu	*Zb*	$\frac{\beta g L \Delta T}{u^2}$	Buoyance/inertial force

4.2.2 Dynamic similarity

In industry, a certain phenomenon is usually comprehensively affected by several factors. At most of the time, it is not easy to study the influence of each factor, thus dimensionless numbers are often

used to replace the investigation on each one. Dimensionless numbers are derived from the dimensional analysis that investigates all the forces that are involved in a specific phenomenon. These numbers usually represents the ratio of one factor with another, and are dimensionless, which makes these numbers model-independent. Accordingly, it is more convenient to use dimensionless numbers to describe the phenomena both in the model and prototype. There are several dimensionless numbers widely used in metallurgical industry, as shown in Table 4-1

In the present study, the flow of matte in furnace can be regarded as the forced viscous flow caused by static pressure of matte and gas phase agitation, so main related forces are inertial force, gravity, viscous force, buoyance and interfacial tension. Amongst those forces, the interfacial tension is relatively small compared to other forces in the flow of a metallurgical bath. Besides, the interfacial tension is often used to investigate the bubble formation process in a bath, which is not a major concern of this study, so the interfacial tension simulation is neglected in this study. Therefore, to establish a cold model, one only needs to take gravity, viscous force, bubble buoyance, and inertial force into consideration. Consequently, Reynolds number and modified Froude number are the corresponding dimensionless numbers to be considered. It must be guaranteed that *Re* and *Fr'* of model are the same with or close to those of the prototype, in order to ensure the flow in model to be similar with that in prototype.

$$Re_{model} = Re_{prototype}$$

$$Fr'_{model} = Fr'_{prototype}$$

Dynamic similarity requires *Re* and *Fr'* of model and prototype to be equal, respectively, which is the condition that guarantees dynamic similarity between the two systems. However, it is not possible to guarantee the two equations at the same time in most cases. In metallurgical containers, the flow is mainly created by gas injection, so the major force that influences the flow of bath is bubble buoyance, while the viscous force of liquid metal phase is relatively small. Therefore, *Fr'* is taken into account as the dimensionless number that guarantees the similarity between the model and the prototype.

For *Fr'* similarity, it is to guarantee *Fr'* of prototype and model equal to each other.

$$Fr'_m = Fr'_p \tag{4.2}$$

That is

$$\frac{\rho_{gm}u_m^2}{(\rho_{lm}-\rho_{gm})gL_m}=\frac{\rho_{gp}u_p^2}{(\rho_{lp}-\rho_{gp})gL_p} \tag{4.3}$$

Where, subscript m — model, p — prototype

u — gas flow velocity, m/s

ρ_l — density of liquid, kg/m^3

ρ_g — density of gas, kg/m^3

g — gravity constant, m/s^2

L — characteristic length, m

Table 4-2 gas flowrate in each lance of Fangyuan's bottom blown furnace

	oxygen branch		air branch		Sum of oxygen and air in each lance
Lance number	Flowrate, Nm^3/h	Pressure, Mpa	Flowrate, Nm^3/h	Pressure, Mpa	Flowrate, Nm^3/h
1	866.53	0.47	424.47	0.52	1291
2	1025.13	0.46	588.47	0.52	1613.6
3	957.08	0.46	540.02	0.52	1497.1
4	931.8	0.47	380.45	0.52	1312.25
5	794.99	0.47	467.47	0.52	1262.46
6	941.82	0.47	464.39	0.52	1406.21
7	973.31	0.46	318.77	0.52	1292.08
8	785.77	0.47	463.33	0.52	1249.1
9	960.08	0.46	513.94	0.52	1474.02
sum	8236.51	/	4161.31	/	12397.82

Substitute line velocity u in Eq. (4.3) with gas flowrate Q, then

$$\frac{\rho_{gm}\left(\frac{Q_m}{\frac{\pi}{4}d_m^2}\right)^2}{(\rho_{lm}-\rho_{gm})gL_m}=\frac{\rho_{gp}\left(\frac{Q_p}{\frac{\pi}{4}d_p^2}\right)^2}{(\rho_{lp}-\rho_{gp})gL_p} \tag{4.4}$$

where d represents lance inner diameter of model and prototype respectively. By Eq. (4.4) flowrate used in model can be gained.

$$Q_m = Q_p \sqrt{\left(\frac{d_m}{d_p}\right)^4 \left(\frac{\rho_{lm} - \rho_{gm}}{\rho_{lp} - \rho_{gp}}\right)\left(\frac{L_m}{L_p}\right)\left(\frac{\rho_{gp}}{\rho_{gm}}\right)} \quad (4.5)$$

In Fangyuan's production, gas flowrate of each lance is shown in Table 4-2. The largest single lance flowrate is 1613.6 Nm^3/h, while smallest is 1249.1 Nm^3/h. Therefore, to simulate the flowrate of industry, gas flow should be between these two values. Put these values into Eq. (4.5), and gas flowrate used in model can be determined.

4.3 Model design

By following principles above, the lab-scale physical model is built up. It is made of acrylic and the size is 1/12 of the prototype. The design blueprint is shown in Figure 4-1, and the well-built mode is in Figure 4-3. It is a horizontal cylindrical container made of transparent acrylic, with lances located at the bottom. The configuration of lances is same with the prototype furnace, *i. e.* five lances in lower row four lances in upper row, where lower row is 7º offset from vertical line and upper row is 22º offset from vertical line. Each lance is controlled by an independent valve and connected with laboratory air compressor. A rotameter in Figure 4-2 is used to monitor the flowrate in each lance. The detailed geometric parameters are shown in Table 4-3.

Table 4-3 Basic designing parameters of lab scale model

	Prototype	Experiment
Average gas flowrate in each lance, m^3/h	1377	0.7038
Lance inner diameter, mm	60[i]	5
Furnace inner diameter, mm	3490	290
Depth of liquid, mm	1200	100
Furnace length, mm	15084	1000[ii]

In metallurgical physical model, water is often used to simulate liquid metal, because kinematic viscosity is close to liquid metal at high temperature, and also water is easy to prepare in experiment. Physical properties of water 20℃ and copper matte 1200℃ is shown in Table 4-4. The kinematic

[i] The prototype lance is comprised of outer annular air lance and inner central oxygen lance. For model experiment, the outer diameter is used.

[ii] Model furnace length is shorter than designed 1/12 of prototype furnace length due to fabrication difficulties.

viscosity is defined by:

$$\nu = \frac{\mu}{\rho}$$

where μ and ρ stand for the dynamic viscosity and density of the fluid, respectively. The dimension of ν is L^2t^{-1}. According to the Newton's law of internal friction, the kinematic viscosity ν also stands for the momentum diffusivity of the fluid. If two fluids have equal kinematic viscosity, the momentum diffuses equally in those two fluids. When the initial condition and boundary condition are the same, the two fluids have the same flow status. In this study, the water under room temperature has close value of kinematic viscosity as liquid matte under 1200ºC, so water can be used in lab-scale model to simulate the flow of liquid matte at a high temperature. Therefore, in this model, water is used to simulate the matte bath in the furnace, and air is used to simulate oxygen-enriched air injection.

Table 4-4 Physical properties of water and copper matte

	Density ($kg \cdot m^{-3}$)	Viscosity ($Pa \cdot s$)	Kinematic viscosity ($m^2 \cdot s^{-1}$)	Surface tension ($N \cdot m^{-1}$)
water	1000	0.89×10^{-3}	0.89×10^{-6}	0.073
Copper matte	4700	4×10^{-3}	0.85×10^{-6}	0.33

As a result, by following the principles of similarity, the lab-scale cold model of the Fangyuan bottom blown copper smelting furnace is built up, with geometric size 1/12 of prototype, using water to simulate molten matte and air to simulate oxygen-enriched air blowing. The current study of fluid dynamics in the bottom blown copper smelting furnace is carried out based on this cold model.

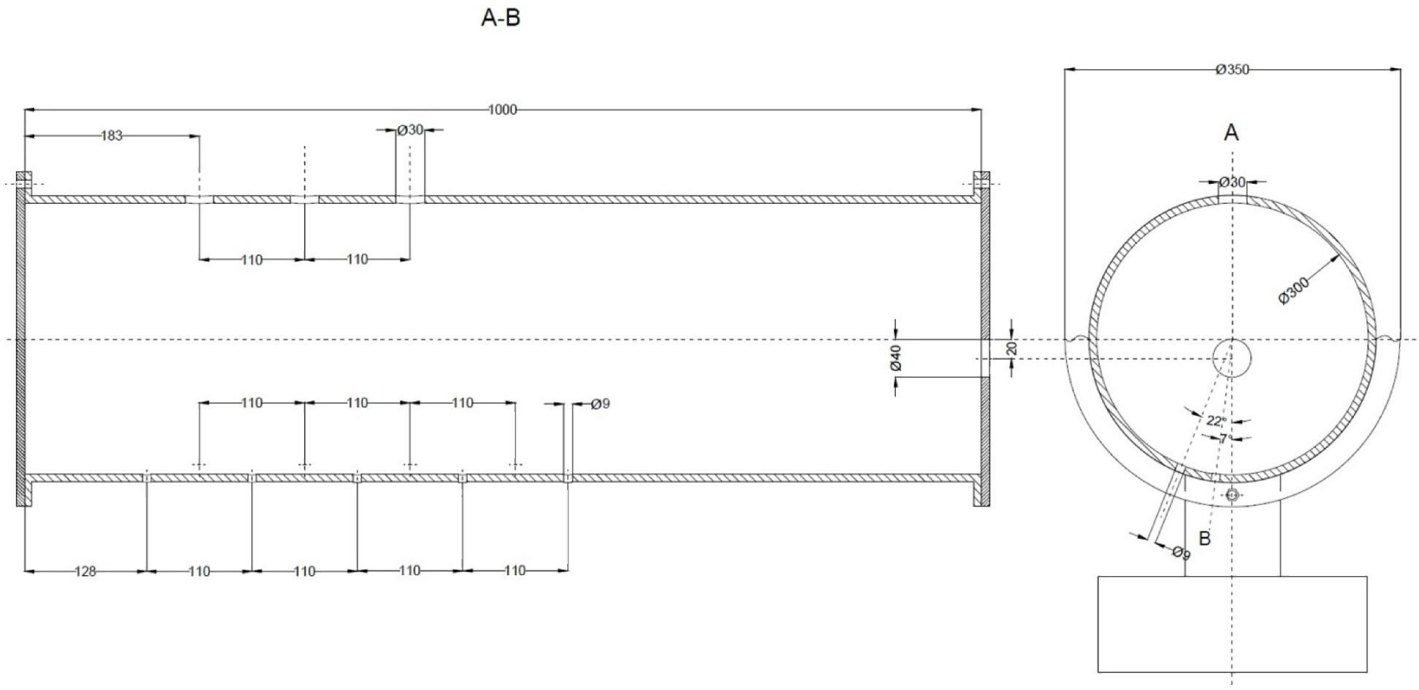

Figure 4-1 Blueprint of water model

Figure 4-2 Rotameter used in experiment to control the compressed air flowrate

(a)

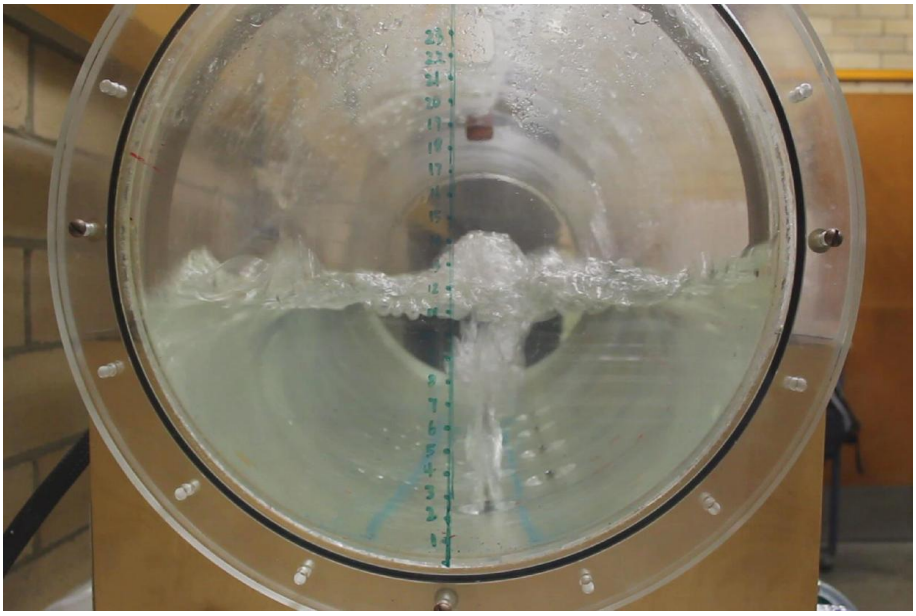

(b)

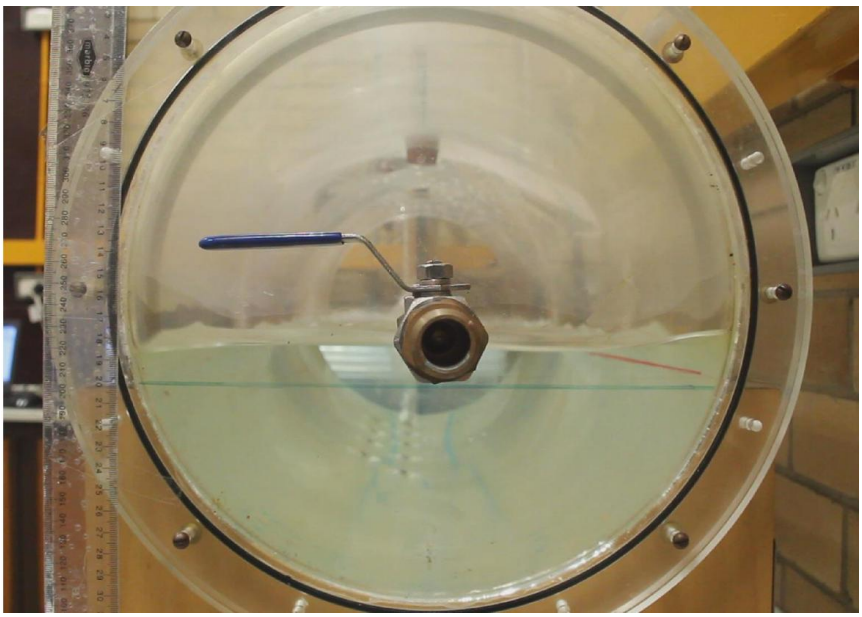

(c)

Figure 4-3 1/12 lab-scale cold model, (a) front view, (b) left view (feed end view), (c) right view (tapping end view)

4.4 References

[1] J. Szekely: *Fluid Flow Phenomena in Metals Processing*, 1979, Academic Press INC, New York, NY, USA, pp.392-418.

[2] R. E. Johnstone and M. W.Thring: *Pilot Plants, Models, and Scale-up Methods in Chemical Engineering*, 1957, McGraw-Hill, London, UK.

[3] H. Lamb: *Hydrodynamics*, 1932, 6th ed., Cambridge University Press, Cambridge, UK.

[4] G. H. Geiger and D. R. Poirier: *Transport Phenomena in Metallurgy*, 1973, Addison-Wesley Pub. Co., Reading, Mass, USA.

[5] R. B. Bird, W. E. Stewart, and E. N. Lightfoot: *Transport Phenomena*, 2007, Rev. 2nd ed., New York, NY, USA.

[6] B. LeMehaute: *An Introduction to Hydrodynamics and Water Waves*, 1976, Springer-Verlag, New York, NY, USA.

[7] Mark E. Schlesinger: *Extractive Metallurgy of Copper*, 5th ed, Elsevier, Saint Louis, MO, USA, 2011,pp.111.

5 Mixing behaviour of single phase in bottom blown copper smelting furnace

Abstract The first commercial bottom blown oxygen copper smelting furnace has been installed and operated at Dongying Fangyuan Nonferrous Metals since 2008. Significant advantages have been demonstrated in this technology mainly due to its bottom blown oxygen-enriched gas. In this study, a scaled-down 1:12 model was set up to simulate the flow behaviour for understanding the mixing phenomena in the furnace. A single lance was used in the present study for gas blowing to establish a reliable research technique and quantitative characterisation of the mixing behaviour. Operating parameters such as horizontal distance from the blowing lance, detector depth, bath height and gas flow rate were adjusted to investigate the mixing time under different conditions. It was found that when the horizontal distance between the lance and detector is within an effective stirring range, the mixing time decreases slightly with increasing the horizontal distance. Outside this range, the mixing time was found to increase with increasing the horizontal distance and it is more significant on the surface. The mixing time always decreases with increasing gas flow rate and bath height. An empirical relationship of mixing time as functions of gas flow rate and bath height has been established first time for the horizontal bottom blown furnace.

Key words: copper smelter, bottom blown, water model, mixing time

5.1 Introduction

Copper sulphide ores are the major source of the world's primary copper. The copper must be chemically separated from sulphur, iron and a wide range of impurity elements in order to produce commercial copper metal. The pyrometallurgical process is the major separation technology which involves a series of high temperature oxidation reactions of the copper sulphide ores by air or oxygen-enriched air. The oxidation reactions include two steps: smelting process to produce matte and converting process to produce copper. Bath smelting is one of the major technologies in copper production because of its high smelting efficiency, low capital cost, low energy consumption and reduced dust production. From the perspective of gas blown regime, developed bath smelting practice can be categorised into three general types: 1) top-submerged blown, including Ausmelt

and Isasmelt; 2) top-suspended blown, such as Mitsubishi smelting; and 3) submerged-side blown, such as Noranda and Teniente smelting.

Recently, Dongying Fangyuan Nonferrous Metals Co. Ltd. (Fangyuan) developed a new bottom-blown copper smelting technology[1-8]. The main equipment of the technology is a horizontal cylindrical reactor that is equipped with 9 oxygen lances at the bottom of the furnace to blow oxygen enriched air into the molten bath. The size of the furnace is Φ 4.4×16.5 m and it is lined with 380 mm thick chrome-magnesia bricks. The nine oxygen lances are arranged in two rows on the bottom. The lower row with five lances is located 7 degrees from the vertical position and the upper row with four lances is located 22 degrees from the vertical position. The angle between the two rows is 15 degrees as shown in Figure 5-1. Reports from industrial operations showed that the volume specific capacity of this reactor is higher than other current copper smelters[9]. Besides, it is autogenous smelting, meaning heat generated by chemical reactions is sufficient to keep bath temperature constant[2]. In molten bath, the first step of the reactions is the melting of concentrate particles and decomposing of high valence sulphides, such as FeS_2 and $CuFeS_2$. And then these sulphides are oxidised to form FeS-Cu_2S matte and iron oxides. Iron oxides generated by those reactions continuously react with SiO_2 in flux to form slag which is insoluble to matte and floats on top of the matte layer. All these reactions occur in molten bath, the mass transfer of the sulphides, matte and slag significantly affects the reaction efficiency of the smelter.

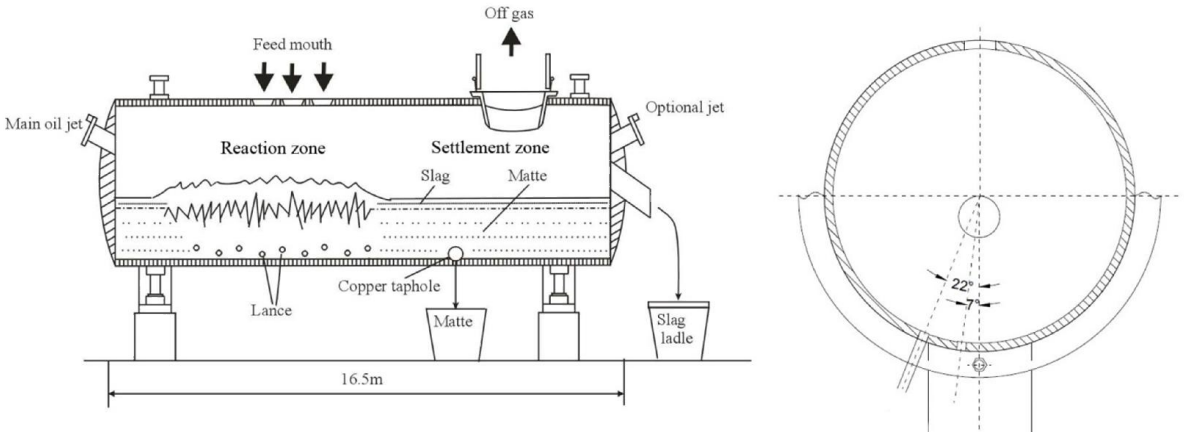

(a) (b)

Figure 5-1 Schematic view from side (a) and tapping end (b) of Fangyuan bottom blown copper smelting furnace

The bottom blown concept was firstly applied in steelmaking, consequently a large number of studies has been carried out on the investigation of the mass transfer phenomena in bottom blown steel refinery ladles or converters[10]. In 1975, Nakanishi *et al.*[11-12] used mixing time as a parameter for investigating the mass transfer efficiency inside model steel refinery ladles. To predict the mixing time, they plotted the mixing time against global rates of specific energy dissipation. Later, Themelis and Goyal[13] further investigated the relationship between mixing time and specific energy dissipation rate for various steelmaking vessels based on Nakanishi's result. Szekely *et al.*[14] then predicted the mixing time in pilot and industrial scale reactors, and noted that mixing time obtained in pilot scale operations tended to be inconsistent with Nakanishi's correlation. Haida[15] carried out experiments in a liquid iron torpedo, and the results showed remarkable influence of the vessel shape on mixing time. Asai *et al*[16] classified fluid motion in refining vessels into three types: flow dominated by molecular viscous forces, predominated by inertial forces and turbulent viscous forces. Their water model experiments showed that at high gas flow rate, mixing time depends on geometry of vessel and a correlation has been obtained from their measurements $\tau_m = 187.7Q^{-0.33}R^{2.03}h^{-1}$. τ_m is the mixing time, Q is the gas flow rate, R is the radius of the vessel and h is the bath height.

Sinha *et al.*[17] reported that position of tracer added and electrode might influence mixing time measurements. Mazumdar and Guthrie[18-20] summarised their empirical relationships for mixing time against gas input energy dissipation rate and parameters of vessel geometry and reported a similar equation to that of Asai *et al*[21] $\tau_m = 25.4Q^{-\frac{1}{3}}R^{\frac{7}{3}}h^{-1}$. Iguchi *et al.*[22] then took viscosity of liquid into consideration and performed the experiments in silicone oil bath. They predicted mixing time as a function of geometry of bath, input gas flow rate and viscosity of liquid $\tau_m = 4700\nu_L^{0.47}Q^{-0.47}R^{1.97}h^{-1}$.

While numerous studies have been reported in vertical reactors, providing a better understanding of the effects of flow rate, geometry of reactor, viscosity of liquid and position of tracer added on mixing time are available, there is only limited information on horizontal reactor which is the shape of the new bottom blowing copper smelting furnace. It is noted that the function of bottom blowing in copper smelter is different from steelmaking vessels.[23-25] In steelmaking, a combination of top

oxygen lance blowing and bottom argon or nitrogen blowing/stirring is widely applied. The purpose of bottom blowing is to supplement the limited stirring created by top oxygen lance. The blown time and intensity are controlled to maximise decarburization. In steel refining, the purpose of bottom blowing is to assist the uniform distribution of temperature and chemical composition. In addition, to suppress the inclusion formation, the stirring energy should be controlled under a certain level to prevent slag entrapment in liquid steel. Furthermore, the geometry of the horizontal bottom blown copper smelter is far different from vertical steelmaking converters or refinery ladles. Hence, the phenomena observed and the data collected for gas bottom blowing in the steelmaking vessels cannot be correctly applied to the copper smelter vessels.

In 1980s, channelled bottom blown smelter was developed in lead smelting industry. Cai *et al*[26] did experiments in physical model of bottom blown lead smelter as well as mathematical simulation to find an optimal lance arrangement and configuration for bottom blown furnace. They firstly conducted dimensional analysis and observed that effective stirring range of each bottom lance could be influenced by three dimensionless numbers. Then mathematical simulation was used to obtain regression equation of the three dimensionless numbers with lance effective stirring range. Finally, physical model was used to validate their results. Later, Liang *et al*[27] did experiments in similar physical model. In his study, a certain amount of tracer liquid was injected into the water bath and its concentration was monitored to obtain mean residence time. Meanwhile, factors including position of separating walls, bottom gas flow rate, liquid flow rate and area of hole on separating walls were all adjusted to obtain the effects on mean residence time.

In 1988, Sahai[28] studied the mixing phenomena in a water model of a side blown cylindrical reactor to understand the characteristics of Noranda copper smelter. The effects of gas injector separation, gas flow rate, depth of water, lateral configuration of injectors, submersion depth of gas injectors, and width of the channel have been investigated.

In summary, the geometry, flow rate level and metallurgical function of Fangyuan bottom blown copper smelter are remarkably different from steelmaking vessels. Its blown behaviour is also different from a side blown cylindrical copper reactor. Therefore, a detailed study into the mixing phenomena in this new smelter needs to be carried out for a better understanding and improvement

of the industrial operations. Since it is extremely difficult to visually observe the flow phenomena and directly measure the properties of the fluid flow field inside an actual reactor, a lab scale water model was used to simulate the flow behaviour of molten bath in this paper. The effects of different operating parameters on the mixing time were investigated to provide fundamental understanding and improvement of industrial scale operations of bottom blown copper smelting furnace.

5.2 Experimental Methodology

5.2.1 Similarity analysis

The model gas flow rate was calculated from the flow rate used in the prototype by considering the modified Froude Number, Fr', which is defined as follows[29]:

$$Fr' = \frac{\rho_g u^2}{(\rho_l - \rho_g) g L} \tag{5.1}$$

where u is the gas flow velocity (m/s), ρ_l is the density of liquid (kg/m^3), ρ_g is the density of gas (kg/m^3), g is the gravity acceleration (m/s^2) and L is the characteristic length (m) which is the bath height in the present study. The principle of the similarity requires the modified Froude Number of the model to be equal to that of the prototype.

$$Fr'_m = Fr'_p \tag{5.2}$$

Gas flow velocity can be represented as a function of gas flow rate

$$u = \frac{Q}{\frac{\pi}{4} d^2} \tag{5.3}$$

where Q is the gas volume flow rate (m^3/s) and d is the lance inner diameter (m). By replacing the gas flow velocity with gas volume flow rate, the following equation that relates the volume flow rate of the model with that of the prototype, can be developed,

$$Q_m = Q_p \sqrt{\left(\frac{d_m}{d_p}\right)^4 \left(\frac{\rho_{lm} - \rho_{gm}}{\rho_{lp} - \rho_{gp}}\right) \left(\frac{L_m}{L_p}\right) \left(\frac{\rho_{gp}}{\rho_{gm}}\right)} \tag{5.4}$$

Table 5-1 Typical data used for simulation calculations

Q_p average gas flowrate of prototype (Nm^3/h)	1377
Q_m corresponding gas flowrate used in model (mL/s)	195
d_p gas inlet inner diameter of prototype(mm)	60
d_m gas inlet inner diameter of model (mm)	5
ρ_{lp} liquid density of prototype (matte) (kg/m^3)	4700[4]
ρ_{lm} liquid density of model (water) (kg/m^3)	1000
ρ_{gp} gas density of prototype (air and O_2) at 1200ºC(kg/m^3)	0.3659
ρ_{gm} gas density of model (air) at 25 ºC (kg/m^3)	1.19
L_p liquid depth of prototype (mm)	1200
L_m liquid depth of model (mm)	100

The typical flowrates in Fangyuan bottom blown furnace are between 1249 and 1614 Nm^3/h for different lances, with average Q_p=1377 Nm^3/h. To simulate the flowrate of industrial furnace, the corresponding average gas flowrate is Q_m=195 mL/s, varying from 170 to 230 mL/s with according to Eq. (5.4) and the data given in Table 5-1. To acquire a wider range of data, the experimental gas flowrate range in the present study is set from 65 mL/s to 450 mL/s. The gas temperature of the prototype is assumed the same with molten bath temperature, i.e. 1200 ºC, as the gas is immediately heated up to the bath temperature upon contacting, so the density of gas in prototype is calculated from standard status by the following formula:

$$\rho_1 = \rho_0 \cdot \frac{T_0}{T_1} \cdot \frac{P_1}{P_0}$$

5.2.2 Experimental setup

Following the principle of similarity, a cold model furnace (1/12 of the prototype size) made of acrylic was developed. The vessel is 1000 mm long and 300 mm in diameter. Similar to the industrial furnace, nine lances with inside diameter 5 mm are arranged in two rows on the bottom. The lower row with five lances is located 7 degrees and the upper row with four lances is located 22 degrees from the vertical position. The distance between the lances in the same row is 110 mm. The kinematic viscosity of water is approximately 0.89×10^{-6} m^2/s at 25 ºC [30], close to that of copper matte 0.8×10^{-6} m^2/s at 1200 ºC (assuming density 4700 kg/m^3, dynamic viscosity 0.0037 Pa·s),

which suggests that both fluids have similar momentum transfer ratio. In the present study, water was used as the fluid to simulate copper matte. The focus of this study was on the flow behaviour, thus chemical reactions were not considered. Air was blown through bottom lances into water bath to simulate the stirring in the vessel. In the present study only single lance was used, and parameters were adjusted to investigate their influence on mixing.

5.2.3 Measurement of mixing time

Mixing time is widely used to evaluate the effectiveness of the mass transfer in metallurgical bath. In this study, the mixing time was determined by using a potassium chloride aqueous solution (4 mol/L) as a tracer. In each experiment, 5 mL of the solution was added by a syringe through a thin alumina tube to the top of the plume. Electrical resistance of the bath was continuously measured using a PARSTAT 2273 electrochemical station at a fixed position. Electrodes, made of two platinum wires with diameter of 0.5 mm and working length of 5 mm, were used in this study. The distance between two platinum wires was set to be 3 mm. The platinum wires were fixed inside the thin alumina tube by insulating glue. The schematic of the setup is shown in Figure 5-2(a).

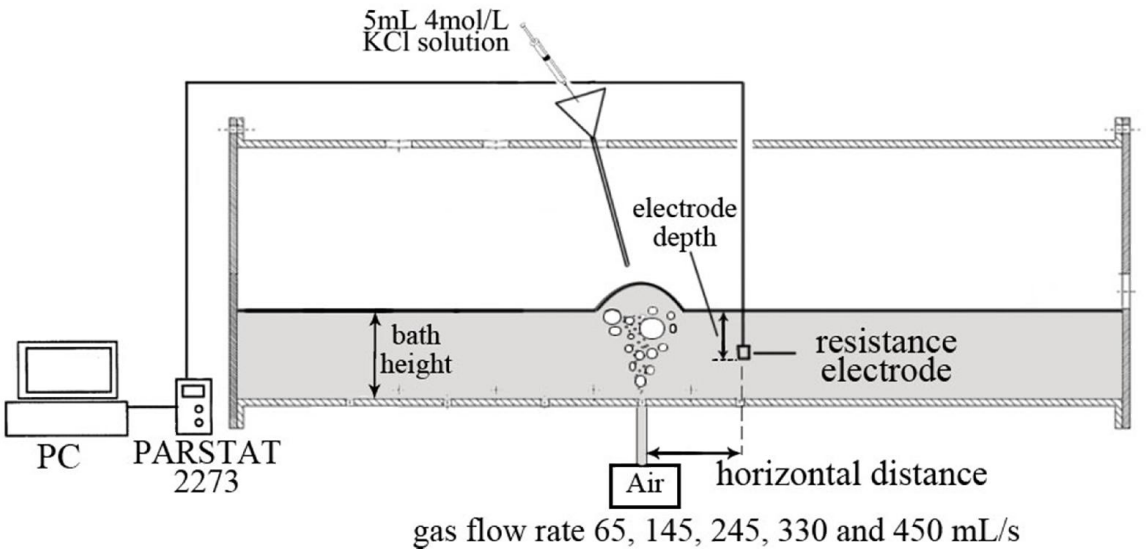

(a)

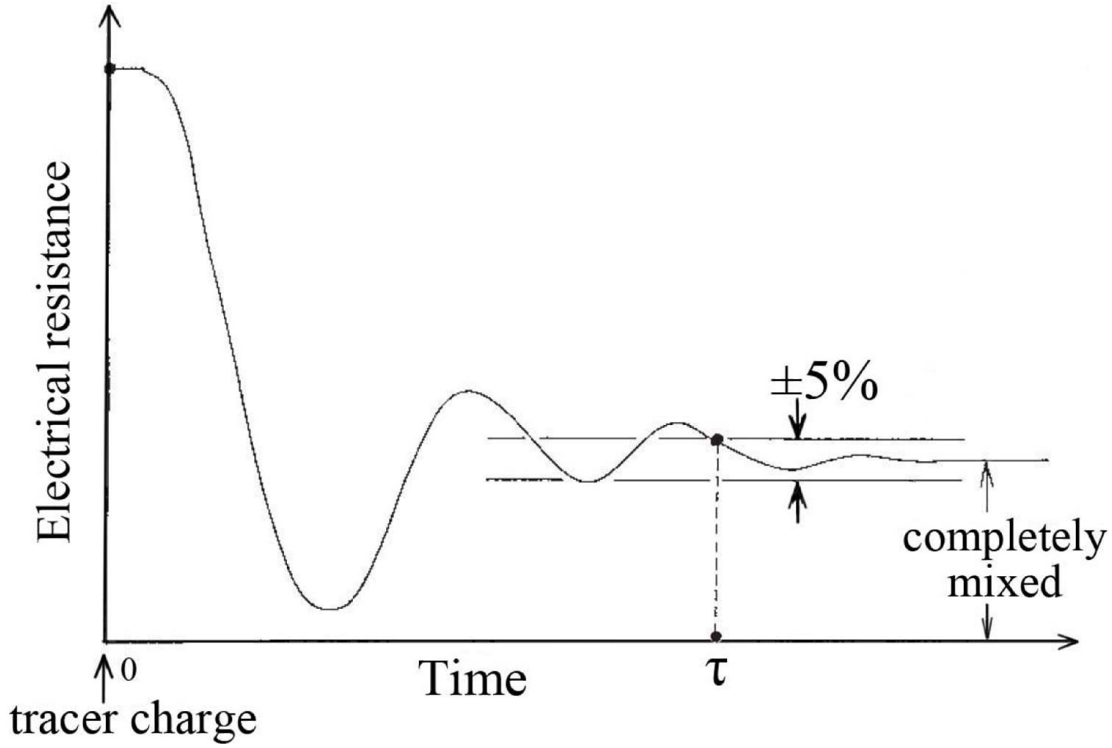

(b)

Figure 5-2 (a) Schematic view of the experimental set up, (b) definition of mixing time based on the steadiness of the solution electrical resistance within 5% variation.

It can be seen from Figure 5-2(b) that when the tracer was added into the water bath the electrical resistance was initially dropped rapidly and then came back to a stable value. In this study, the mixing time was defined as the period from the moment the tracer was introduced to the bath to the moment at which the fluctuation of electrical resistance was within ±5 %. It would correspond to the bath that is 95% well mixed [48]. The experiment at the same condition was repeated at least 3 times to obtain mean values of the mixing time.

5.2.4 Experimental parameters

A number of experimental parameters considered in this study include horizontal distance, electrode depth in the bath, bath height and input gas flowrate. The horizontal distance was measured between the electrode and the blowing lance, by changing blowing lance while the electrode location was fixed. The details of the parameters used in the study are provided in Table 5-2.

Table 5-2 Experimental variables and values

Experimental variables	Variation values
Horizontal distance (mm)	110, 220, 330, 440
Electrode depth (cm from the surface)	1.5, 5, 10
Bath height (cm)	7, 10, 13, 16
Input gas flowrate (mL/s)	65, 145, 150, 245, 330, 450

5.3 Results and discussions

5.3.1 Influence of horizontal distance

Figure 5-3 shows the relationship between mixing time and horizontal distance from the blowing lance to the electrode at 150 mL/s gas flowrate, 10 cm bath height and 3 different depths of the electrode. It can be seen from the figure that, at different electrode depths, the mixing time initially decreases slightly and then increases rapidly with increasing the horizontal distance. The turning point is at 220, 270 and 310 mm respectively when the electrode is on surface, middle and bottom of the bath. At a given depth of the bath, the mixing time is not sensitive to the distance between the lance and the electrode within a limit. This result is similar to that reported by Iguchi *et al*[48] carried out in an upright cylindrical vessel. The effective stirring range D_e was defined similar to that described by Cai *et al*[31]. However, the effective stirring range they reported was based on the observation of the plastic balls on the surface. It was not real quantitative measurements and only the information on the surface was provided.

It can be seen from Figure 5-3 that within 220mm the mixing time is almost independent of electrode depth indicating that the mixing strength and efficiency are similar along the vertical direction. However, D_e is different at different depths of the bath and increases with increasing the depth, or, on the other word, D_e decreases along the direction away from the lance located at the bottom. When the horizontal distance between the electrode and the lance is greater than D_e, the mixing time increases rapidly with increasing the distance. In addition, the mixing time measured at the surface is increased much faster than those at the middle and bottom.

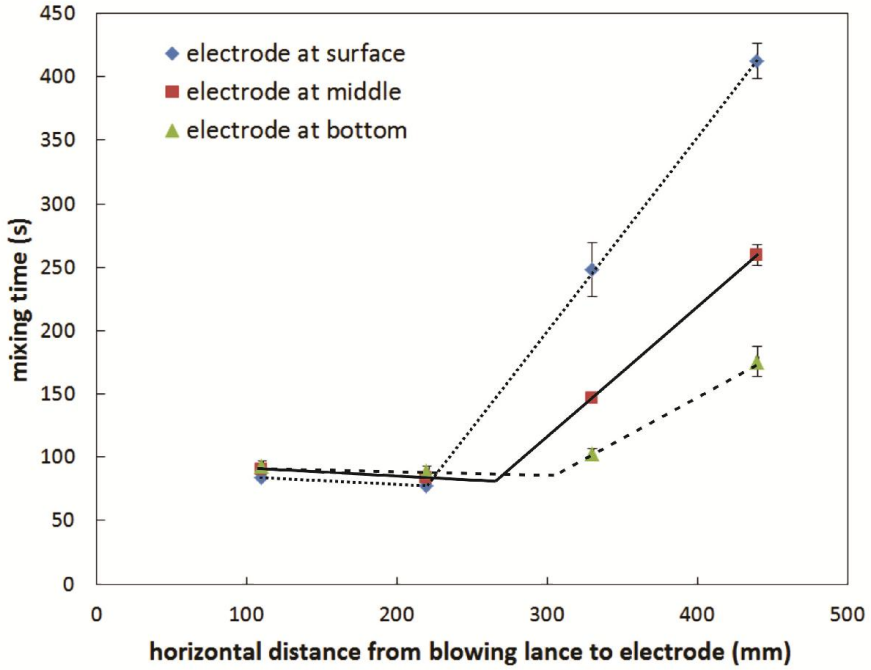

Figure 5-3 Mixing time vs horizontal distance, at gas flowrate 150mL/s, bath height 10cm

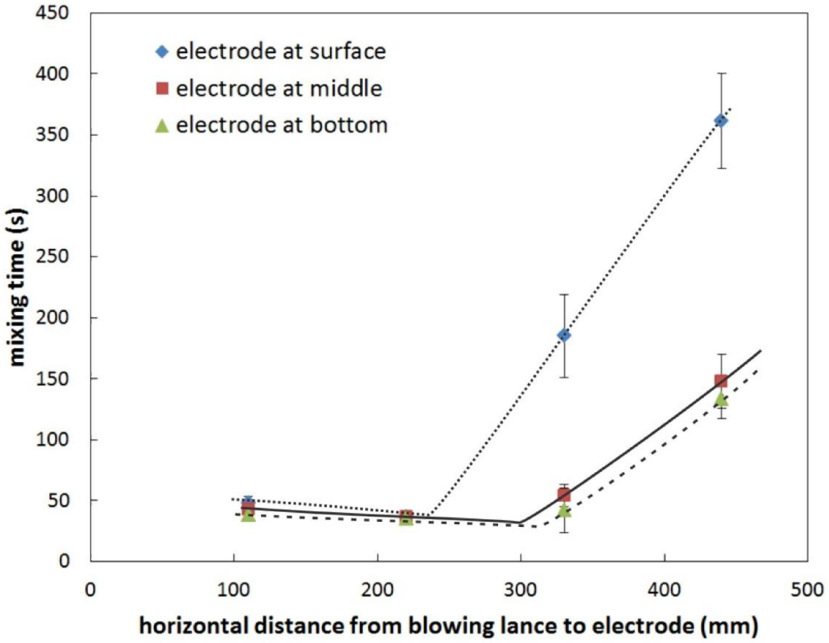

Figure 5-4 Mixing time vs horizontal distance, at gas flowrate 450mL/s, bath height 10cm

Figure 5-4 shows the relationship between mixing time and horizontal distance at 450 mL/s gas flowrate, 10 cm bath height and three different depths of the electrode. The results are similar to that obtained at 150 mL/s gas flowrate and the effective stirring range D_e is 230, 300 and 310 mm respectively at the surface, middle and bottom of the bath. It seems that higher flowrate does not

affect the effective stirring range at the bottom but increases D_e at surface and middle areas.

5.3.2 Influence of gas flowrate

Figure 5-5 compares the mixing behaviours on the surface between different gas flowrates. It can be seen clearly that higher flowrate results in higher mixing efficiency and larger effective stirring range. When the injection gas flowrate is increased from 150 to 450 mL/s the minimum mixing time is decreased from 75 to 35 seconds. Accordingly, the effective stirring range is increased from 220 to 230 mm on the surface.

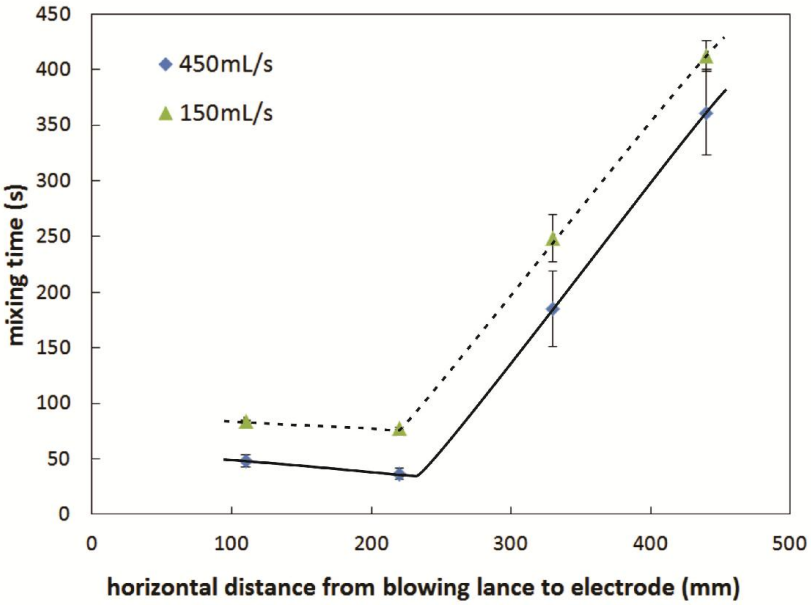

Figure 5-5 Mixing time measured at surface vs horizontal distance, bath height 10cm

The similar trends are observed in the middle and bottom of the bath as shown in Figures 6 and 7 respectively. It can be seen from Figure 5-6 that, increase of the injection gas flowrate from 150 to 450 mL/s results in the decrease of the minimum mixing time from 75 to 25 seconds in the middle area. Accordingly, the effective stirring range is increased from 270 to 300 mm. On the bottom of the bath, Figure 7 shows that increase of the injection gas flowrate from 150 to 450 mL/s results in the decrease of the minimum mixing time from 85 to 25 seconds and the effective stirring range is increased from 300 to 310 mm.

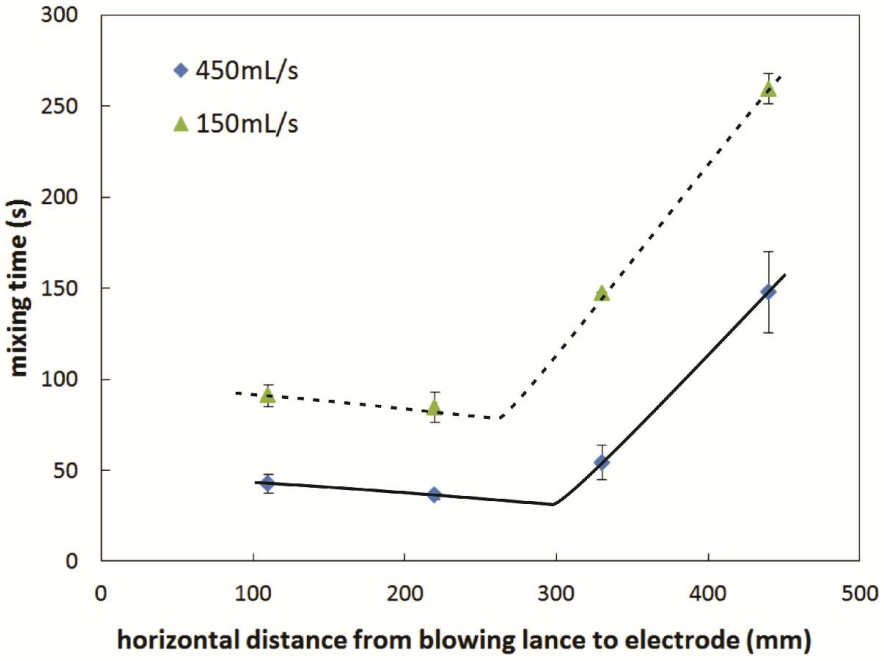

Figure 5-6 Mixing time measured at middle area vs horizontal distance, bath height 10cm

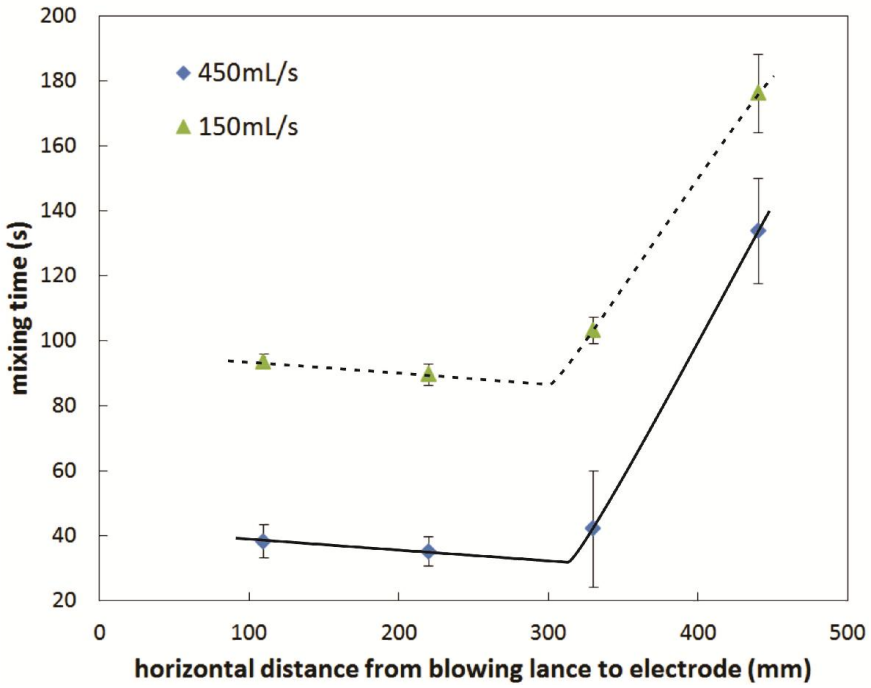

Figure 5-7 Mixing time measured at bottom area vs horizontal distance, bath height 10cm

5.3.3 Influence of bath height

To evaluate the influence of bath height on mixing behaviour, the experiments were carried out at

horizontal distance from lance to electrode at 110 and 220 mm, and gas flowrate at 450 mL/s. Bath height was changed from 7, 10, 13 to 16 cm. At each bath height, electrode was placed at surface (1.5 cm depth), middle (3.5, 5, 6.5 and 8 cm depth corresponding to each bath height) and bottom as well.

Figure 5-8 shows mixing time as a function of bath height at horizontal distance 110 mm and gas flowrate 450 mL/s. It can be seen that at a given bath height, no significant variation of mixing time was observed as the electrode position was changed. The average mixing time at each bath height is correlated to the bath height giving the following dependence:

$$\tau = 0.587H^{-1.828} \quad (5.5)$$

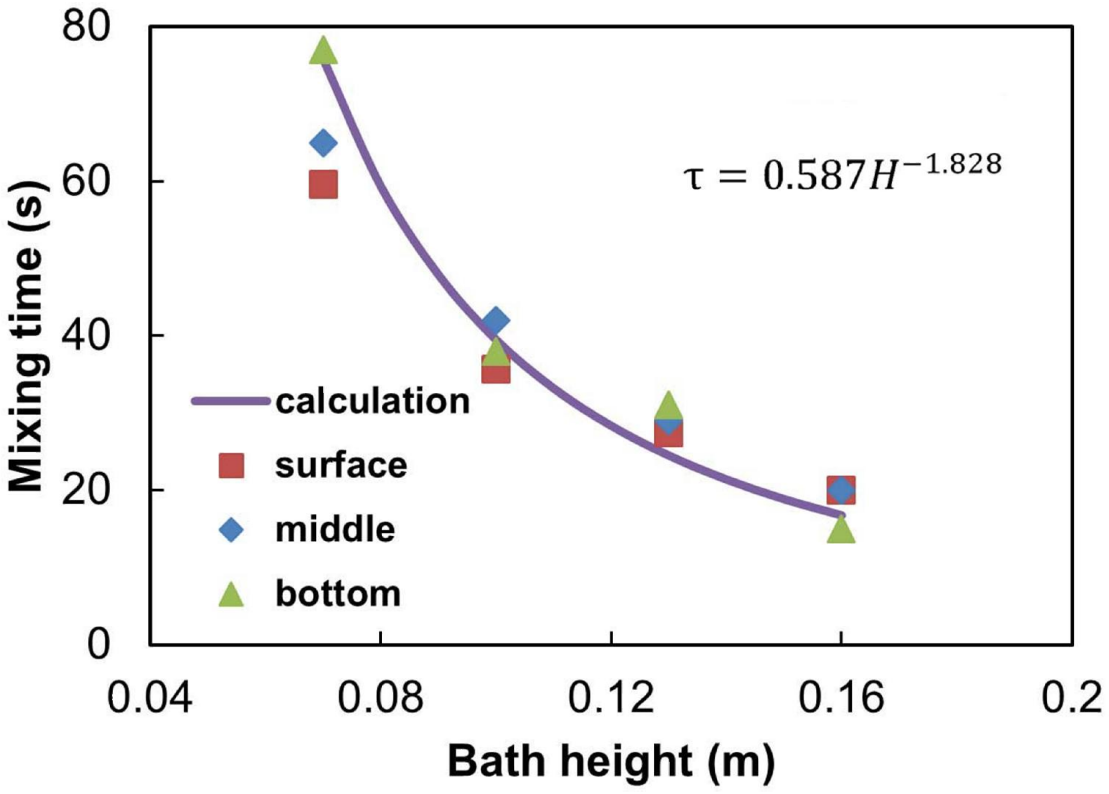

Figure 5-8 Mixing time vs bath height at gas flowrate 450 mL/s and horizontal distance 110 mm

Clearly Eq. (5.5) and Figure 5-8 show that mixing time decreases rapidly with increasing bath height at certain range and then decreases slowly if the bath height continuously increases. When the horizontal distance between the lance and electrode was increased to 220 mm, the average value of mixing time measured at the three different electrode depths is correlated to the bath height as

$$\tau = 1.881H^{-1.295} \quad (5.6)$$

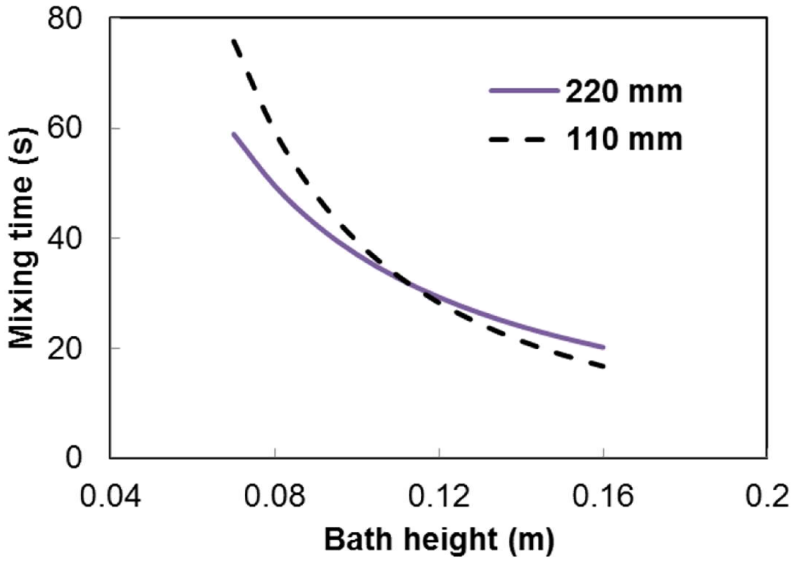

Figure 5-9 Mixing time vs bath height at gas flowrate 450 mL/s and different horizontal distances

Similar to the horizontal distance 110 mm, mixing time decreases rapidly with increasing bath height at certain range and then decreases slowly if the bath height continuously increases. However, it can be seen from Figure 5-9 that at distance far from the lance (220 mm), the changes in mixing time is less significant than that close to the lance (110 mm). At bath height below 0.11 m the mixing time decreases with increasing horizontal distance indicating the effective stirring range is greater than 220 mm. However, it can be seen from Figure 5-9 that when the bath height is above 0.11 m, the mixing time at 110 mm is lower than that at 220 mm. This indicates that the effective stirring range is less than 220 mm if the bath height is greater than 0.11 m.

5.3.4 Mixing behaviour for horizontal bottom blown furnace

The discussions in previous sections have shown that effective stirring range can be experimentally determined with the technique developed in the present study. Within the effective stirring range the mixing time is almost the same from the surface to the bottom of the bath. Both injection gas flowrate and bath height have significant effects on the mixing time. Systematic experiments were carried out to quantitate mixing time as functions of gas flowrate and bath height. The horizontal distance from lance to electrode was fixed at 110 mm and electrode was fixed at middle bath height. The gas flowrate varies 65, 145, 245, 330 and 450 mL/s and the bath height varies 0.07, 0.10, 0.13

and 0.16 m, respectively.

The results are shown in Table 5-3 and Figure 5-10. Analyses of these experimental results show that mixing time τ can be expressed as functions of gas flowrate Q and bath height h:

$$\tau = 37.5Q^{-0.39}H^{-1.08} \quad (5.7)$$

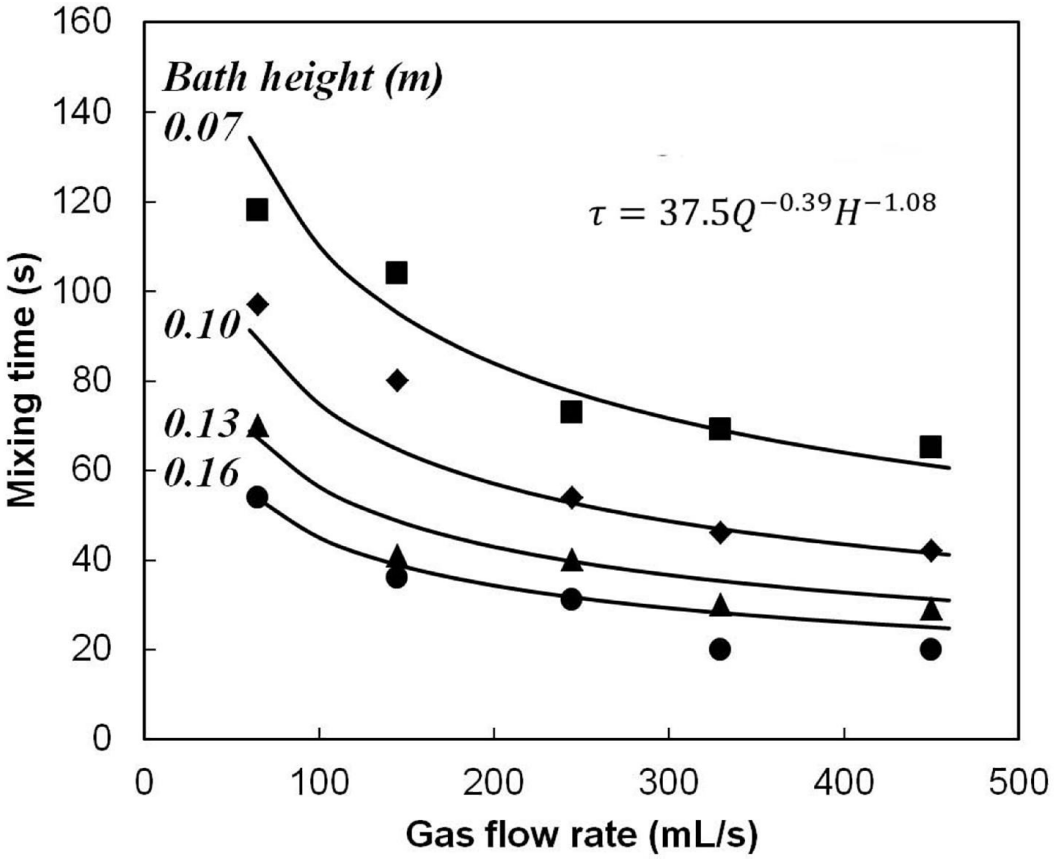

Figure 5-10 Mixing time vs flowrate at fixed distance of lance to electrode 110 mm and electrode fixed at middle bath

Table 5-3 Mixing time (s) at horizontal distance 110 mm and middle electrode

Gas flowrate (mL/s)	Bath height 0.07m	Bath height 0.110m	Bath height 0.13m	Bath height 0.16m
65	118	97	70	54
145	104	80	41	36
245	73	54	40	31
330	69	46	30	20
450	65	42	29	20

Asai *et al*[33], Mazumdar and Guthrie[39] and Iguchi *et al*[52] have reported similar relationships to predict mixing time from gas flowrate and bath height for steelmaking ladle. However, the bottom blown copper smelting furnace investigated in the present study is horizontal which has different geometry from the steelmaking ladle. It can be seen from Eq. (5.7) that the absolute value of exponent constant (1.08) for H is slightly higher in horizontal bottom blown furnace than that in steel ladle (1.0). This indicates that mixing time is more sensitive to the bath height in horizontal bottom blown furnace than that in steel ladle. The absolute value of exponent constant (0.39) for Q in horizontal bottom blown furnace is within the range of that in steel ladle (0.33 to 0.47).

5.4 Industrial applications

Bottom blown copper smelting furnace operated in Fangyuan has shown significant advantages. Fluid dynamics play a major role in describing the behaviours of the liquid bath in the bottom blown copper smelting furnace. Mixing behaviour of the bath is directly associated with the reaction rate or capacity of the furnace to treat copper concentrate. Systematic studies are required to fully characterise the fluid dynamics of the bottom blown copper smelting furnace. As the first study into the fluid dynamics of the bottom blown copper smelting furnace, a number of important findings have been obtained through well-designed experiments.

1. Effective stirring range can be accurately determined for a single lance which is one of the important parameters to design the number of lances and distance between the lances. An optimum number and distance of the lances will enable the bath to be efficiently mixed with minimum energy and gas consumptions.
2. Within the effective stirring range, the mixing time is not sensitive to the vertical locations. However, the effective stirring range is smaller on the surface and mixing energy decreases much faster at the surface beyond the range. In bottom blown copper smelting furnace, most reactions occur on the surface of the bath as the copper concentrate is fed from the top. It is therefore important to ensure the surface area in the reaction zone is fully covered within effective stirring area by proper arrangement of the lances.
3. Mixing time τ can be expressed as functions of gas flowrate Q and bath height H:

$$\tau = 37.5Q^{-0.39}H^{-1.08} \quad (5.7)$$

This is the first quantitative expression of the mixing time for horizontal bottom blown

furnace. Required injection gas flowrate and bath height can be calculated from this equation according to the productivity.

4. Further investigations are required to evaluate the effects of liquid viscosity, multi-layer bath, solid phase present, angle of the lance and multi-lances on mixing behaviour of the horizontal bottom blown furnace in order to more closely simulate the industrial operation.

5.5 Conclusions

A lab scale cold model has been developed for investigating mass transfer in the bottom blown copper smelting furnace. Mixing time in this cold model was measured to examine the characteristics of the fluid dynamics in horizontal bottom blown furnace. It was found that:

1) Within effective stirring range, mixing time changed little with horizontal or vertical distance. Outside the effective stirring range, mixing time increases with increasing horizontal distance and the increment is much greater on the surface of the bath.
2) Within effective stirring range, mixing time decreases with increasing bath height and gas flowrate. However, the effective stirring range can be reduced with increasing the bath height.
3) An empirical prediction of mixing time from gas flowrate and bath height is established first time for horizontal bottom blown furnace:

$$\tau = 37.5Q^{-0.39}H^{-1.08} \qquad (5.7)$$

These findings will provide a better understanding of blowing patterns in the new bottom blown furnace for the copper industry. For a further understanding and optimisation of field trials and production, further work in this area would be required.

5.6 References

[1] Z. Cui, D. Shen, and Z. Wang: *You Se Jin Shu [Nonferrous Metals]*, 2010, No. 3, pp. 17-20.

[2] B. Zhao, Z. Cui, and Z. Wang: *Int. Symp. High-Temp. Metall. Process., 4th,* 2013, pp. 1-10.

[3] J. Yan: *Proc. Copper 2013—Cobre 2013 Int. Conf.*, 2013, pp.873-887.

[4] B. Li, J. Jiang, and K. Wei et al: *Proc. Copper 2013—Cobre 2013 Int. Conf.*, 2013, pp.889-896.

[5] L. Feng: *Proc. Copper 2013—Cobre 2013 Int. Conf.*, 2013, pp.897-909.

[6] Z. Cui, Z. Wang and B. Zhao: *Proc. Copper 2013—Cobre 2013 Int. Conf.*, 2013, pp.923-933.

[7] Z. Cui, Z. Wang and R. Li: *Proc. Copper 2013—Cobre 2013 Int. Conf.*, 2013, pp.935-943.

[8] Z. Cui, Z. Wang and J. Zheng et al: *Proc. Copper 2013—Cobre 2013 Int. Conf.*, 2013, pp.1047-1057.

[9] X. Hao, Z. Lu, and K. Wei et al: *Proc. Copper 2013—Cobre 2013 Int. Conf.*, 2013, pp.1035-1045.

[10] D. Mazumdar and J. W. Evans: *ISIJ Int.*, 2004, vol. 44, No. 3, pp. 447-461

[11] K. Nakanishi, T. Fujii and J. Szekely: *Ironmaking Steelmaking*, 1975, No. 3, pp. 190-195.

[12] K. Nakanishi, J. Szekely, T. Fujii, Y. Mihara, and S. Iwaoka: *Metall. Trans. B*, 1975, vol. 6B, pp. 111-118.

[13] N. J. Themelis and P. Goyal: *Can. Metall. Q.*, 1983, vol. 22, No. 3, pp. 313-320.

[14] J. Szekely, T. Lehner, and C W. Chang: *Ironmaking Steelmaking*, 1979, vol. 3, pp. 285-93.

[15] O. Haida, T. Emi, S. Yamada, and F. Sudo: *SCANINJECT, Int. Conf. Injection Metall., Proc.*, 2nd, Lulea, Sweden, 1980, pp. 20:1-20:20

[16] S. Asai, T. Okamoto, J. He, and I. Muchi: *Trans. Iron Steel Inst. Jpn.*, 1983, vol. 23, pp.43-50.

[17] U. P. Sinha and M. J. McNallan: *Metall. Trans. B*, 1985, vol. 16B, pp. 850-53.

[18] D. Mazumdar and R. I. L. Guthrie: *Metall. Trans. B*, 1986, vol. 17B, pp. 725-733.

[19] D. Mazumdar: *Metall. Trans. B*, 1989, vol. 20B, pp. 967-969.

[20] D. Mazumdar: *Metall. Trans. B*, 1990, vol. 21B, pp. 925-928.

[21] S. Asai, T. Okamoto, J. He, and I. Muchi: *Trans. Iron Steel Inst. Jpn.*, 1983, vol. 23, pp.43-50.

[22] M. Iguchi, K. Nakamura and R. Tsujino: *Metall. Trans. B,* 1998, vol. 29B, pp. 569-575.

[23] C. Su, J. Chou, and S. Liu: *Mater. Trans.*, 2009, vol. 50, No. 6, pp. 1502-1509.

[24] C. Su, J. Chou, S. Liu, and C. Chiang: *Mater. Trans.*, 2010, vol. 51, No. 9, pp. 1594-1601.

[25] C. Su, J. Chou, and S. Liu: *Mater. Trans.*, 2010, vol. 51, No. 9, pp. 1602-1608.

[26] C. Cai, Y. Liang and Z. Qian: *The Chinese Journal of process engineering*, 1985, No. 4, pp. 113-121.

[27] Y. Liang, C. Cai and Z. Qian: *Chemical Metallurgy*, 1986, vol. 7, No. 1, pp. 45-53.

[28] Y. Sahai: *Metall. Trans. B*, 1988, vol. 19B, pp. 603-612.

[29] K. Krishnapisharody and G. A. Irons: *Metall. Trans. B*, 2013, vol. 44B, pp.1486-1498.

[30] W. E. Forsythe: Smithsonian Physical Tables, 9th rev. ed., Knovel, New York City, NY, USA, 2003, pp. 319.

[31] C. Cai, Y. Liang and Z. Qian: *The Chinese Journal of process engineering*, 1985, No. 4, pp. 113-121.

6 Mixing behaviour of multiphase in bottom blown copper smelting furnace

Abstract A lab-scale cold model study was carried out to understand the effect of a slag layer on mixing behaviour of the novel bottom blown copper smelting furnace. In this study, a single lance was used and experimental variables including water height, gas flowrate, oil layer height and oil viscosity were adjusted to investigate the impact of each on mixing. It was found that the mixing time was decreasing with increasing water height and gas flowrate at a greater rate than that of oil free, while it was increasing with increasing oil layer height and oil viscosity, where the rate with an oil layer was much greater. An overall empirical relationship with these variables was correlated, and it showed good prediction of mixing time at different conditions. The correlation was then generalised to a model-independent format for wider use, which provides guidelines for industrial operations.

Key words: copper smelting, bottom blown furnace, cold model, mixing time

6.1 Introduction

Previous study discussed the mixing behaviour without the upper immiscible phase in the bottom blown copper smelting furnace[1]. An effective stirring range was estimated and an empirical relationship of mixing time in terms of factors such as flowrate and bath height was also proposed. However, in most metallurgical containers, there is always a slag layer with substantial thickness existing on liquid metal. Typically, in the bottom blown copper smelting furnace, the height of the slag layer can reach about 1/3 of matte layer, which necessarily impacts the flow dynamics of the matte phase. Therefore, it is significant to study the mixing behaviour with a top immiscible phase.

Mixing phenomenon in gas stirred ladle has been extensively studied back in decades, and a great deal of information on this topic can be found in literature[2]. Among those, most authors reported their studies carried out in slag-free cold models. By such models, empirical or semi-empirical correlations of mixing time against variables such as bath height, container dimension, flowrate, and

nozzle configuration were given to predict effect of each variable on mixing. Whereas only a few studies took the overlying slag layer into consideration[3-12].

Kim and Fruehan[6] reported the presence of second phase, *i. e.* oil, in a water model of a steelmaking ladle, increases the mixing time significantly, indicating its resistance to the recirculatory velocity of fluid near the surface. Mazumdar *et al*.[8-10] also studied the behaviour of the upper slag layer on the steelmaking ladle using an oil-water system, and noticed the interaction mechanism between oil and water phase on the interface. These authors studied the formation of the plume eye in oil layer and its consumption of input stirring energy, and pointed out the significant relationship between the plume eye area and input energy. Han[12] conducted both experiments and numerical simulation to investigate the characteristics of flow in a model of gas stirred ladle with an oil layer. It was found that the plume eye size increased with gas flowrate and decreased with the oil layer thickness. Moreover, the flow pattern in the presence of oil layer was found to form distorted and localised recirculating loop near the side wall below the oil layer, which eventually extended the mixing time in the bath. Yonezawa and Schwerdtfeger[13-16] conducted several studies, using a mercury bath with oil layer and large scale water models to investigate features of the spout height in presence of a slag layer. These authors also carried out industrial experiments in a 350 t steel ladle to validate the results. It was reported in these studies the spout height were fluctuating strongly and long-term average values were collected and used to correlate empirical relationships with operational parameters. Yonezawa *et al*. [16-17] also studied the area of the plume eye in the slag layer and reported correlated dimensionless area of the plume eye in terms of the gas flow rate and bath height. Krishnapisharody and Irons[11] also focused on the size of plume in the slag layer, and obtained the same tendency of the plume eye size with gas flowrate and oil layer thickness. These authors further found that the eye size increased with increasing the lower phase depth, and less dense upper phase resulted into a smaller eye size. A mechanistic model regarding the dimensionless eye size was expressed in terms of the density ratio and Froude number based plume velocity to predict the eye size change. Mazumdar and Guthrie[18] studied the energy dissipation in slag covered steel bath by using oil-water system and divided the stirring energy consumption into five parts: turbulence, bubble, wall friction, plume eye formation and slag metal interface. In this manner, the mixing in the lower phase is linked with the spout height formation and features of the

slag layer. Amaro-Villeda[3] applied this model to study the mixing time in model of steel ladle with different bottom nozzle configurations.

Most of these studies focused on the formation of the plume eye in the slag layer and the effect on bath recirculation but did not give explicit mixing time correlations with operational variables. Limited reports were found to address this topic. Patil[19] investigated experimental mixing phenomenon in water models of slag covered, gas stirred ladles, and then developed explicit empirical correlations to estimate mixing times. Besides, at their experimental condition, the gas flowrate was relatively low to keep the slag layer almost intact, and the slag layer is only 1-13% of bulk depth, which enables the authors to develop mixing time correlations on the basis of slag free models. Patil's explicit mixing time relationship with operational variables predicts mixing time at required dynamic condition very well, but the low flowrate and thin slag layer is only applicable to limited metallurgical containers. Furthermore, in most cases of literature that studies the effect of the upper layer, the height of overlying slag layer is limited to about 10% of bulk height and gas flowrate is constrained to a relatively low value to avoid a large amount of entrainment between two phases, as the ladle metallurgy requires. Khajavi and Barati[20] reported a study that investigated mixing time in a thick slag covered metallurgical bath. The authors carried experimental studies in kerosene-water and silicone oil-water system and used effective bath height that combined both lower and upper layer height to correlate the relationship with mixing time. Their results provide guidelines for industrial processes such as COREX and CRISP steelmaking technologies. However, the mixing behaviour with a slag layer in horizontal cylindrical furnaces that are widely used in nonferrous metallurgy has not been studied.

In the current study, the metallurgical function of Fangyuang bottom blown copper smelting furnace differs from steelmaking ladles significantly[21]. Accordingly, mixing theories obtained in steelmaking ladles is not applicable in this novel smelter. Besides its horizontal cylindrical geometry and dimension, and the slag layer exists constantly about 1/3 of matte layer height[22]. Meanwhile, the gas blown from the bottom stirs the slag and matte layer to much intensive extent. Therefore, the mixing behaviour in bottom copper smelting furnace should be investigated specifically.

6.2 Experimental methodology

In common metallurgical containers, the flow is dominated by the inertial and gravitational forces, which means the viscous forces of liquid are negligibly small. Therefore, in the absence of overlying layer, many studies exclude the viscosity of bulk and express mixing time in terms of operating variables in the following form:

$$\tau = f(H, Q\ h, g,) \tag{6.1}$$

However, in the presence of an overlying layer, this expression is not sufficient to characterize the features of mixing time, especially with a thick overlying layer. Mazumdar[10] reported the mixing time obtained with a relatively thin overlying layer and low flowrates and suggested that the depth and physical properties of the upper layer would exert noticeable influence upon bulk flow and mixing. Typical physical dynamic properties of slag layer include viscosity, interfacial tension and density. Among those viscosity is the most concerned because the apparent viscosity of industrial slag of bottom blown copper smelting furnace varies in a wide range due to different contents of entrained solid phase[23]. Therefore, viscosity is the main property of the upper layer considered in the present study. The expression of mixing time then can be extended to:

$$\tau = f(H, Q, h, \nu_s, R, g,) \tag{6.2}$$

where, H stands for the lower phase height (water or matte), Q stands for the gas flowrate, h stands for the upper phase height (oil or slag), ν_s stands for the viscosity of upper layer, R stands for the radius of furnace and g is the accelerate due to gravity. The radius of furnace R depends on the model furnace geometry and g remains constant 9.8 m/s^2, while the rest of them are industry corresponded variables which this study will investigate. Eq. (6.2) shows the relationship of the mixing time with the combination of operational variables, and its explicit form can be obtained by experimental work that is designed following the principles of similarity[24].

The detailed cold model design has been introduced in previous study[1], so it is not repeated in this chapter. In this experiment, as discussed in Chapter 4, water is still used to simulate copper matte because the kinematic viscosity of water at room temperature is close to the liquid matte at 1200ºC, which means that the momentum diffusivity of the two fluids are close to each other and the flow status of the two tends to be similar if initial and boundary condition are set the same. Likewise, the

choosing of experimental liquid to simulate the liquid slag layer must follow the same rule. In Fangyuan practice, the viscosity of full liquid phase of slag is normally around 0.2 Pa·s[23]. To consider a wide range of simulation and the presence of solid particles in slag, the minimum 0.05 Pa·s and the maximum 0.7 Pa·s are taken as extreme conditions. To guarantee the principles of similarity, Eq.(6.3) must be satisfied when selecting the silicone oils. As a result, the corresponding silicone oils with kinematic viscosity 10, 50 and 200 cSt were selected as shown in Table 6-1.

$$\nu = \frac{\mu_{slag}}{\rho_{slag}} = \frac{\mu_{oil}}{\rho_{oil}} \tag{6.3}$$

Table 6-1 Physical parameters of experimental fluids corresponding to fluids in prototype at 1200ºC

Top phase	Min I	Ave II	Max III	Lower phase	-
Slag density kg/m^3	3500	3500	3500	Matte density kg/m^3	4700
Slag viscosity Pa·s	0.05	0.2	0.7	Matte viscosity Pa·s	4×10^{-3}
Slag kinematic viscosity cSt	14.29	57.14	200.00	Matte kinematic viscosity cSt	0.85
Si-oil density kg/m^3	935	960	970	Water density kg/m^3	0.89×10^{-3}
Si-oil kinematic viscosity cSt	10	50	200	Water kinematic viscosity cSt	0.89

$$Q_m = Q_p \sqrt{\left(\frac{d_m}{d_p}\right)^4 \left(\frac{\rho_{lm} - \rho_{gm}}{\rho_{lp} - \rho_{gp}}\right)\left(\frac{L_m}{L_p}\right)\left(\frac{\rho_{gp}}{\rho_{gm}}\right)} \tag{6.4}$$

Experimental setup is shown in Figure 6-1, the silicone oil was applied onto water, and its height was adjusted as desired. The 4 mol/L potassium chloride solution was used as tracer, and was injected on to the spout via a thin alumina tube. Platinum electrode was placed at the bottom of furnace near the tip of the right-most lance, and it was connected to PARSTAT 2273 electrochemical device to monitor the electrical resistance of bath continuously. For the sake of simplicity, only single lance (lance 7) was used for blowing, and its horizontal distance from the electrode was fixed at 110mm to monitor the mixing behaviour close to plume zone. Air flowrate was still determined by guaranteeing the modified Froude number equality between model and industrial prototype as shown in Eq.(6.4), and was controlled by the rotameter to the desired values. Prior to each experiment the bath was constantly blown for 20 min at the corresponding flowrate because the container was relatively large and the effect of single lance blowing takes a long time to form a steady flow field in such a container. The mixing time was defined as the time lapse from the

moment the tracer was introduced to the bath to the moment at which the fluctuation of electrical resistance was less than ±5%. Each experimental condition was repeated at least once to confirm the average value.

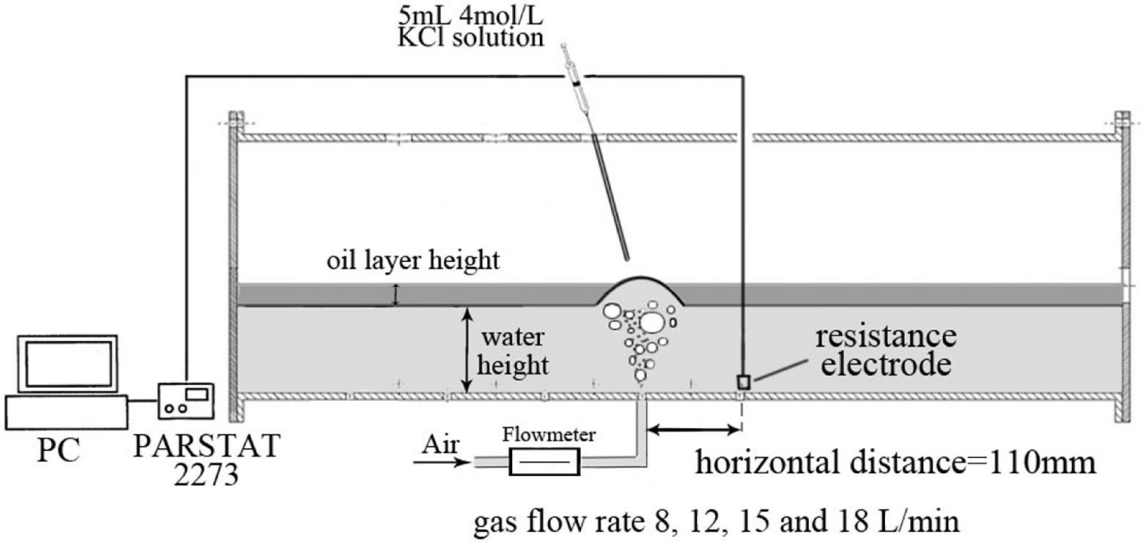

Figure 6-1 Experimental setup of mixing time measure with presence of top oil layer

Table 6-2 Experimental variables and values

Horizontal distance from lance to electrode mm	110
Vertical location of electrode	Close to bottom (not touching)
Water height cm	7, 8, 9, 10
Silicone oil height cm	1, 2, 3
Silicone oil kinematic viscosity cSt	10, 50, 200
In put air flowrate L/min	8, 12, 15,18

In preliminary experiment, the electrode was placed at mid bath depth. It was found that the rising plume quickly emulsifies silicone oil and a large amount of oil droplets were formed in water. These oil droplets flew with turbulence and easily attached onto the electrode, which frequently caused abrupt peaks of electrical resistance and affected the measuring of mixing time. It was noticed that most of these droplets could not reach the bottom of bath because of buoyance. Therefore, on the contrary to previous study, electrode location in this study must be fixed at the bottom of bath to avoid influence of oil attachment. Furthermore, there was still some attachments taking place even electrode was placed at bottom, so the current solution was to slightly flick the rod of electrode to remove the droplets, and accordingly ignore the corresponding abrupt peaks on mixing curve.

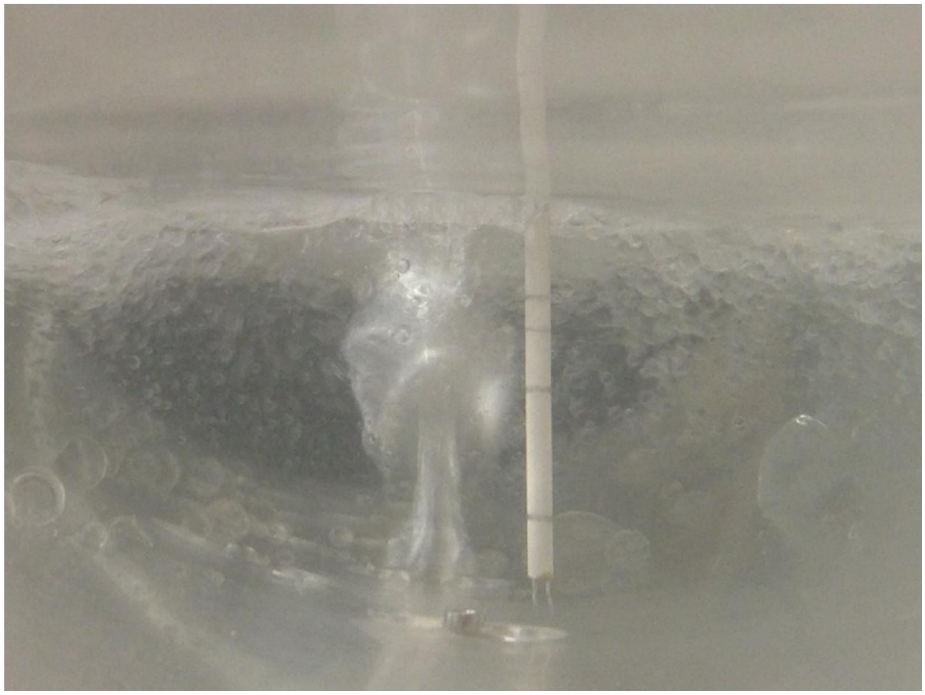

Figure 6-2 Oil droplets entrained in water during gas stirring

6.3 Results and discussion

6.3.1 Influence of water height

To investigate the influence of water height, the silicone oil II (50cSt) was used, and its height was fixed at 3 cm. As shown in Figure 6-3, despite large error bars on data dots, the mixing time of 3 cm oil still shows decreasing trend with water height at a given air flowrate and oil height. The solid circles in Figure 6-3 is calculated by empirical equation summarised in previous chapter Eq. (5.7). To compare the mixing time at the two conditions, it is found that the absolute mixing time of oil covered condition is much higher and the decreasing rate of mixing time against water height is much higher than the oil free condition. The oil free mixing time, however, is shown close to horizontal compared to the decreasing rate of oil covered condition.

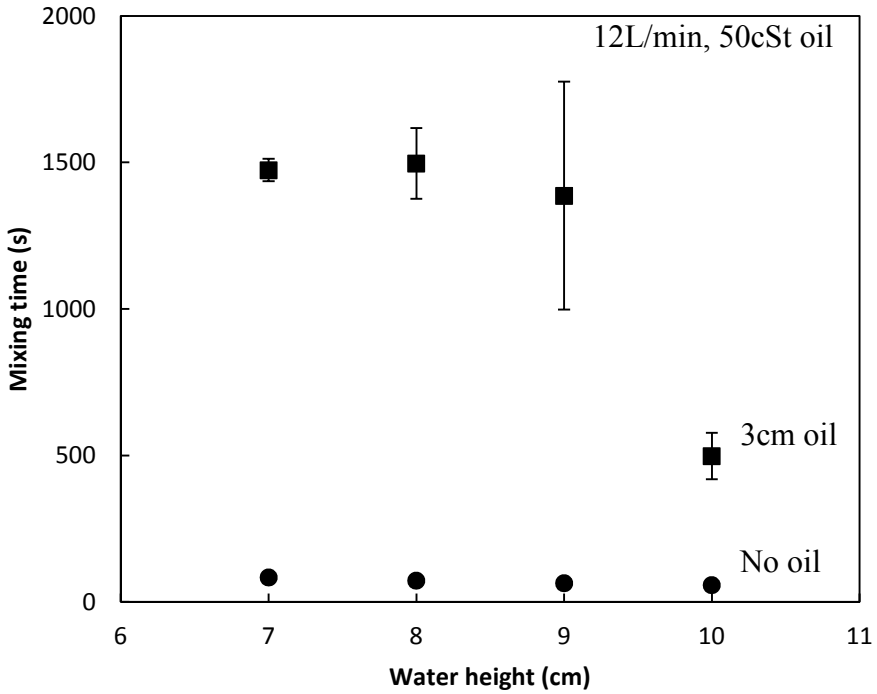

Figure 6-3 Comparison of oil covered and oil free mixing time against water height, 12L/min, 50cSt oil

6.3.2 Influence of air flowrate

To investigate the influence of gas flowrate, the silicone oil II (50cSt) is used, and its height was fixed at 3cm, and water depth was fixed at 7cm, while the gas flow rate was increased from minimum to maximum as shown in Table 6-2. The mixing time against flowrate is plotted in Figure 6-4. It is shown that at a certain water and oil layer height, the measured mixing time is much higher than the absence of oil layer, which is similar to the Figure 6-3. Likewise, the mixing time is decreasing much faster with flowrate compared to the absence of oil layer. The comparison of current study from oil free result is discussed in later sections.

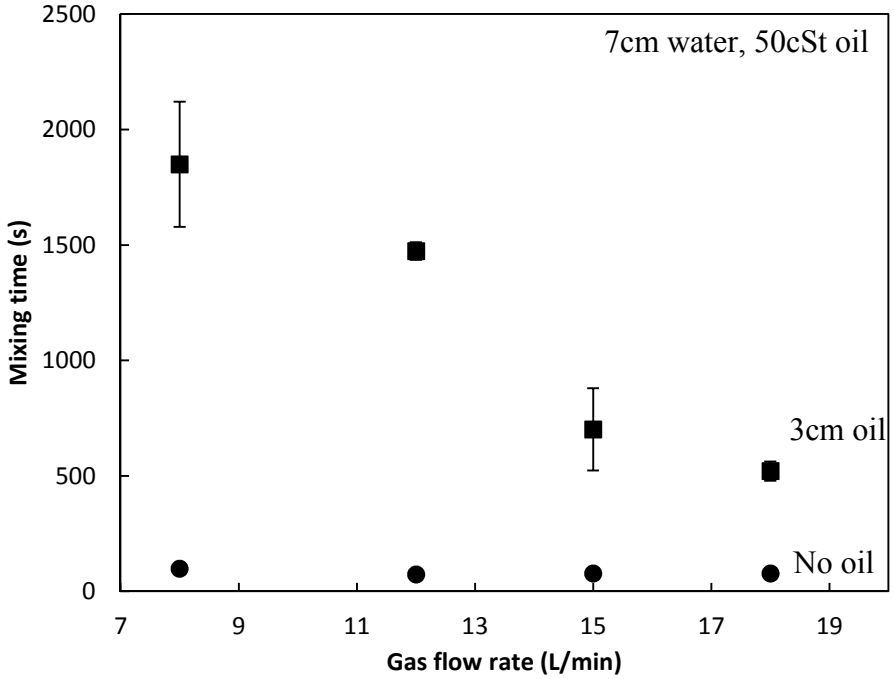

Figure 6-4 Comparison of oil covered and oil free mixing time against gas flowrate, 7cm water, 50cSt oil

6.3.3 Influence of oil height

The influence of oil height was investigated by setting water height 7cm, gas flowrate 12L/min, and using silicone oil II (50cSt). The oil height was changed from 1-3cm. The relationship of mixing time against oil height is shown in Figure 6-5, the mixing time is increasing fast with oil height. For comparison, the oil height in the current study is 14-42% of the water height, while the upper layer heights in most previous researchers' models were only around 10%. This means even the upper layer height reaches a greater range, it still exerts influence on the mixing behaviour of lower layer.

6.3.4 Influence of oil viscosity

The influence of oil viscosity was measured by setting water height 7 cm, oil height 3 cm, and gas flowrate 12L/min. The oils with different viscosities were used to carry out experiment. From silicone oil I to III, the viscosity was changed from 10 to 200cSt, and the result is shown in Figure 6-6. It is found that the mixing time is also increasing with oil viscosity, but the increasing rate is lower than oil height, which means the influence of oil viscosity is not as great as the layer height. Detailed comparison of these four variables is discussed in the following section.

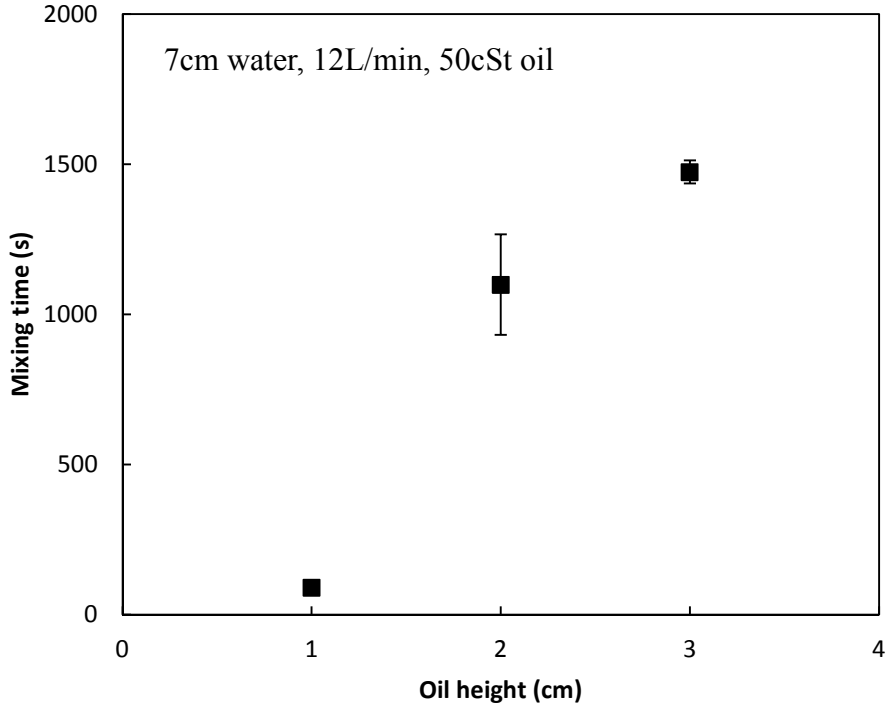

Figure 6-5 Oil covered mixing time against oil height, 7cm water, 12L/min, 50cSt oil

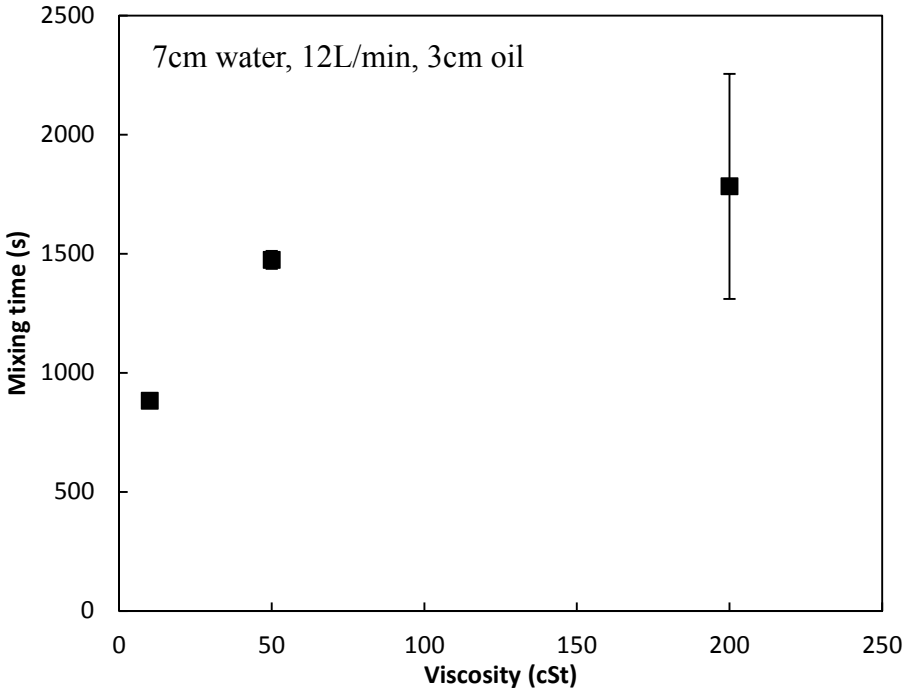

Figure 6-6 Oil covered mixing time against oil viscosity, 7cm water, 12L/min, 3cm oil

6.3.5 Correlation of mixing time with variables

Figure 6-3 to Figure 6-6 each shows the influence of each single variable on the mixing time of bottom blown furnace. To acquire a more general relationship for the better understanding of mixing behaviour in the presence of the upper layer, one needs to consider all variables together, *i. e.* the explicit form of Eq. (6.2). Figure 6-3 and Figure 6-4 show the relationship of the mixing time with water height and gas flowrate, respectively. It is evident that the absolute value of the mixing time with overlying oil is much longer than that of oil free. Meanwhile, though the mixing time with oil layer still shows a decreasing trend with respect to flowrate and water height, it is more sensitive to the change of the two variables than the oil free condition. Figure 6-5and Figure 6-6 show the influence of oil height and oil viscosity on mixing time. In both figures, the mixing time is showing increasing trend. From the absolute value of correlated exponent, it is found that mixing time is more sensitive to oil layer height than viscosity.

On the other hand, many data dots in Figure 6-3 to Figure 6-6 have large error bars, which indicate the experimental uncertainty is around ±30%. One possible reason is that the great gas flowrate emulsifies the overlying silicone oil and shatters oil into a large number of droplets with various sizes as shown in Figure 6-2, which affects the mixing of the water phase. These droplets are entrained into the water phase and flow with turbulence. Though some of them are able to return to oil layer by the buoyance and the flow upwards, a large number of droplets still constantly exist in the water phase due to continuous blowing. Therefore, the mixing behaviour in the water phase is always affected by these entrained oil droplets, which accordingly causes large experimental deviation. Another reason to account for the experimental uncertainty is that the rising plume onto which the tracer is charged oscillates from time to time. The oscillating or rotation of the plume which causes standing waves on bath surface has been discussed in previous study[25], but the oscillation of the plume in the presence of the oil layer needs further study. As a result, the intermittently unstable plume disperses tracer charged atop in a different manner each time, which consequently leads to large deviation by each experiment. In summary, in spite of the large deviation of each measurement, the statistical average mixing time under a certain experimental condition can be obtained by several repetitions.

Table 6-3 Experimental and predicted mixing time under different conditions

H m	Q m^3/s	h m	v_s m^2/s	Experimental mixing time τ s	Predicted mixing time τ s
0.07	0.0002	0.03	0.00005	1474	1320
0.08	0.0002	0.03	0.00005	1496	1076
0.09	0.0002	0.03	0.00005	1386	898
0.1	0.0002	0.03	0.00005	498	764
0.07	0.000133	0.03	0.00005	1849	2663
0.07	0.00025	0.03	0.00005	701	897
0.07	0.0003	0.03	0.00005	520	654
0.07	0.0002	0.01	0.00005	90	116
0.07	0.0002	0.02	0.00005	1099	539
0.07	0.0002	0.03	0.00001	881	902
0.07	0.0002	0.03	0.0002	1782	1832

To acquire the explicit form of Eq. (6.2), those four variables *H, Q, h,* v_s are correlated in an overall multiple regression, which provides:

$$\tau = 0.21H^{-1.53}Q^{-1.73}h^{2.21}v_s{}^{0.24} \qquad (6.5)$$

where the variables are in SI unit, and the R-square value is 0.715. The effectiveness of correlation is shown in Figure 6-7. Given the ±30% uncertainty of experiment due to transient of turbulence and the two possible additional mechanisms discussed above, this regression is reasonable. Hence, the relationship of mixing time against each variable can be plotted using the overall correlation, as shown in Figure 6-8 to Figure 6-11 . For better presenting the tendency of data, both of the axes are shown in logarithmic format. In these figures, a set of different experimental conditions was used to validate the prediction to confirm the prediction of Eq. (6.5), *e.g.* 18L/min gas flowrate or 1 cm oil height. It is found that in spite of deviation at several points, the Eq. (6.5) provides good prediction of mixing time under different conditions. The Figure 6-12 shows the set of 18 L/min and 1 cm oil height experiment to fit with Eq.(6.5). It is shown that the experimental result of 18 L/min and 1cm oil height is 1.17 times of Eq. (6.5) prediction, with R-square 0.704. Under such complicated mixing condition, this prediction is acceptable[7]. Therefore, Eq. (6.5) is an plausible empirical

equation derived from this lab-scale model to predict the mixing behaviour in the bottom blown copper smelting furnace.

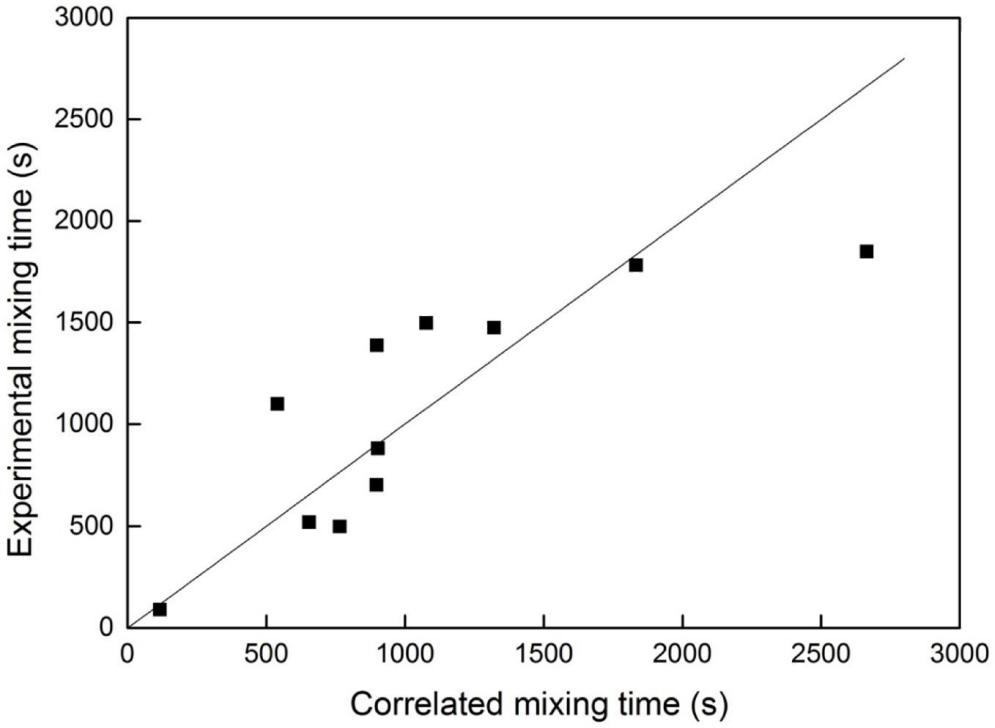

Figure 6-7 Effectiveness of regression to illustrate the adequacy of Eq. (6.5)

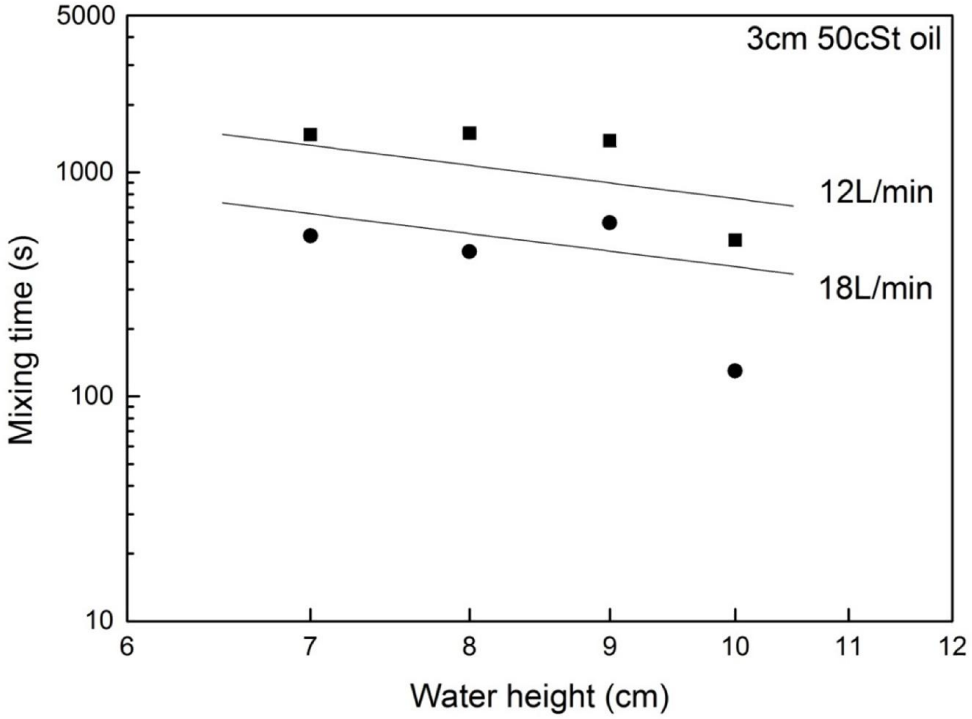

Figure 6-8 Comparison of experimental data and Eq. (6.5) against water height in log-log coordinate to illustrate the trend

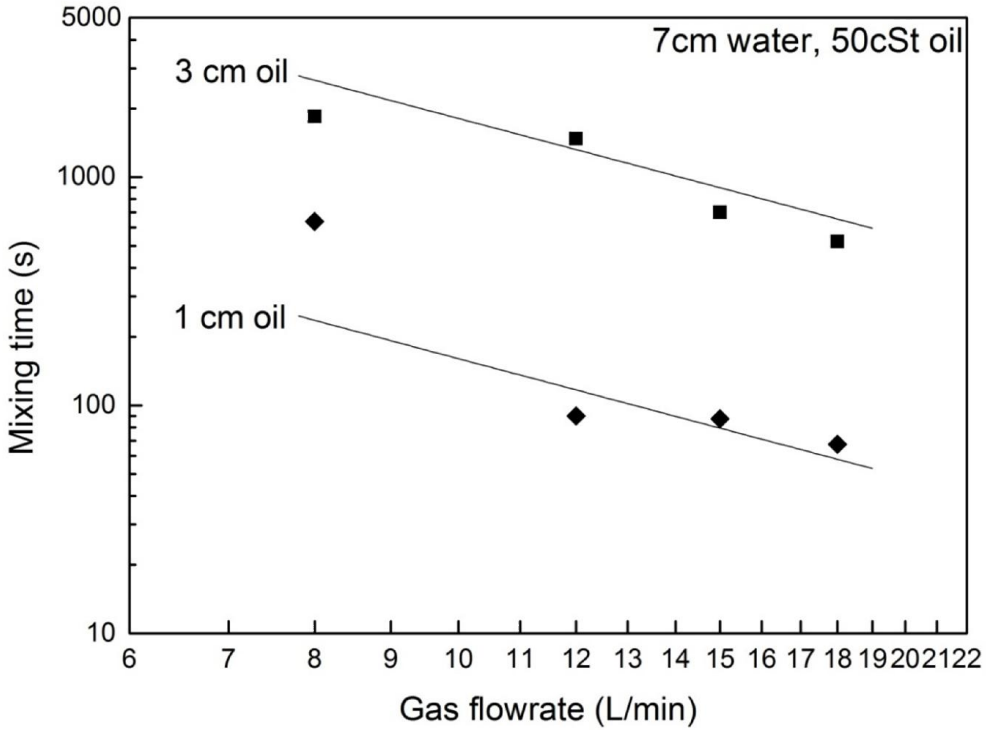

Figure 6-9 Comparison of experimental data and Eq. (6.5) against gas flowrate in log-log coordinate to illustrate the trend

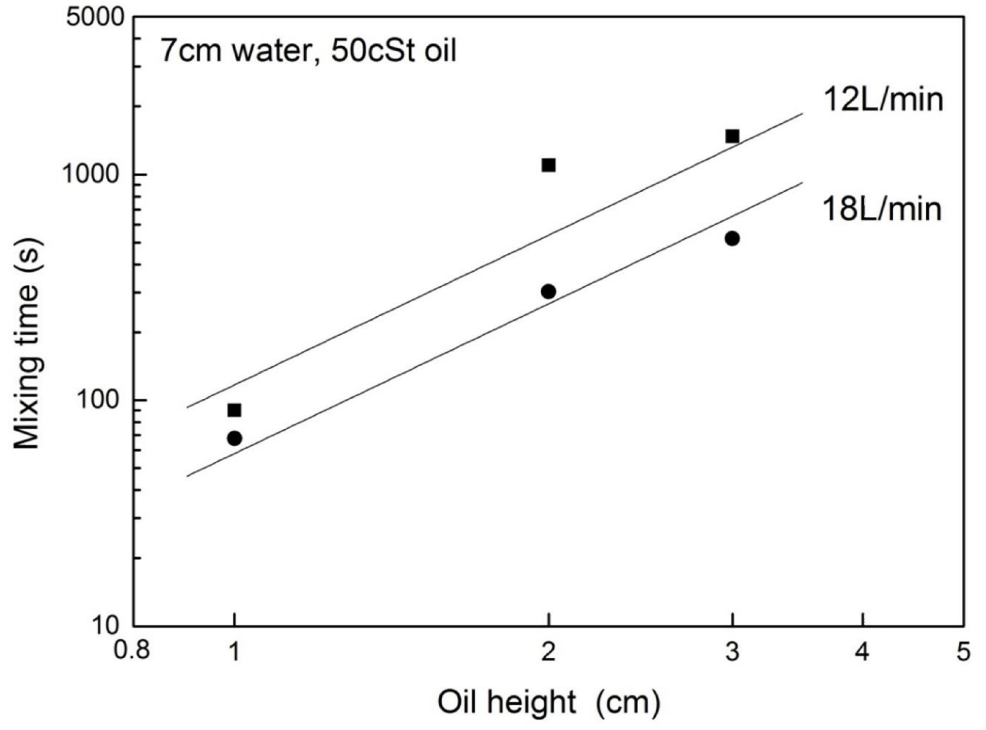

Figure 6-10 Comparison of experimental data and Eq. (6.5) against oil height in log-log coordinate to illustrate the trend

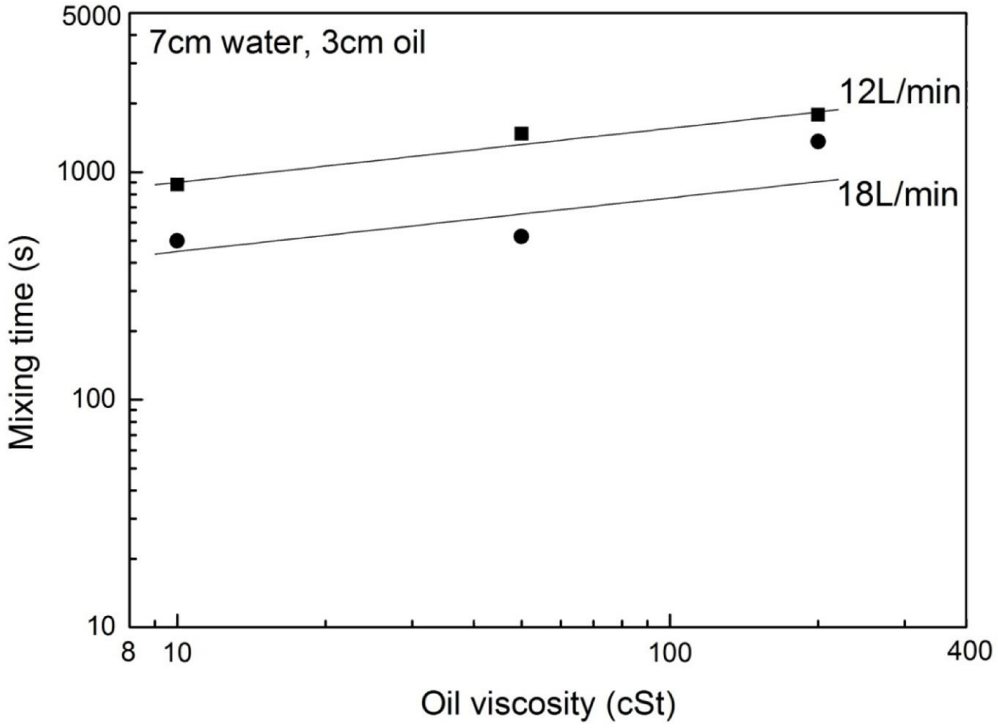

Figure 6-11 Comparison of experimental data and Eq. (6.5) against oil viscosity in log-log coordinate to illustrate the trend

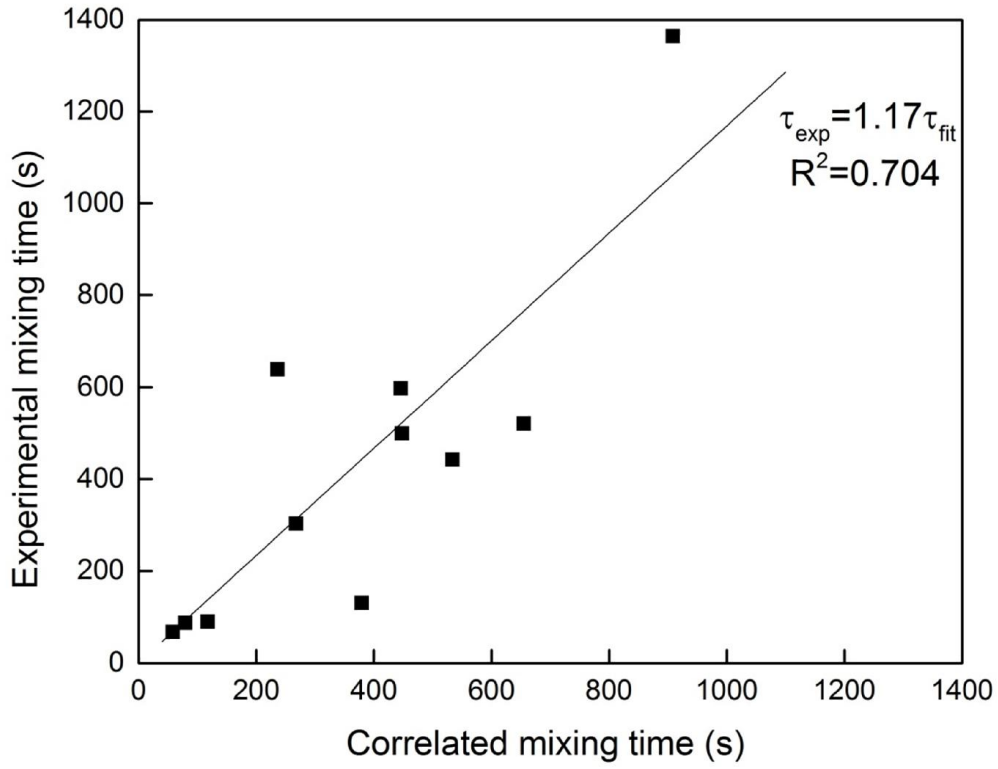

Figure 6-12 Validating the correlation by using different combination of variables

Table 6-4 Validating the effectiveness of correlation by using different combinations of variables

H m	Q m^3/s	h m	v_s m^2/s	Experimental mixing time τ s	Predicted mixing time τ s
0.07	0.0003	0.03	0.00005	520	654
0.08	0.0003	0.03	0.00005	442	533
0.09	0.0003	0.03	0.00005	597.5	445
0.1	0.0003	0.03	0.00005	130	379
0.07	0.000133	0.01	0.00005	639	235
0.07	0.0002	0.01	0.00005	90	116
0.07	0.00025	0.01	0.00005	87	79
0.07	0.0003	0.01	0.00005	67	57
0.07	0.0003	0.02	0.00005	302	267
0.07	0.0003	0.03	0.00001	499	447
0.07	0.0003	0.03	0.0002	1364	908

The effect of the water height and gas flowrate variation without an upper layer has been discussed in previous paper[1], and Eq.7 in the paper was given to summarise the relationship between mixing time and water height in the absence of an upper layer. Rearrange Eq. 7 in SI unit one obtains:

$$\tau = 0.17Q^{-0.39}H^{-1.08} \quad (6.6)$$

To compare Eq.(6.5) with Eq.(6.6), one may notice that the Eq.(6.6) was obtained when the monitoring electrode was placed at mid bath depth while Eq.(6.5) at bottom. However, as stated in the previous study, the mixing time measured at mid bath depth and bottom are quite close, given the electrode was fixed at 110mm from blowing lance. Taking this result in to account, Eq.(6.5) and Eq.(6.6) are comparable.

From Eq.(6.5) to Eq.(6.6), one may easily find that the mixing time is significantly increased, which indicates the remarkable influence exerted by the overlying phase on the mixing of the lower phase. In the case of present study, given height oil layer height and great gas flowrate, emulsion and phase entrainment take place extensively, which causes the mixing process prolonged as much as tenfold

more. Previous researchers Patil *et al.*[7] reported a relationship between the slag covered and the slag free mixing time in the axisymmetric steelmaking ladles, which was expressed:

$$\tau_{slag} = \tau_{slag-free} G \tag{6.7}$$

where,

$$G \approx 6\left(\frac{h}{H}\right)^{0.3} \nu_s^{0.033} \left(\frac{\rho_s}{\rho_L}\right)^{-0.044} \tag{6.8}$$

By embodying a factor *G*, the mixing time with a thin oil layer is linked with that of oil free under the same other conditions. Taking the parameters of experiment the authors reported into Eq.(6.8), one obtains $G \approx 2.2$, which indicates the mixing time with a thin upper layer is about twofold times of oil free. Noticeably, this relationship is only valid in steelmaking shaped vessels with (i) $0.5<H/D<2.0$, (ii) ε_m~0.01W/kg, and (iii) $\nu_L=10^{-6}m^2/s$. Under similar condition, Mazumdar and Guthrie[9] investigated the stirring energy dissipation by an overlying layer and reported the reversed flow formed at the plume eye that counteracts against the rising plume, which accordingly reduces bulk recirculation rate and prolongs mixing time. However, in the present study, the situation is considerably more complicated, as emulsion and phase entrainment are non-negligible. Simply taking present experimental parameters into Eq.(6.8), one obtains $G \approx 3.4$, which is far less than measured. Therefore, the empirical equation acquired in thin overlying layer model with low gas flowrate is not applicable in the bottom blown copper smelting furnace.

From Eq. (6.6) to Eq.(6.5), the absolute values of exponents on *H* is increased from1.08 to 1.53, which means the mixing time is more sensitive to the change of the water height in the presence of an oil layer. Furthermore, the absolute value of exponent on *Q* is also increased, from 0.39 to 1.73. Considering the exponent of *H* is still close to that of oil free, the increment of exponent on *Q* is considerably large. In most studies regarding to the relationship of mixing time against gas flowrate, the exponent is around -0.33 to -0.58. Even in the presence of upper layer, as Mazumdar[9]and Khajavi[20] reported, the correlated exponent is close to -0.33. Considering Khajavi's study was also conducted with a thick upper layer, the large exponent absolute value on *Q* of the present study is possibly caused by the special geometry of the furnace. The exponent on the overlying layer height *h* is of the greatest value among the four, which indicates the upper layer height is the most significant factor influencing mixing. As the sign is positive, it means the increasing upper layer

height leads to prolonged mixing time. This tendency is consistent with conclusions gained in cold models of steelmaking ladles except for a much greater absolute value. On the contrary, the absolute value of exponent on v_s is the smallest, which indicates the viscosity of the upper layer has the least influence on mixing. This conclusion agrees with previous studies done in cold models of steelmaking ladles.

6.4 Industrial application

Eq.(6.5) is correlated using the data acquired in the current lab-scale model with a fixed characteristic length radius R = 0.145 m. For more general use of this correlation, a model-independent format of equation should be induced. The Eq. (6.5) is acquired on the basis of Eq.(6.2), with the characteristic length of model R fixed. By applying Rayleigh's method of dimensional analysis and using R and g as independent dimensions[24], the Eq. (6.2) can be represented into

$$\frac{\tau}{R^{\frac{1}{2}}g^{-\frac{1}{2}}} = C_0\left(\frac{H}{R}\right)^a\left(\frac{Q}{R^{\frac{5}{2}}g^{\frac{1}{2}}}\right)^b\left(\frac{h}{R}\right)^c\left(\frac{\nu_s}{R^{\frac{3}{2}}g^{\frac{1}{2}}}\right)^d \qquad (6.9)$$

where on the right side in each bracket, it is a dimensionless variable corresponding to the original variable, and the term on left side is dimensionless mixing time. Constants C_0 a b c and d are determined by experiments, in which C_0 is dependent on experimental setup such as blowing lance angle, electrode location and definition of mixing time, while the value a b c and d indicate the influence of each dimensionless variable on the dimensionless mixing time[5,19].

By rearranging Eq. (6.5) into the format of Eq.(6.9), one obtains the dimensionless format

$$\frac{\tau}{R^{\frac{1}{2}}g^{-\frac{1}{2}}} = 182\left(\frac{H}{R}\right)^{-1.53}\left(\frac{Q}{R^{\frac{5}{2}}g^{\frac{1}{2}}}\right)^{-1.73}\left(\frac{h}{R}\right)^{2.21}\left(\frac{\nu_s}{R^{\frac{3}{2}}g^{\frac{1}{2}}}\right)^{0.24} \qquad (6.10)$$

Therefore, Eq. (6.10) provides the model-independent empirical relationship to predict mixing time in the bottom blown copper smelting furnace. Ideally, given fixed experimental setup including lance configuration, electrode location and so on, the dimensionless mixing time acquired in models

of different sizes should be equivalent, accordingly the mixing time in the prototype furnace can be predicted by

$$\frac{\tau_m}{R_m^{\frac{1}{2}} g^{-\frac{1}{2}}} = \frac{\tau_p}{R_p^{\frac{1}{2}} g^{-\frac{1}{2}}} \tag{6.11}$$

$$\frac{\tau_m}{\tau_p} = \left(\frac{R_m}{R_p}\right)^{\frac{1}{2}} = \lambda^{\frac{1}{2}} \tag{6.12}$$

In current study, λ=1/12, leading to

$$\tau_p = \tau_m \sqrt{12} \tag{6.13}$$

Thus Eq. (6.13) connected mixing time of the model with the prototype by geometrical ratio. In spite of complication of industrial practices such as high temperature, different physical properties of liquids, intensive chemical reactions, and so on, the equation as well as data obtained in the present study still provides a method to extrapolate the mixing behaviour in bottom blown copper smelting furnace.

For example, when water depth is 7 cm, gas flowrate 12 L/min, oil layer height 3 cm, and oil viscosity 50 cSt, the mixing time obtained in current model is 1474 s. Taking it into Eq.(6.13), it yields 5120 s, *i.e.* 85 min, which indicates that under normal smelting condition, the agitation of single lance blowing takes up to 85 min to drive the nearby molten bath reach homogeneity. This time is considerably long in industrial practice. Therefore, in such a large metallurgy reactor, the mass transfer driven by a single bottom lance blowing is too limited. Currently, Fangyuan plant sets up nine lances for blowing, but the configuration of lances is still an issue that requires further study in future.

To obtain optimal mass transfer in industrial practice, it is desirable to keep a relatively deeper matte layer and a lower slag layer. Probably it is an option to prolong the matte tapping interval and shorten the slag tapping interval. The high viscosity slag is detrimental to mass transfer in matte, but its effect is less concerned compared to the slag layer height. Therefore, the solid particles entrained in slag layer which increases apparent slag viscosity remarkably does not cause a big issue in mixing behaviour. Increasing gas flowrate is beneficial for the mixing, but it becomes less effective at large flowrate.

6.5 Conclusions

A lab-scale cold model study was carried out to investigate mixing behaviour with second layer in the bottom blown copper smelting furnace. Mixing time in this cold model was measured to examine the influence of operational variables on mixing in the presence of an upper layer. It was found that:

1) Mixing time is decreasing with increasing water height and gas flowrate like the trend of oil free, but the decreasing rate is faster, which means the mixing is more sensitive to the water height and flowrate change in the presence of the second phase.
2) Mixing time is increasing with increasing oil height and oil viscosity, but the increasing rate against oil height is much greater than against oil viscosity. This means the layer height of the second phase is the main factor that influences mixing rather than viscosity.
3) The following overall empirical relationship of mixing time is obtained from experiment, and it shows good prediction of mixing time under different conditions.

$$\tau = 0.21 H^{-1.53} Q^{-1.73} h^{2.21} {\nu_s}^{0.24} \qquad (6.5)$$

4) The prediction of mixing time is generalised to model-independent format, which provides guidelines for industrial operation of the bottom blown copper smelting furnace.

6.6 References

[1] L. Shui, Z. Cui, X. Ma, M. A. Rhamdhani, A. Nguyen, and B. Zhao: *Metall. Mater. Trans. B*, 2015, Vol. 46B, pp. 1218-1225.

[2] D. Mazumdar and R. I. L. Guthrie: *Metall. Trans. B,* 1986,Vol. 17B, pp.725-733.

[3] A. M. Amaro-Villeda, M. A. Ramirez-Argaez and A. N. Conejo: *ISIJ Int.*, 2014, Vol. 54, No. 1, pp. 1-8.

[4] L. T. Khajavi and M. Barati: *Metall. Trans. B*, 1982, vol.13B, pp. 193-202.

[5] J. Mandal, S. Patil, M. Madan and D. Mazumdar: *Metall. Trans. B*, 2005, Vol.36B, 479-487.

[6] S. H. Kim and R. J. Fruehan: *Metall. Trans. B*, 1987, Vol. 18B, 381-390.

[7] S. P. Patil, D. Satish, M. Peranandhanathan and D. Mazumdar: *ISIJ Int.*, 2010, Vol. 50, No. 8, pp. 1117-1124.

[8] D. Mazumdar, H. Nakajima, and R. I. L. Guthrie: *Metall. Trans. B,* 1988*,* Vol. 19B, pp. 507-511.

[9] D. Mazumdar and R. I. L. Guthrie: *Metall. Trans. B*, 2010, Vol. 41B, pp. 976-989.

[10] D. Mazumdar and J. W. Evans: *Metall. Trans. B*, 2004, Vol. 35B, pp. 400-404.

[11] K. Krishnapisharody and G. A. Irons: *Metall. Trans. B*, 2006, Vol. 37B, pp. 763-772.

[12] J. W. Han, S. H. Heo, D. H. Kam, B. D. You, J. J. Pak and H. S. Song: *ISIJ Int.*, 2001, Vol. 41, No. 10, pp. 1165-1173.

[13] K. Yonezawa and K. Schwerdtfeger: *Metall. Mater. Trans. B*, 1999,vol. 30B, pp. 655-60

[14] K. Yonezawa and K. Schwerdtfeger: *Metall. Mater. Trans. B*, 2000, vol. 31B, pp. 461-68.

[15] K. Yonezawa and K. Schwerdtfeger: *Metall. Mater. Trans. B*, 1999,vol. 30B, pp. 411-18.

[16] K. Yonezawa and K. Schwerdtfeger: *ISIJ Int.*, 2004,vol. 44, pp. 217-19.

[17] Subagyo, G.A. Brooks, and G.A. Irons: *ISIJ Int.*, 2003,vol. 43, pp. 262-65.

[18] D. Mazumdar and R. Guthrie: *Metall. Mater. Trans*. *B*, 2010,41B, pp.976-989.

[19] S. P. Patil, D. Satish, M. Peranandhanathan and D. Mazumdar: *ISIJ Int.*, 2010, Vol. 50, No. 8, pp. 1117-1124.

[20] L. T. Khajavi and M. Barati: *Metall. Mater. Trans*. *B*, 2010, 41B, pp. 86-93.

[21] Z. Cui, D. Shen, and Z. Wang: *You Se Jin Shu[Nonferrous Metals]*, 2010, No. 3, pp. 17-20.

[22] B. Zhao, Z. Cui, and Z. Wang: *Int. Symp. High-Temp. Metall. Process.*, 4th, 2013, pp. 1-10.

[23] M. Chen and B. Zhao: *Proceeding of Copper-Cobre 2013*, Santiago, Chile, 2013, pp. 799-812.

[24] J. Szekely: Fluid Flow Phenomena in Metals Processing, 1979, Academic Press INC, New York, NY, USA, pp.392-418.

[25] L. Shui, Z. Cui, X. Ma, M. A. Rhamdhani, A. Nguyen, and B. Zhao: *Metall. Mater. Trans*. *B*, 2015, In Press.

7 Surface standing wave formation in bottom blown copper smelting furnace

Abstract The waves formed on bath surface play important role in the bottom blown copper smelting furnace operations. Simulation experiments have been carried out on model of the bottom blown furnace to investigate features of the waves formed on bath surface. It was found that the ripples, the 1st asymmetric standing wave and the 1st symmetric standing wave were able to occur in this model, and empirical occurrence boundaries have been determined. The amplitude and frequency of the standing waves have been systematically investigated. It was found that the amplitude of the 1st asymmetric standing wave is much greater than the 1st symmetric standing wave and the ripples; and the amplitude is found to increase with increasing bath height and flowrate but decrease with blowing angle. The frequency of the 1st asymmetric standing wave is found increasing with bath height but independent of flowrate and blowing angle.

Key words: copper smelting, bottom blown, water model, surface wave, bath oscillation

7.1 Introduction

Gas bottom injection has been widely applied in metallurgical processes, such as steelmaking converter and ladle refining. The injection creates gas-liquid two-phase plume zone above the orifice and the rising of the plume drives recirculation of liquid in the vessel. This circulating flow of liquid phase enhances the mixing and chemical reactions in the liquid greatly [1-2]. Meanwhile, the rising plume is able to set up bath sloshing motion in upright cylindrical container or standing waves in Peirce-Smith converter. It was reported that the liquid in the container is violently agitated which brings powerful mixing in bath at the presence of sloshing or standing waves. On the other hand, spitting, splashing and refractory abrasion were also found corresponded to this phenomenon[3-12].

One of the earliest reports of this phenomenon was given by Thomas[3], who studied the relationship between bath sloshing motion and its influence on the ejection of molten metal in steelmaking converter. The author also noticed abrasion of the refractory material with presence of this

phenomenon. Later researchers [4-6] found in water model that the sloshing of bath was created by rotating of gas plume which only occurs when the gas flowrate is above a critical value. It was also found that this rotation wave is determined by gas flowrate, bath depth and nozzle configuration. Schwarz [7-8] proposed a mechanism of the bath sloshing motion. According to this mechanism, the sloshing motion is occurring when the buoyancy force on bubbles which are displaced from the centre line as a result of the oscillation is sufficient to sustain the oscillation. A mathematical model of this mechanism was also developed to predict period and amplitude of the sloshing motion. Xie and Oeters[9-10] studied wave motion quantitatively in water/air ladle model and Wood's metal /nitrogen ladle. They investigated the critical condition of oscillation occurrence, and used simple pendulum model to predict period and amplitude of bath oscillation. Iguchi [11-12] classified sloshing motion of bath in upright cylindrical container into two types by ratio of bath depth over diameter, and then gave four sub-boundaries of its occurrence condition.

Similar bath sloshing was also reported in horizontal cylindrical containers like copper Peirce-Smith converter. In such vessels, the geometry of bath is different from steelmaking ladles and the gas injection is not absolutely from bottom but with some offset angles, instead. Different geometries of container and offset of blowing angle made the bath motion appear differently from that in upright cylindrical container. Kootz and Gille [13] found in their model of Pierce-Smith converter that there were 3 general types of surface motions. They were termed (1) the 1st asymmetric standing wave, (2) the 1st symmetric standing wave and (3) the 2nd asymmetric standing wave, as shown in Figure 7-1.

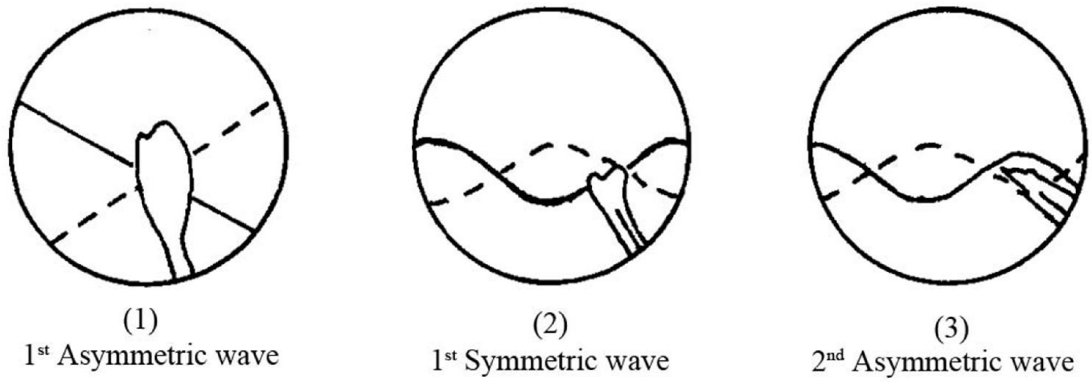

Figure 7-1 Definitions of the wave types in the PS converter model of Kootz and Gille[13]

Richards[14] studied slopping and splashing of copper Peirce-Smith converter in a 1/4th scaled

sectional model with geometry Ø762 ×265 mm. It was found that a "standing wave" appears abruptly at a critical buoyancy power per unit mass. This standing wave is related to splashing and hence limitations on converter capacity. Liow and Gray [15-17] continued this study in water model and found that the occurrence of a standing wave was found to be determined by the bath depth and tuyere submergence.

Researches related to bath sloshing have been done in upright cylindrical containers and Peirce-Smith converters, but little information was found in large horizontal channelled reactors such as bottom blown copper smelting furnace.

7.2 Experimental methodology

7.2.1 General procedure for observation of standing waves occurrence

To investigate the condition under which the standing wave was occurring in bottom blown copper smelting furnace, gas flowrate, lance angle and bath depth were adjusted as variables. For the sake of simplicity, the present study focuses on the effect of single lance blowing, so only the 1st lance from left side in Figure 7-2 was used for gas injection.

Figure 7-2 the 1/12 lab scale model used in this study

For each bath height and lance angle, air with a fixed flowrate was blown into the bath to examine if the 1st asymmetric standing wave occurred. Prior to starting, a period of 5 min was needed for the

bath to calm down. Upon starting, air flow was turned on and smoothly increased to the fixed value to avoid sudden gas surge. The bath was stirred constantly for 20 min at each flowrate to ensure the motion of bath reached steady, and then a video recorder was employed to record bath motion for analysis. After each experiment, the model furnace was drained and refilled fresh water for the next experiment, because the motion of bath took a long time to calm down and may affect next experiment. The lowest flowrate used was 150 mL/s. If one flowrate could not generate the 1st asymmetric standing wave during 20 min, a greater flowrate would be used in the next experiment, until it reached the value at which the 1st asymmetric standing wave occurred or the maximum 550 mL/s.

7.2.2 Measurement of wave amplitude

The amplitude of wave is defined as the height from still water surface to the highest point that bath surface can reach by blowing as shown in Figure 7-3. A ruler was fixed on the tapping end wall of the furnace for this measurement. Under each experimental condition, 20 min blowing was required for bath motion to reach steady, and then a video camera was used to record the wave at tapping end. Amplitude of wave was measured from the video recording, and the height of 30 continuous peaks of the wave was collected to obtain the average amplitude.

7.2.3 Measurement of wave frequency

When the standing wave was occurring, the motion of wave was also recorded. By slowing down playback speed, the time for the standing wave to complete 30 vibrations was counted, and its average wave frequency was determined as the reciprocal of this time divided by 30.

7.3 Results and discussions

7.3.1 Occurrence condition of standing waves

At a given bath depth and lance angle, flowrate was increased by 33mL/s in each experiment, until the critical flowrate was found. Then the bath depth and lance angle were varied to investigate wave shapes under different physical conditions. As a result, three different shapes of wave were observed: ripples only, the 1st asymmetric standing wave and 1st symmetric standing wave as shown in Figure 7-1, which is consistent with Kootz and Gille's work [13]. However, the occurrence of 2nd

asymmetric standing wave reported in their study was not observed in the present study.

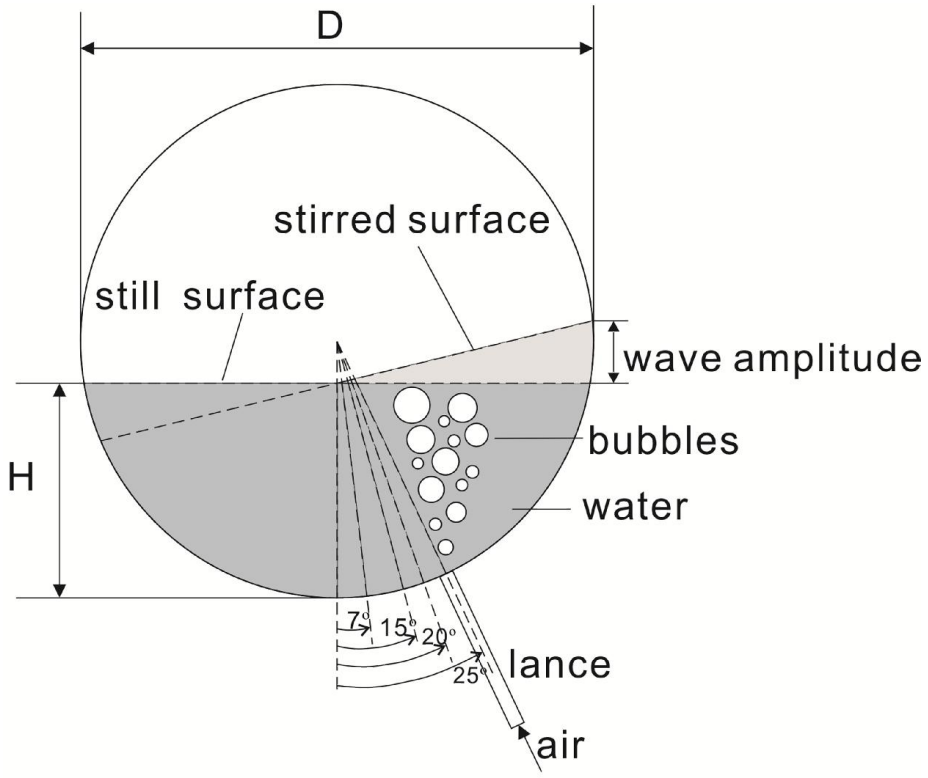

Figure 7-3 Schematic diagram of lance angle adjustment in experiment

When lance angle was 7º, 15º or 20º, at low flowrates, the gas plume was rising almost vertically from bottom to surface, creating small peaks and troughs on surface, as shown in Figure 7-4 (a). It was termed "ripples only" to distinguish from the latter two shapes. The ripples created by plume were propagating towards the tapping end Figure 7-4 (b), which made the surface shape alike. When the flowrate exceeded a certain critical value, the plume started to rotate around the lance tip. This rotating motion of plume was so intensive that the bath was quickly driven following this rotatory trend. However the rotation of entire bath did not occur because the length of furnace is much greater than its width, which made the bath swirling in upright cylindrical container difficult to form in this container. Instead, the bath was swinging from one side to the other at the same frequency of the rotating plume forming the 1st asymmetric standing wave, as shown in Figure 7-4 (c). This asymmetric standing wave was also intensive enough to transmit to the tapping end and forced the bath surface there to form the same standing wave at the same frequency (Figure 7-4 (d)), in an opposite phase. During this motion, the entire bath was swinging uniformly and an analogous motion of bath was reported by previous researchers when a container of water was moving back and forth in a horizontal line in a harmonic motion[18]. Greater amplitude was observed and splashes

occurred frequently on the surface of the bath.

When the lance angle was 25º, at low flowrates, only ripples were observed, but at greater flowrate the plume started to rotate as well. However, as the angle offset was larger than previous experiments, this rotation was stirring the bath in a different manner, resulted in the appearance of the 1st symmetric standing wave (Figure 7-4 (e)). Compared to the 1st asymmetric wave, the 1st symmetric standing wave did not occur abruptly after gas flowrate reached a clear critical value. On the contrary, it firstly appeared with ripples and gradually became more distinguished with increasing flowrate. In addition, as the length of furnace was much greater than PS converter, the wave shape at feed end may not be the same as tapping end. Although this 1st symmetric standing wave was distinguishable at feed end, it was not able to transmit to tap end (Figure 7-4 (f)), where there were only small ripples on bath surface like shown in Figure 7-4 (b).

It was noticed that the behaviour of rising plume was closely associated with the occurrence of the 1st asymmetric and 1st symmetric standing waves. When flowrate was low and plume was rising directly upward, it did not create large rises and falls of bath surface. There were only ripples on bath surface. However, when the plume started to rotate, it led to the rise of bath surface at one side and fall on the other side. Especially, if the blowing lance was located at the centre of the bottom or a small offset from the centre, it led to half bath rising and the other falling which is the 1st asymmetric standing wave as shown in Figure 7-5. On the contrary, if the blowing lance was offset from the centre at a large angle, 25º for example, the rotating plume only reached the middle of the bath and made the middle part rise and fall, and the opposite side of the bath was forced to follow the rise and fall of middle part so the 1st symmetric standing wave was formed, as shown in Figure 7-6.

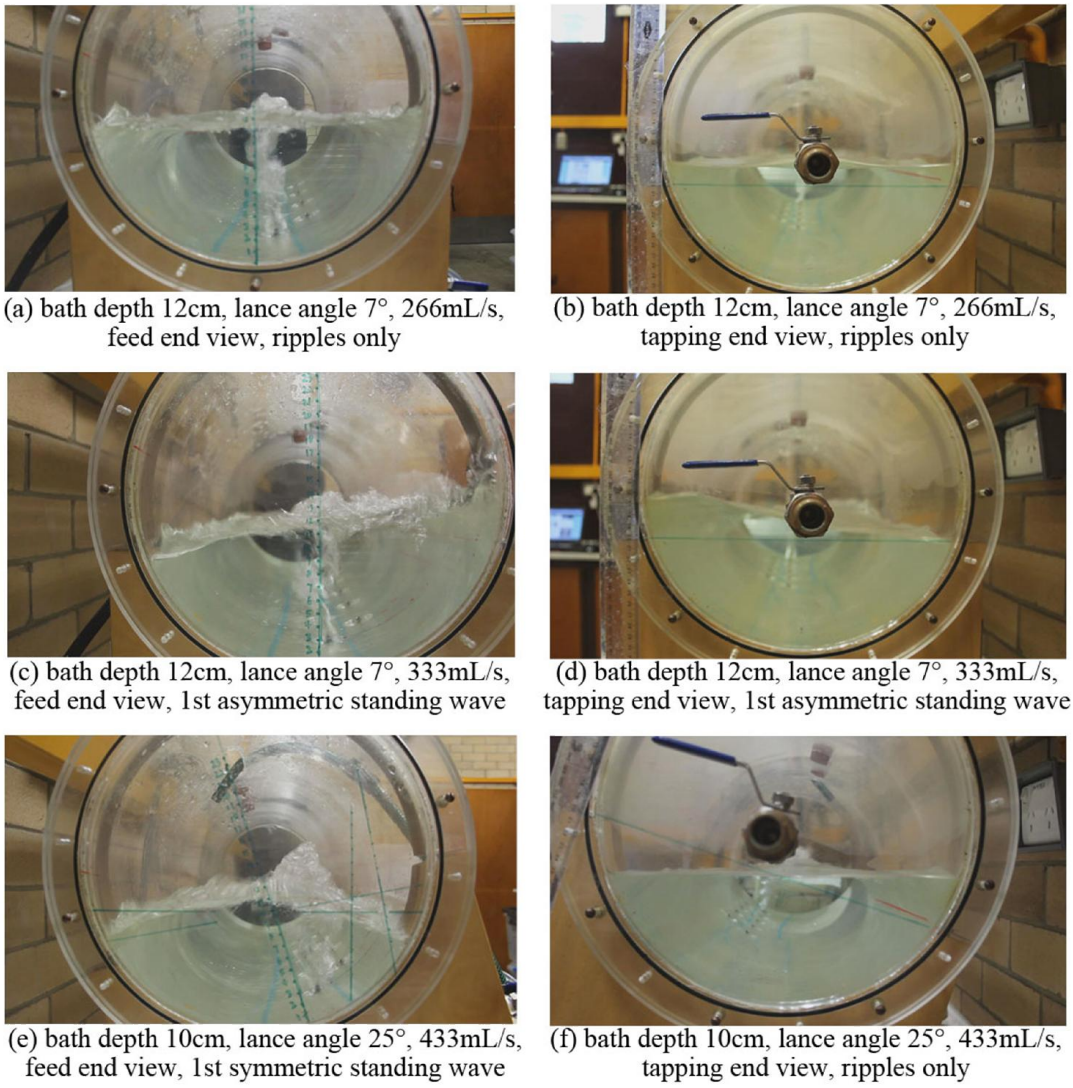

(a) bath depth 12cm, lance angle 7°, 266mL/s, feed end view, ripples only

(b) bath depth 12cm, lance angle 7°, 266mL/s, tapping end view, ripples only

(c) bath depth 12cm, lance angle 7°, 333mL/s, feed end view, 1st asymmetric standing wave

(d) bath depth 12cm, lance angle 7°, 333mL/s, tapping end view, 1st asymmetric standing wave

(e) bath depth 10cm, lance angle 25°, 433mL/s, feed end view, 1st symmetric standing wave

(f) bath depth 10cm, lance angle 25°, 433mL/s, tapping end view, ripples only

Figure 7-4 Typical shapes of wave at feed end and tapping end

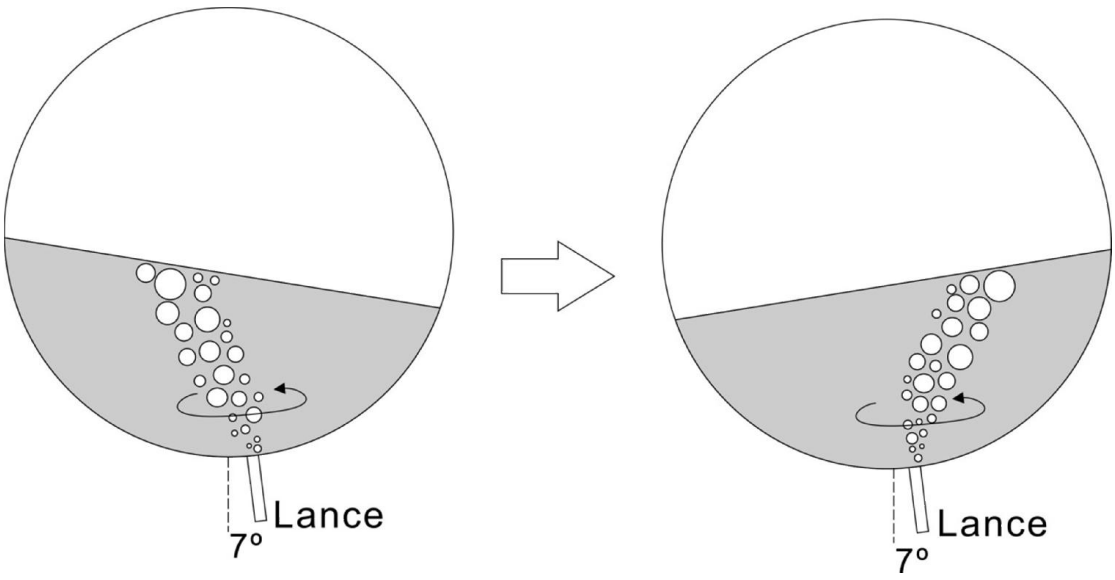

Figure 7-5 Formation of the 1st asymmetric standing wave (1st AS wave)

In the present study, the occurrence condition of the 1st asymmetric standing wave when blowing angle is less than 20º can be described by two sub-boundaries which are combinations of aspect ratio and flowrate.

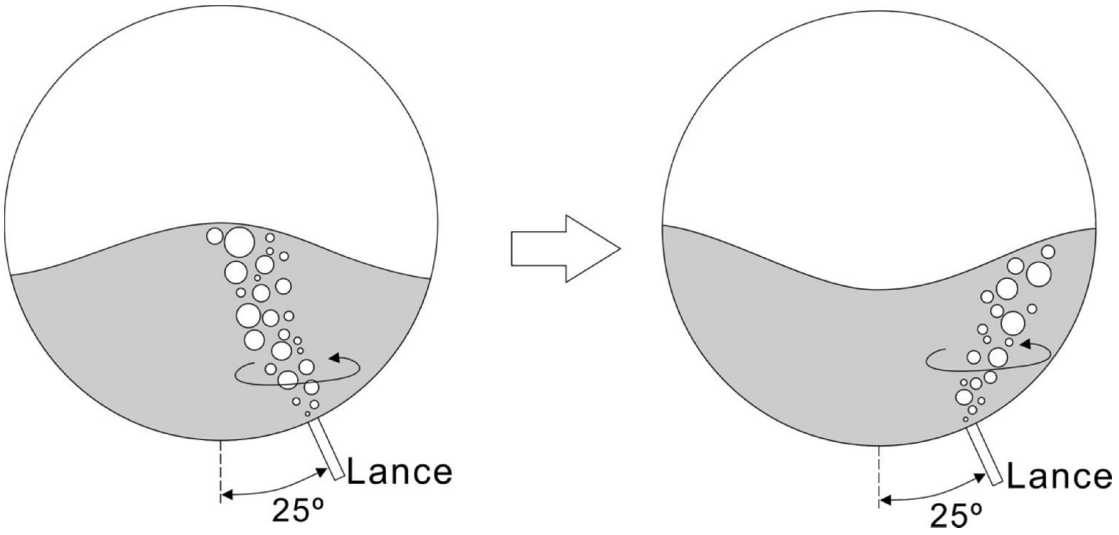

Figure 7-6 Formation of the 1st symmetric standing wave (1st S wave)

Sub-boundary 1

According to Iguchi's[12] study in a vertical cylindrical container, the Sub-boundary 1 can be expressed in terms of aspect ratio H/D and a modified Froude number Fr_{mD},

$$\frac{H}{D} = 0.036 Fr_{mD}^{-0.1} \alpha^{0.084} \tag{7.1}$$

Where Fr_{mD} is dimensionless number expressed in term of gas flowrate,

$$Fr_{mD} = \frac{Q_g^2}{gD^5} \tag{7.2}$$

and Q_g is the gas flowrate (mL/s), D is the container inner diameter (cm), α is the blowing angle offset from vertical line (radian), and g is the acceleration of gravity (980 cm/s^2).

Sub-boundary 2

A correlation based on modified Weber number was given in vertical cylinder container. Likewise, in correlation of bottom blown copper smelting furnace, modified Weber number was also used.

$$\frac{H}{D} = 0.63 We^{0.44} \alpha^{-0.39} \tag{7.3}$$

where We is dimensionless number

$$We = \frac{\rho_L Q_g^2}{\sigma D^3} \tag{7.4}$$

ρ_L is the liquid density (kg/m^3), σ is the surface tension of liquid (dyn/cm), D is the container inner diameter (mm), Q_g is the gas flowrate (mL/s).

Figure 7-7 shows the conditions for the occurrence of the 1st asymmetric standing waves. The solid curves show the correlated boundaries while dots show the experimental results. It can be seen that, in general, the boundaries of different blowing angles are alike in shape. On the right side of the boundary, the 1st asymmetric standing wave is present, while on the left side there are only minor ripples. Plotting results of three angles together with Iguchi's in Figure 7-8, it is found that the region for the occurrence of the 1st asymmetric standing waves is shifted to higher gas flowrate as the angle of blowing is increased. Iguchi[11-12] investigated the wave shapes in upright cylindrical containers, and proposed four sub-boundaries to describe the occurrence of rotary wave of bath. In the present study, the standing waves are also created by the rotary motion of uprising plume, so the boundary lines of occurrence condition are similar in shape. The sub-boundary 1 in the present study is close to that in the case of upright container, i.e. a horizontal boundary line at value equal to H/D =0.3 where below this line no standing wave or bath swirling occurs. The sub-boundary 2 also follows a similar increasing trend with that of upright cylindrical container, which means that larger bath depth requires greater flowrate to create the 1st asymmetric standing wave. However, as the geometry of furnace and smelting condition are different, the boundary lines are more complicated compared to that of upright cylindrical container. When the aspect ratio was increased to 0.5, the shape of the wave was limited by the geometry of furnace and became difficult to recognize. This does not happen in an upright container so the sub-boundary 2 trends can extend further. Additionally, Iguchi also reported a sub-boundary 3 when H/D> 1 and a sub-boundary 4 at far greater We. In the present study, sub-boundary 3 is not considered because the aspect ratio never exceeds 0.5 in bottom blown copper smelting furnace; and sub-boundary 4 requires far too great flowrate to reach, so it is not considered, either.

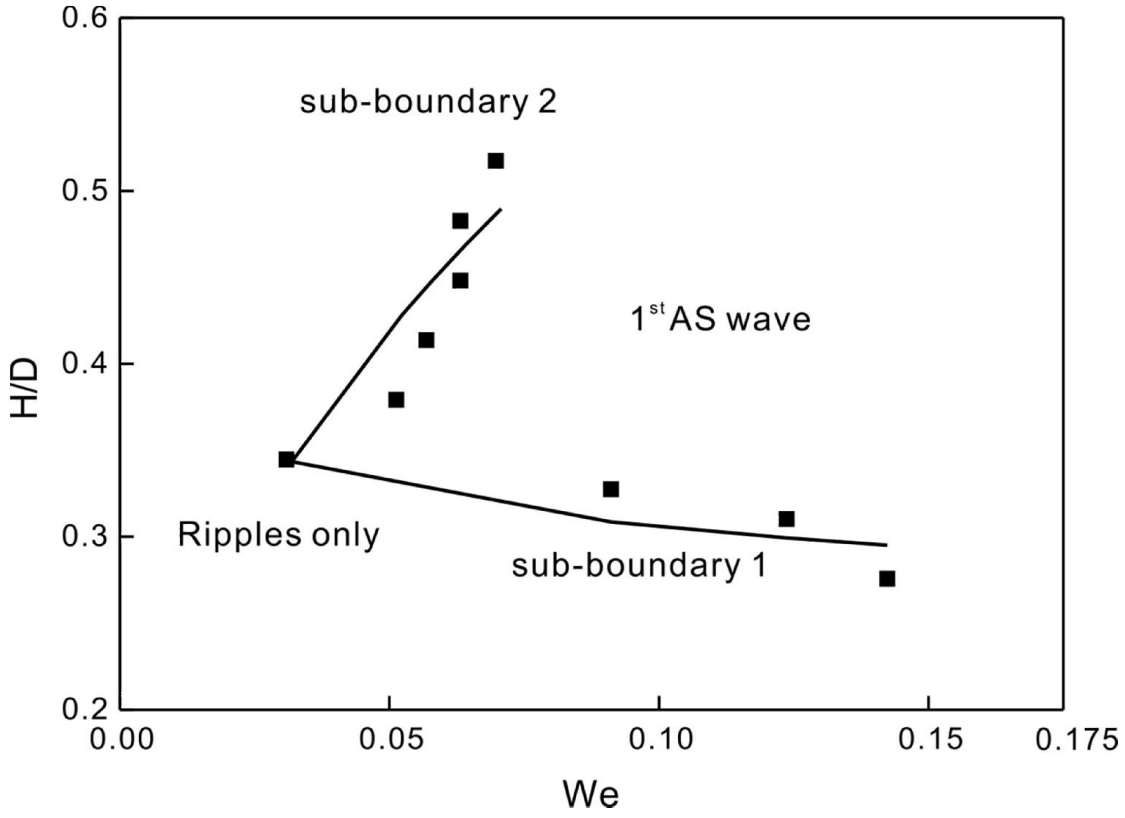
sub-boundary 2
1st AS wave
Ripples only
sub-boundary 1
H/D
We
0.6
0.5
0.4
0.3
0.2
0.00
0.05
0.10
0.15
0.175

(a) 7º

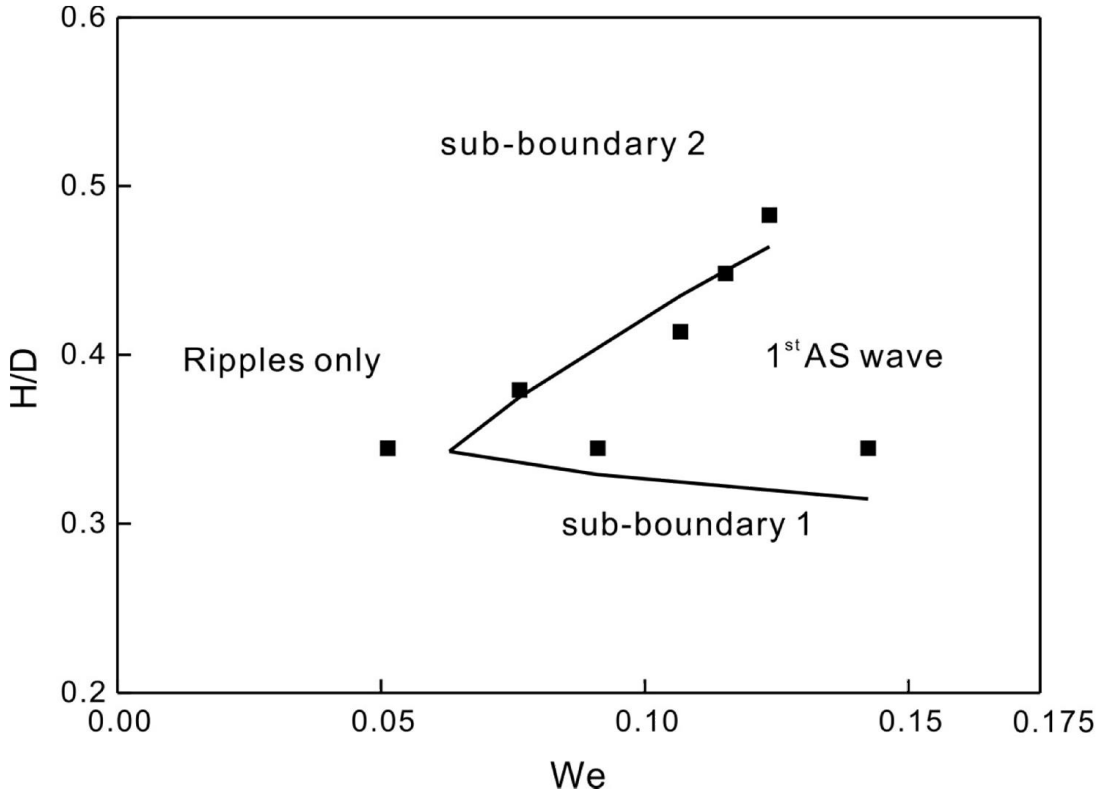
sub-boundary 2
Ripples only
1st AS wave
sub-boundary 1
H/D
We
0.6
0.5
0.4
0.3
0.2
0.00
0.05
0.10
0.15
0.175

(b) 15º

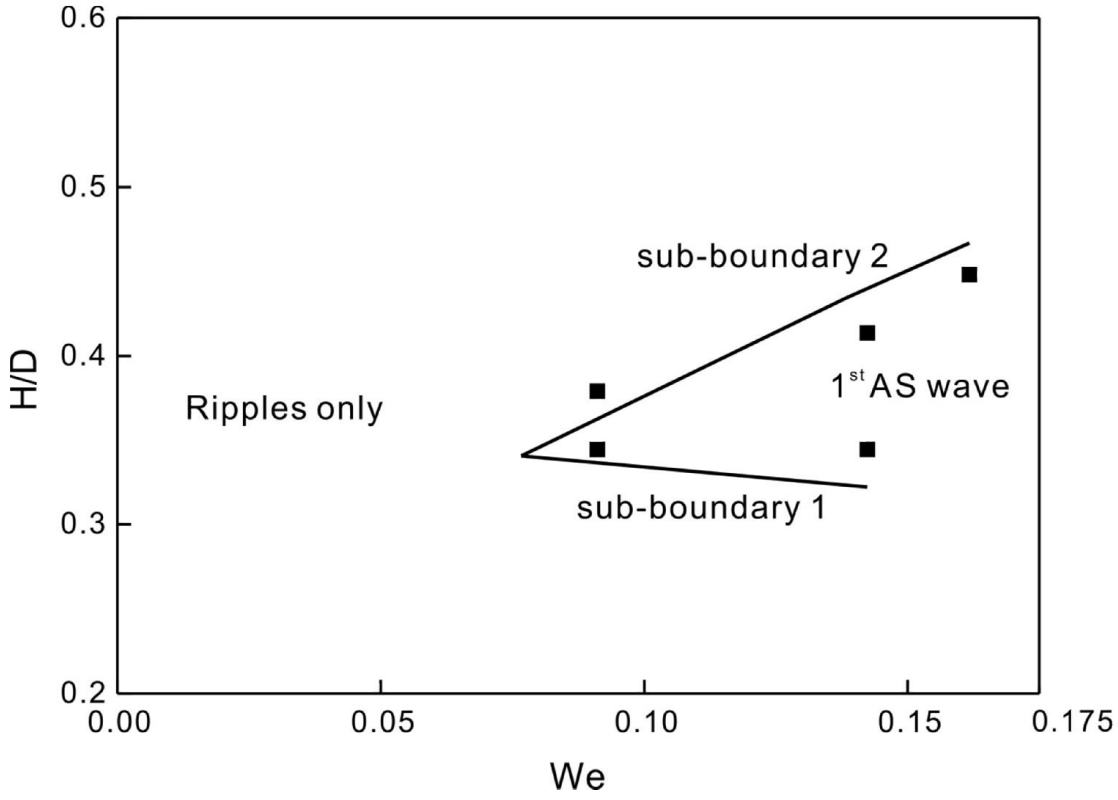

(c) 20º

Figure 7-7 Occurrence condition of the 1st asymmetric standing wave at (a) 7º, (b) 15º and (c) 20º blowing

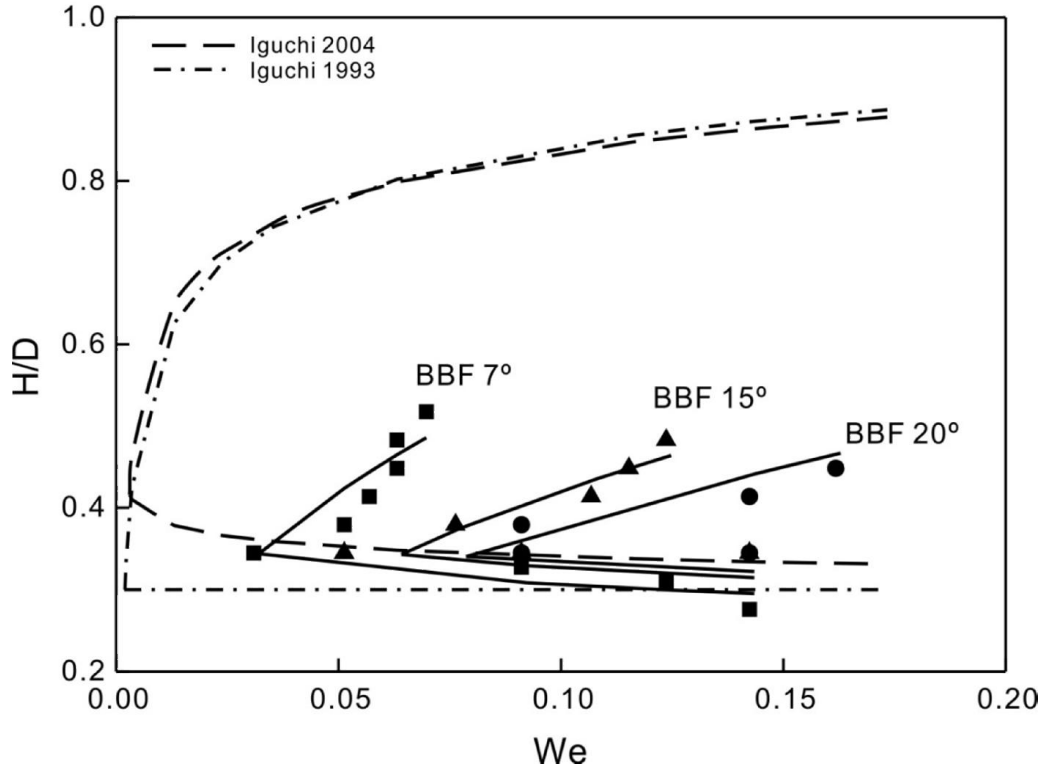

Figure 7-8 The 1st AS wave boundary in BBF model compared with Iguchi's boundary in upright cylindrical container

When the blowing angle was increased to 25º, the 1st asymmetric wave did not occur anymore. Instead, the 1st symmetric wave was present at certain combination of aspect ratio and flowrate. The 1st symmetric wave did not occur as suddenly as 1st asymmetric wave but gradually became more distinguishable, so its boundary curve was blurred. Figure 7-9 show approximate boundary of the 1st symmetric wave of blowing at 25º angle.

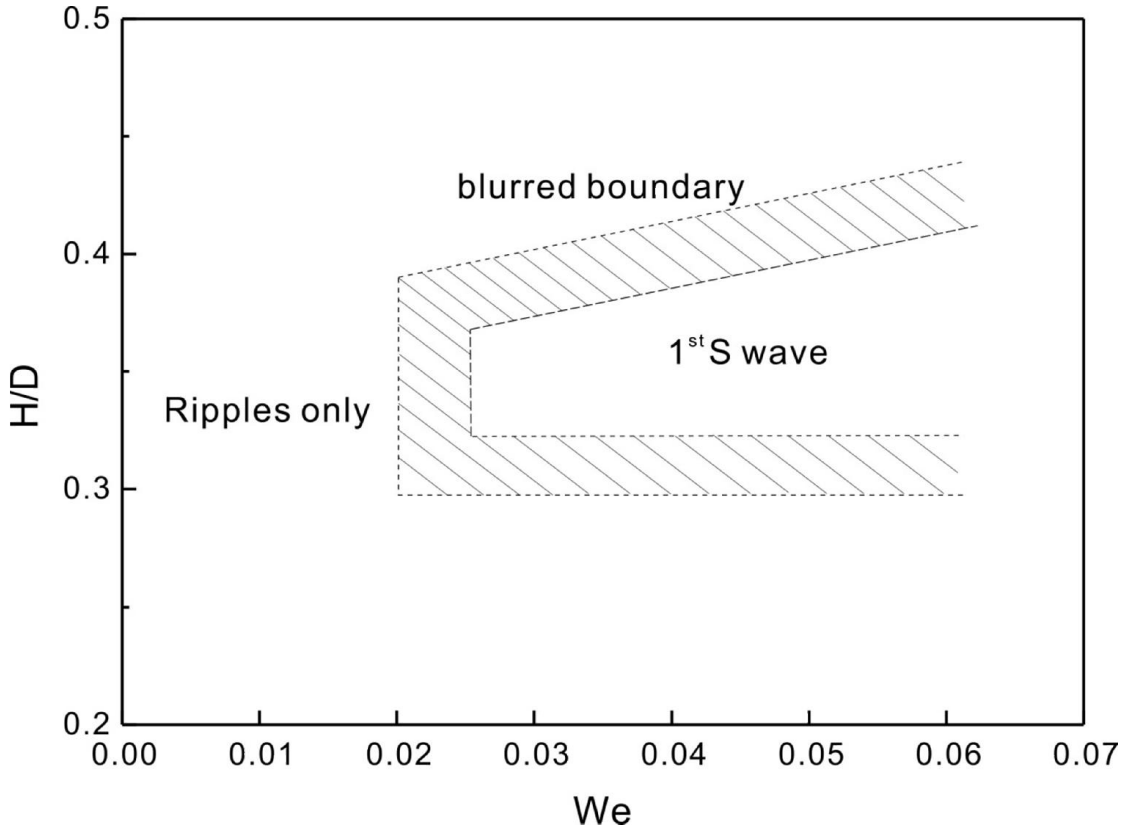

Figure 7-9 Approximate occurrence condition of the 1st symmetric standing wave at 25º blowing

7.3.2 Wave amplitude

Experimental result showed that the amplitude of wave was significantly relevant with the shape of wave. Taking the 7º blowing for example, when the bath depth was 7cm (H/D =0.24), referring to Figure 7-7 (a) there were only ripples from minimum to maximum flowrate, so the amplitude is small and increasing slowly with flowrate as shown in Figure 7-10 (a). When the bath depth was increased to 10cm (H/D =0.34), the amplitude measured was much higher than that of 7cm, and was increasing faster with flowrate. It was because, as shown in Figure 7-7 (a), the 1st asymmetric standing wave was present since 233mL/s (We=0.03) at 10cm bath depth (H/D =0.34), so this standing wave was present in the whole range of Figure 7-10 (a), which accordingly brought up amplitude to the extent much higher than the H/D =0.24. When the bath depth was increased to

13cm (H/D =0.45), referring to Figure 7-7 (a), it was found that the 1st asymmetric standing wave was present since 333mL/s (We=0.063). Therefore, as shown in Figure 7-10 (a), the first two dots of H/D =0.45 where the flowrate was lower than 333mL/s were much lower than the latter ones and close to that of H/D =0.24. Contrarily, when the flowrate was increased to 333mL/s and greater, the 1st asymmetric standing wave occurred, so a big rise was shown from the second dot to the third dot of the H/D =0.45 curve in Figure 7-10 (a). Regarding the 1st symmetric standing wave created by 25º blowing, as shown in Figure 7-10 (d), the amplitude was as small as that of ripples, even though the 13cm bath depth (H/D =0.45) curve rose faster than the other two, it was still much lower compared to those of other angles.

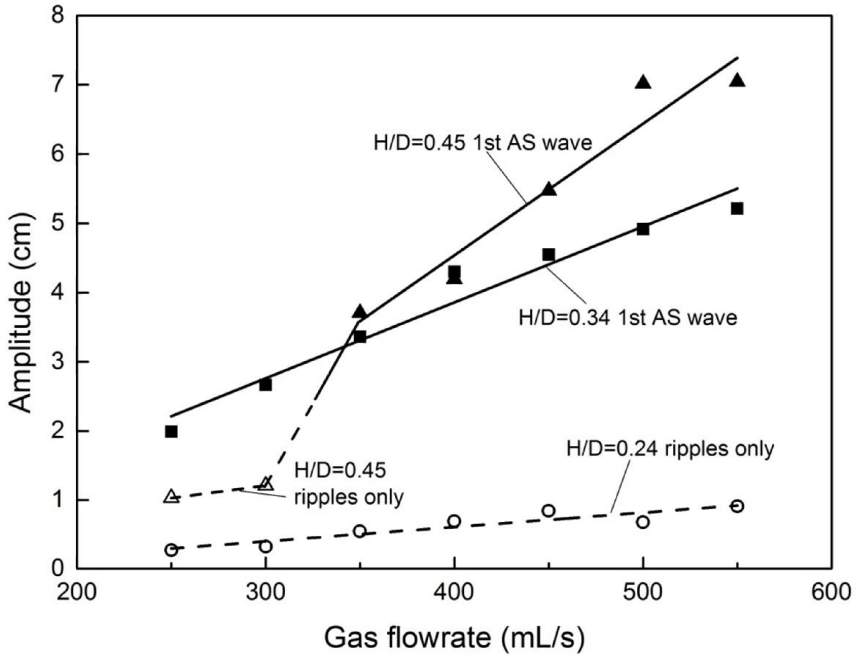

(a) 7º

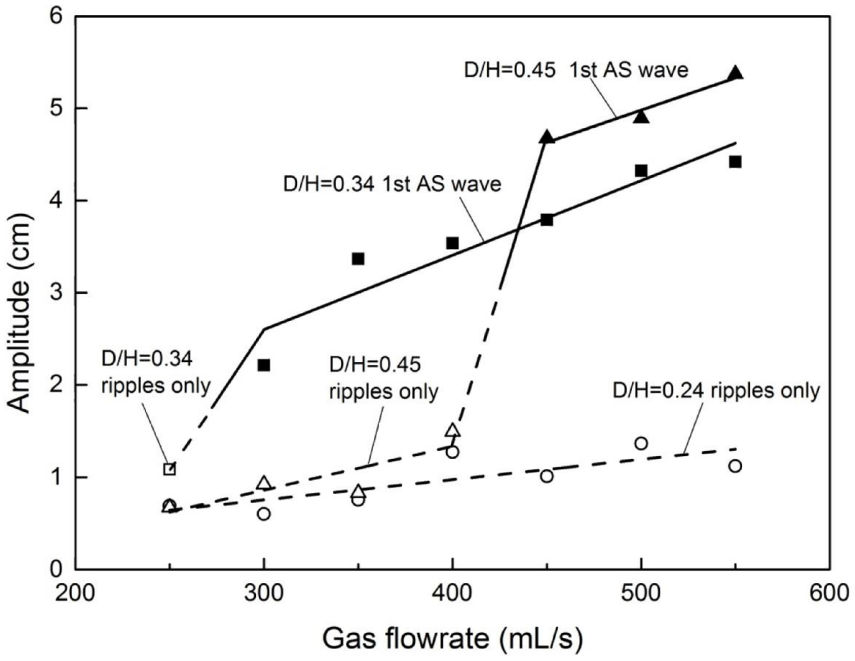
D/H=0.45 1st AS wave
D/H=0.34 1st AS wave
D/H=0.34
ripples only
D/H=0.45
ripples only
D/H=0.24 ripples only
Amplitude (cm)
Gas flowrate (mL/s)
0
1
2
3
4
5
6
200
300
400
500
600

(b) 15º

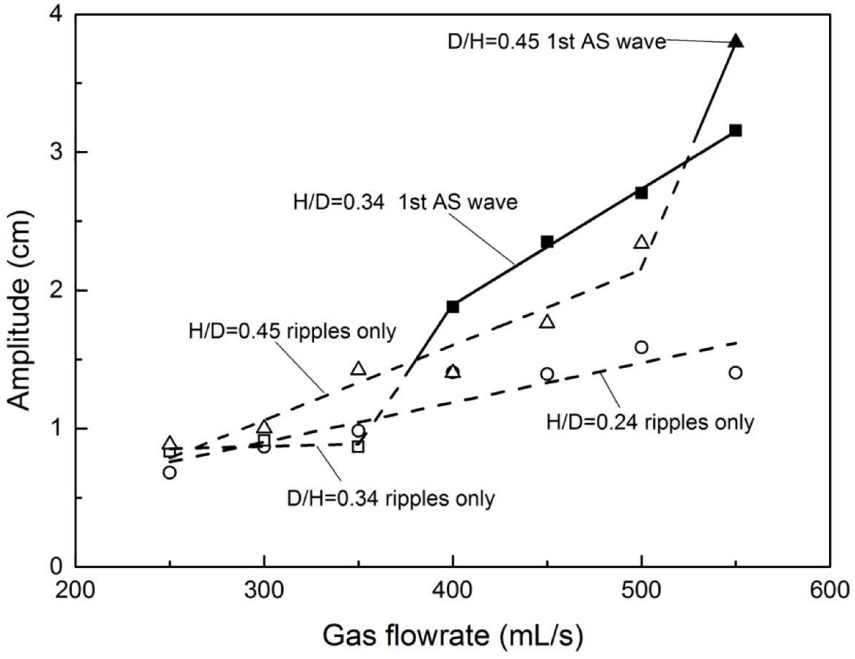
D/H=0.45 1st AS wave
H/D=0.34 1st AS wave
H/D=0.45 ripples only
H/D=0.24 ripples only
D/H=0.34 ripples only
Amplitude (cm)
Gas flowrate (mL/s)
0
1
2
3
4
200
300
400
500
600

(c) 20º

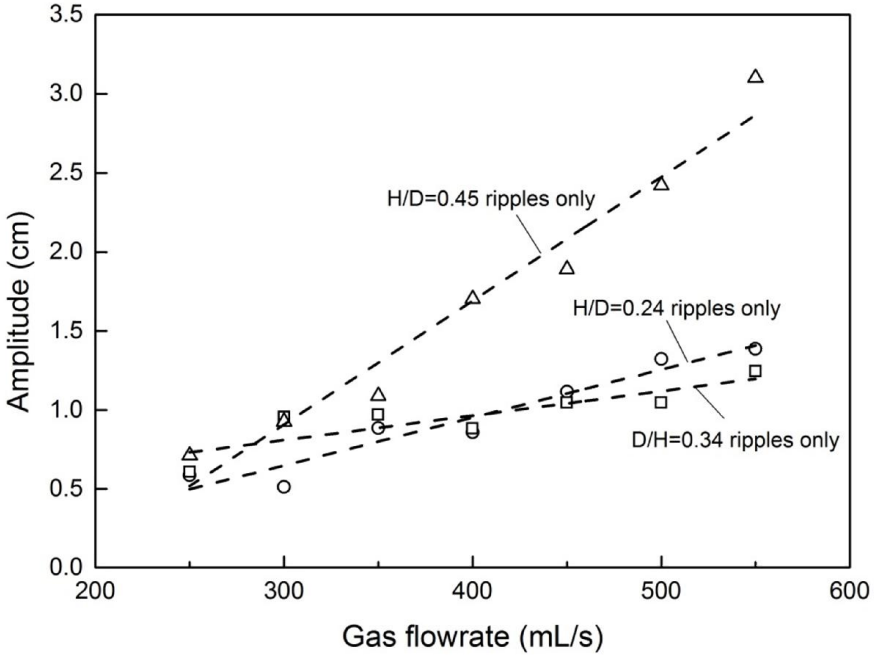

(d) 25º

Figure 7-10 Amplitude of wave at 7º, 15º, 20º and 25º blowing, solid dots and lines represent the presence of 1st AS wave

Table 7-1 Amplitude measured at tapping end

Amplitude	Blowing angle											
(cm)	7º			15º			20º			25º		
Flowrate	Bath depth (cm)			Bath depth (cm)			Bath depth (cm)			Bath depth (cm)		
(mL/s)	7	10	13	7	10	13	7	10	13	7	10	13
250	0.27	1.99	1.03	0.69	1.08	0.67	0.68	0.83	0.88	0.59	0.61	0.71
300	0.32	2.67	1.21	0.60	2.21	0.92	0.87	0.91	1.00	0.51	0.96	0.93
350	0.54	3.36	3.70	0.76	3.37	0.83	0.98	0.87	1.42	0.89	0.97	1.09
400	0.69	4.30	4.19	1.27	3.54	1.49	1.41	1.88	1.40	0.86	0.88	1.70
450	0.84	4.54	5.47	1.01	3.79	4.67	1.39	2.35	1.76	1.12	1.05	1.89
500	0.67	4.91	7.02	1.37	4.32	4.89	1.59	2.70	2.34	1.32	1.05	2.42
550	0.91	5.21	7.04	1.12	4.42	5.37	1.40	3.16	3.80	1.39	1.25	3.10

By summarising the features in Figure 7-10 and Table 7-1, general conclusion was obtained as follows.

(1) Smaller offset angle blowing creates greater amplitude

(2) If the 1st asymmetric standing wave is absent, deeper bath depth creates slightly greater amplitude

(3) If the 1st asymmetric standing wave is present, amplitude is significantly increased to a level much greater than that of absent, and increases faster with flowrate.

(4) If the 1st asymmetric standing wave is present in both bath depths, the deeper bath depth still creates greater amplitude

(5) The amplitude of 1st symmetric standing wave is as small as ripples.

7.3.3 Wave frequency

Ripples and the 1st symmetric standing wave did not generate large amplitude at the tapping end, so there were many small peaks and troughs at the tapping end, which was not considered for frequency measurement. Therefore only the frequency of the 1st asymmetric standing wave was investigated. Figure 7-11 shows that the frequency of the 1st asymmetric standing wave at 7º blowing does not change with flowrate. Instead, it is only increasing with bath depth, and 15º and 20º show the same trend, which are not given here.

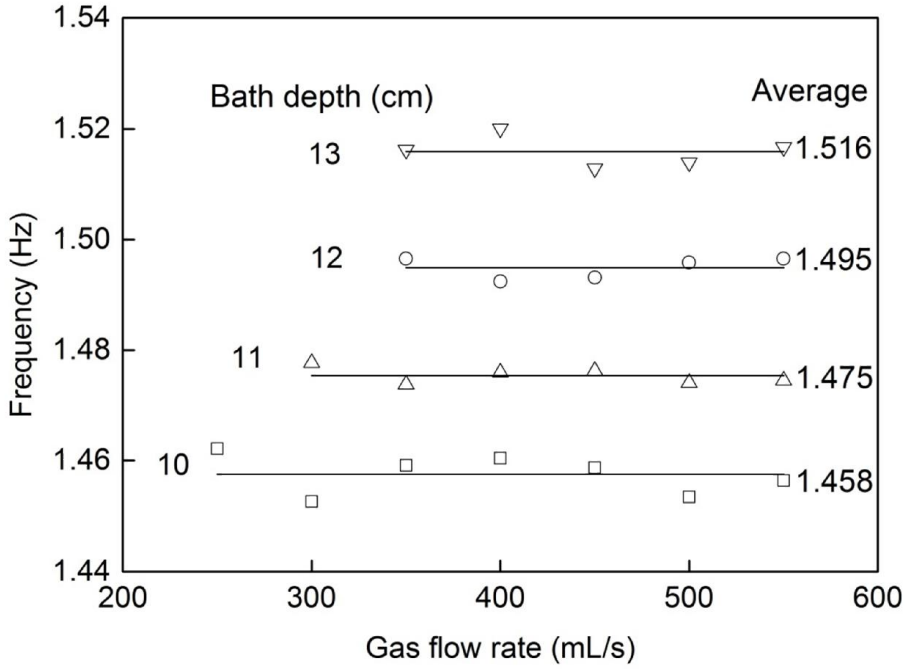

Figure 7-11 Frequency of the 1st asymmetric standing wave at 7º blowing

By using the dimensional analysis, the dimensionless frequency that is model-independent can be derived in terms of natural frequency obtained in a specific model:

$$\alpha = 2\pi f \sqrt{\frac{R}{g}} \tag{7.5}$$

where α denotes the dimensionless frequency, f denotes the natural frequency obtained in specific model (Hz), R denotes the radius of the model (m), and g denotes the acceleration of gravity ($9.8 m/s^2$).

Figure 7-12 shows dimensionless frequency plotted against aspect ratio H/D. It is found that data of different blowing angles almost overlap, and follow the same increasing trend with bath depth. This indicates that the frequency of the 1st asymmetric wave is independent of blowing angle, and only slightly increases with bath depth. The frequency dispersion of surface gravity waves can be expressed as[19]:

$$f = \sqrt{\frac{g}{2\pi\lambda}\tanh\left(\frac{2\pi h}{\lambda}\right)} \tag{7.6}$$

where λ denotes the wavelength, h denotes the depth of bath, and f denotes the wave frequency. Based on this formula, Rosales[20] reported an approximate analytical approach to calculate the frequency of standing waves in Teniente converter, which employs the theory of frequency dispersion for surface gravity waves:

$$\alpha = \sqrt{\frac{n\pi}{4(\eta(1-\eta))^{\frac{1}{2}}}\tanh\left(\frac{n\pi}{2}\left(\frac{\eta}{1-\eta}\right)^{\frac{1}{2}}\right)} \tag{7.7}$$

where α is the dimensionless frequency, n denotes the node of a specific standing wave, in the case of 1st asymmetric wave n=1, and η denotes the aspect ratio H/D. In present study, the wave is also generated by gas agitation and gravity, so data agree well with Eq. (7.7), with deviation less than 4%.

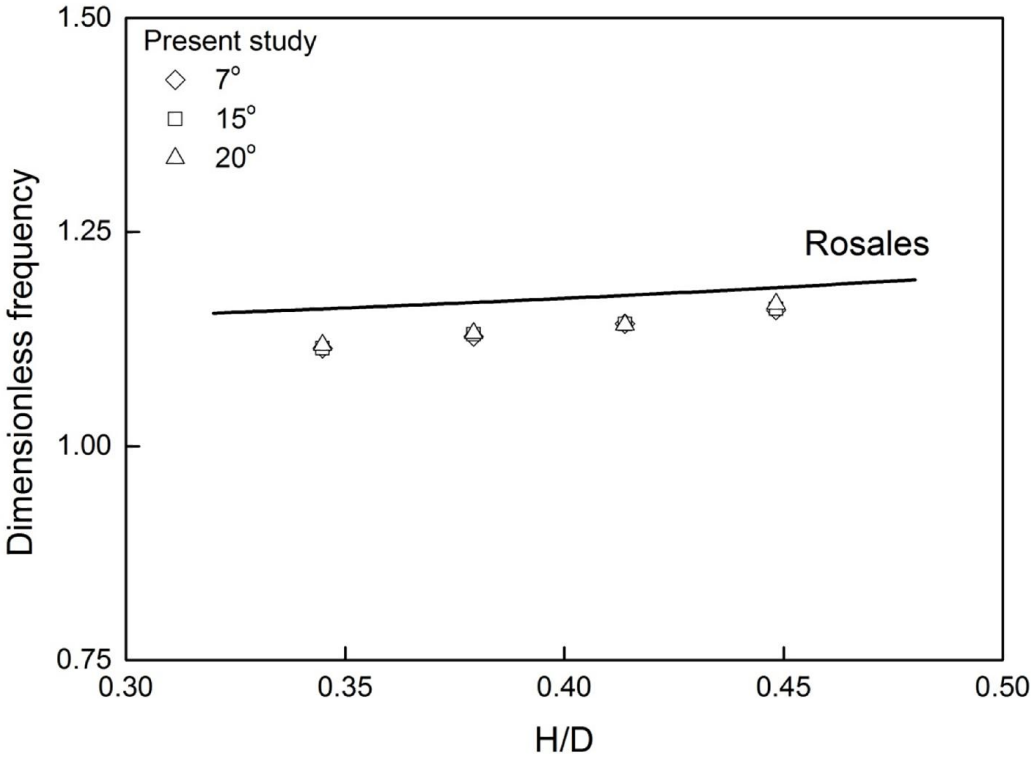

Figure 7-12 Comparison of experimental data to Rosales' analytical solution

7.4 Industrial application

In industrial practice, the 1st asymmetric standing wave is possibly relevant to the advantages of Fangyuan bottom blown furnace mentioned in introduction section. For example, the high amplitude of 1st asymmetric standing wave may work on the settlement of matte droplets in top slag layer, which influences copper content in slag. Therefore, further study on the mechanism of this effect is needed in future. On the other hand, the vibration of the 1st asymmetric wave is able to increase friction between molten bath and refractory and accelerate wearing. According to results of present study, it is possible to reduce this wearing by reducing bath depth, as the frequency of the 1st asymmetric standing is decreasing with bath depth, and lower frequency reduces friction between molten bath and refractory. Changing gas injection flowrate or blowing angle is not to be considered as options to reduce the 1st asymmetric wave friction, since frequency is independent with these two parameters.

The Eq. (7.1) and (7.2) in present study provide information for industry to generate or avoid the 1st asymmetric standing wave by varying bath depth H and flowrate Q_g in bottom blown copper

smelting furnace. In industrial practice, taking 7º blowing lance for example, at fixed furnace diameter D=3.5 m and a certain bath depth H=1.2 m that make aspect ratio H/D=0.34, one may refer to Figure 7-7 (a) and adjust Q_g to make We greater than 0.03 for obtaining 1st asymmetric standing wave, or to make We less than 0.03 for obtaining only ripples on surface. Likewise, at a given flowrate Q_g that makes We=0.05 for example, one can obtain the 1st asymmetric wave by controlling bath depth between 1.12 and 1.44 m ($0.32<H/D<0.41$), out of which one obtains ripples only. Other blowing angles follow the same rule.

7.5 Conclusions

(1) Three different types of surface waves were observed in lab scale model of bottom blown copper smelting furnace. The 1st asymmetric standing wave was the most significant type among the three because it leaded the entire bath to swing laterally, even at the tapping end.

(2) The 1st asymmetric standing wave occurs only at certain combination of bath height and gas flowrate, which can be analyzed in two sub-boundaries. Additionally, as the lance angle was increased, the critical bath height and flowrate for the occurrence was also increasing. Empirical correlations can be obtained as follows:

Sub-boundary 1

$$\frac{H}{D} = 0.036 Fr_{mD}^{-0.1} \alpha^{0.084} \tag{7.1}$$

Sub-boundary 2

$$\frac{H}{D} = 0.63 We^{0.44} \alpha^{-0.39} \tag{7.3}$$

When blowing angle was increased to 25º, the 1st asymmetric standing wave was substituted by the 1st symmetric standing wave, and its occurrence condition was not as clear as the former one.

(3) The measured amplitude of several conditions showed that tapping end amplitude was increasing with flowrate and bath height, and when the 1st symmetric standing wave occurred, the amplitude was remarkably increased.

(4) The frequency of the 1st asymmetric standing wave did not change with flowrate or blowing angle, but was slightly increasing with bath height.

7.6 References

[1] Y. Sahai and R. I. L. Guthrie: *Metall. Trans. B*, 1982, vol.13B, pp. 193-202.

[2] Y. Sahai and R. I. L. Guthrie: *Metall. Trans. B*, 1982, vol.13B, pp. 203-211.

[3] K. Thomas: *Stahl u. Eisen*, 1930, vol. 50, pp. 1665/674 and 1708/718.

[4] P. Leroy and G. Cohen de Lara: *Rev. Metall.,* 1958, vol. 55, pp. 75-97 and 186-200.

[5] A. Etienne: *Metal. Rep.,* 1975, No. 43, pp. 13-21.

[6] Y. Kato, K. Nakanishi, T. Nozaki, K. Suzuki and T. Emi: *Trans. ISIJ*, 1985, vol. 25, pp. 459-466.

[7] M.P. Schwarz: *Proc*. *Australas. Fluid Mech. Conf.*, *10th*, University of Melbourne, Melbourne, VIC, Australia, 1989, pp. 3.29-3.32.

[8] M. P. Schwarz: *Appl. Math. Modelling*, 1996, vol. 20, pp. 41-51.

[9] Y. Xie and F. Oeters: *Steel Res.*, 1992, vol.63, No. 6, 227-233.

[10] Y. Xie and F. Oeters: *Steel Res.*, 1992, vol.63, No. 7, 277-280.

[11] M. Iguchi, S. Hosohara, T. Koga, R. Yamaguchi and Z. Morita: *ISIJ Int.*, 1993, vol. 33, No. 10, pp. 1037-1044.

[12] M. Iguchi, D. Iguchi, Y. Sasaki, T. Kumagai and S. Yokoya: *ISIJ Int.*, 2004, vol. 44, No. 10, pp. 1623-1628.

[13] T. Kootz and G. Gille: *Stahl Eisen,* 1948, vol. 48, pp. 287-294.

[14] G.G. Richards, K.J. Legeard, A.A. Bustos, J.K. Brimacombe and D. Jorgensen: *Reinhardt Schuhmann Int. Symp. Innovative Technol. React. Des. Extr. Metall., Proc. Symp.,* D.R. Gaskell, ed., Colorado Springs, CO, TMS-AIME, Warrendale, PA, 1986, pp. 385-403.

[15] J. L. Liow and N. B. Gray: *Proc*. *Australas. Fluid Mech. Conf.*, *10th,* University of Melbourne, Melbourne, VIC, Australia, 1989, pp.14.33-14.36.

[16] J. L. Liow and N. B. Gray: *Metall. Trans. B,* 1990, vol. 21B, pp. 657-664.

[17] J. L. Liow and N. B. Gray: *Metall. Trans. B,* 1990, vol. 21B, pp. 987-996.

[18] C. Tsai and Z. Qian: *Trans. ISIJ*, 1986, vol. 26, pp. 139-144.

[19] H. Lamb: *Hydrodynamics*, 1932, 6th ed., Cambridge University Press, Cambridge, UK.

[20] M. Rosales, P. Ruz and R. Fuentes: *Proc. Copper 2003-Cobre 2003 Hermann Schwarze Symp.*, C. Diaz, C. Landolt and T. Utigard, ed., Santiago, Chile, Vol. IV, pp. 485-498.

8 Behaviour of longitudinal wave in bottom blown copper smelting furnace

Abstract Simulation experiment was carried out on a lab-scale cold model of the Fangyuan bottom blown copper smelting furnace to investigate characteristics of the surface longitudinal wave on the molten bath during smelting. In this study, all nine lances were used for blowing, and other experimental variables including gas flowrate in each lance, water level, oil level and oil viscosity were adjusted according to the principles of similar to ensure the experimental dynamic condition corresponding to industrial operation. It is found that the amplitude trend of the longitudinal wave along the furnace length is dependent on the combination of gas flowrate and bath level, and three typical trends were observed. At the gas flowrate corresponding to industrial flowrate, the amplitude of wave is increasing with the water level, but remains almost stable with the oil level. A higher viscosity oil layer leads to lower amplitude of wave, while a lower viscosity oil layer leads to the rising of amplitude near the tapping end. The amplitude of wave at the edge of the tapping end is found always higher than at the centre. The frequency of the longitudinal wave is not affected by the water level, oil level or oil viscosity.

Key words: copper smelting, bottom blown furnace, cold model ,surface wave

8.1 Introduction

Previous study found that different types of transversal waves were able to take place at certain conditions[1]. On the other hand, out of the critical occurrence boundary, there were small ripples continuously transmitting from the reaction zone to the tapping end across the settlement zone. As these ripples are uniformly transmitting along the length of the furnace, the term longitudinal wave is used to describe the uniform feature of these ripples in this study[2]. Though the longitudinal wave have relatively small amplitude, the impact on wearing of furnace refractory can be accumulative with time[3-4]. In addition, the peaks and troughs on bath surface still have influence on the settling of matte droplets and the tapping of slag[5].

8.2 Experimental methodology

To investigate features of the longitudinal wave and its effect on smelting, water model experiment is carried out. The structure of the water model has been introduced in previous studies, so it is not repeated in this chapter[6]. The previous study investigated the formation of standing waves on single phase bath surface. In this study, in order to make the simulation further closer to the prototype, the slag layer is taken into consideration. Therefore, silicone oils with different viscosities are used to simulate the slag layer. In Fangyuan practice, the viscosity of full liquid phase of slag is normally around 0.2 Pa·s[7]. To consider a wide range of simulation and the presence of solid particles in slag, the minimum 0.05 Pa·s and the maximum 0.7 Pa·s are taken as extreme conditions. To guarantee the principles of similarity, Eq.(8.1) must be satisfied when selecting silicone oils[8]. As a result, the corresponding silicone oils with kinematic viscosity 10, 50 and 200 cSt are selected as shown in Table 8-1.

$$\nu = \frac{\mu_{slag}}{\rho_{slag}} = \frac{\mu_{oil}}{\rho_{oil}} \tag{8.1}$$

Table 8-1 Physical parameters of experimental fluids corresponding to fluids in prototype at 1200ºC

Top phase	Min I	Ave II	Max III	Lower phase	-
Slag density kg/m^3	3500	3500	3500	Matte density kg/m^3	4700
Slag viscosity Pa·s	0.05	0.2	0.7	Matte viscosity Pa·s	4×10^{-3}
Slag kinematic viscosity cSt	14.29	57.14	200.00	Matte kinematic viscosity cSt	0.85
Si-oil density kg/m^3	935	960	970	Water density kg/m^3	0.89×10^{-3}
Si-oil kinematic viscosity cSt	10	50	200	Water kinematic viscosity cSt	0.89

To simulate the formation of longitudinal wave in the settlement zone, all nine lances are used to blow compressed air to stir the silicone oil covered bath. The gas flowrate used in each lance is calculated by Eq. (8.2).

$$Q_m = Q_p \sqrt{\left(\frac{d_m}{d_p}\right)^4 \left(\frac{\rho_{lm} - \rho_{gm}}{\rho_{lp} - \rho_{gp}}\right) \left(\frac{L_m}{L_p}\right) \left(\frac{\rho_{gp}}{\rho_{gm}}\right)} \tag{8.2}$$

The longitudinal wave is transmitting from the reaction zone to the tapping end of furnace. Compared to standing waves, it is not an overall synchronised motion of bath. Instead, there are many small peaks and troughs created in the reaction zone transmitting in the settlement zone. As

there is no separating dam between the reaction and settlement zone, the longitudinal wave is directly transmitting and attenuating along the furnace length. Therefore, several monitoring points along the furnace length are selected. As shown in Figure 8-1, rulers with millimetre scale are setup vertically onto the he side wall of the settlement zone as well as the end wall to monitor the wave transmission at each position[9]. Regarding rulers on the side wall, the scales on the right edge are used for measurement, and as shown in Figure 8-2, the horizontal distance from the last lance to the right edge of each ruler is 35, 190 and 345 mm, respectively. This horizontal distance represents how far the wave has transmitted from the reaction zone where it is created. A video camera is used to record the wave shape at each ruler.

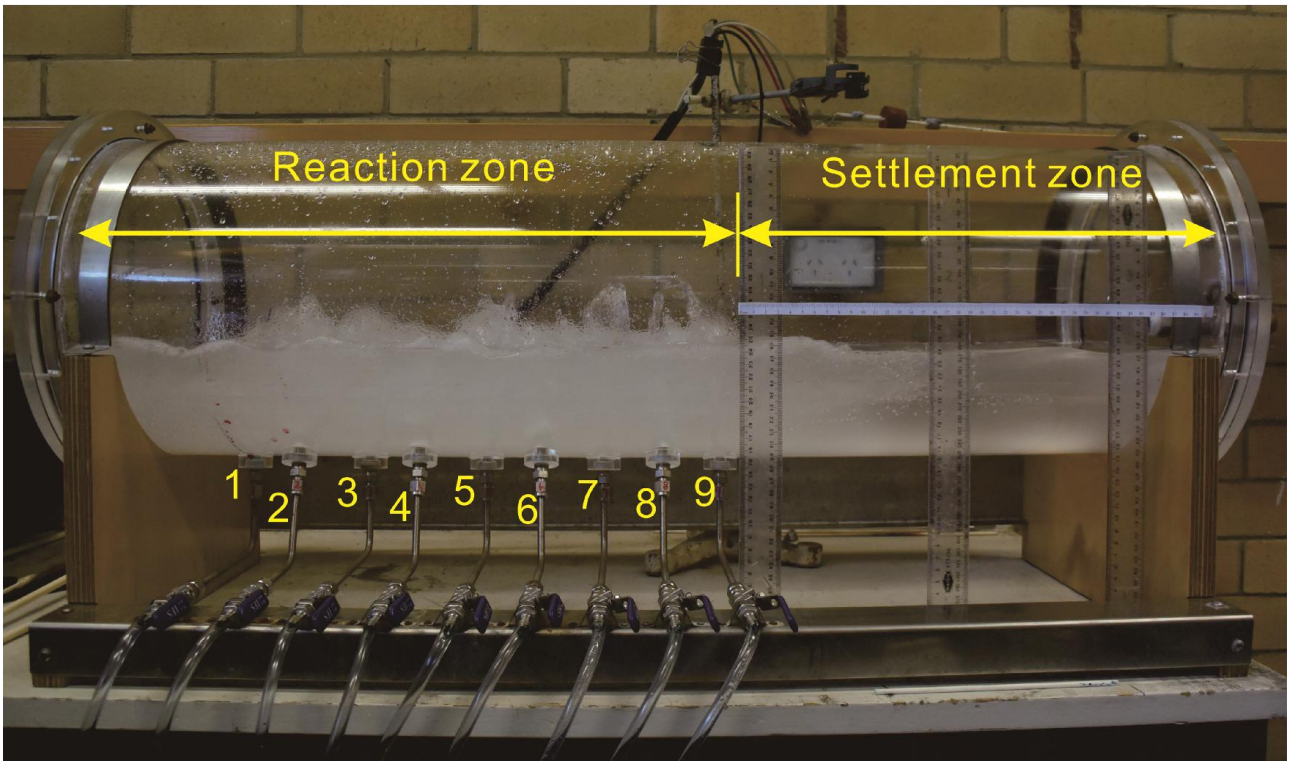

Figure 8-1 Experimental setup

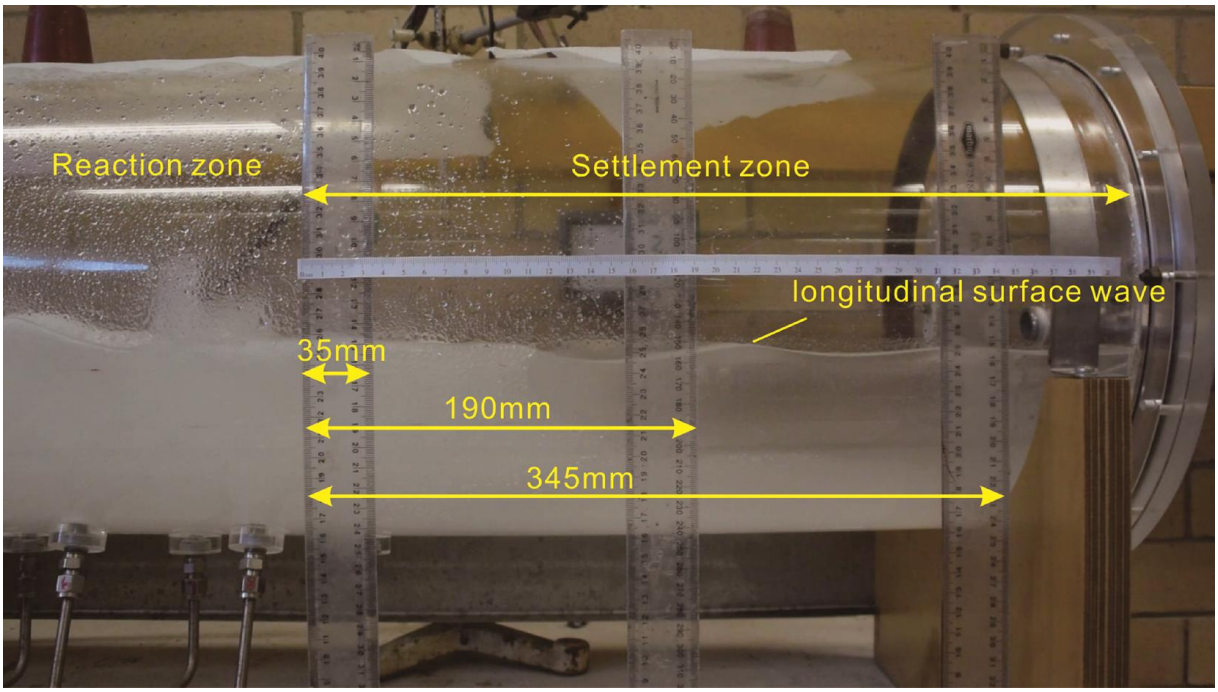

Figure 8-2 Positioning of side wall rulers for measurement of longitudinal wave along the settlement zone

The amplitude of longitudinal wave at each position is recorded by video as shown in Figure 8-3. In data processing, the video is slowed down and the bath surface height of 30 continuous peaks and troughs are picked up from video. Usually, the amplitude of the wave is the height difference from the high or low point of bath surface to the still surface level. However, in experiment once the gas stirring is started, the average bath surface level in settlement zone is considerably higher than still because gas injection forms plume eye in reaction zone and pushes the upper oil layer to the settlement zone. It is also difficult to identify the average bath surface level on the ruler scale as the surface keeps vibrating once gas stirring started. As a result, in order to identify an average surface level for comparison in the current study, the mean value of the 30 points (including peaks and troughs) is taken as the average bath surface level, and the absolute value of the height difference from the average surface level to each high point or low point is termed as amplitude of the peak or trough. The mean amplitude value of the 30 points is taken as the amplitude of the monitoring position, and then the other continuous 30 high and low points are selected to confirm the value. The mean value of the two groups is used as the final amplitude value of the monitoring point[10].

The frequency of the longitudinal wave is also measured by slowing down video play speed. At each measuring ruler, the time for the wave to complete 30 vibrations was counted, and its average

wave frequency was determined as the reciprocal of this time divided by 30.

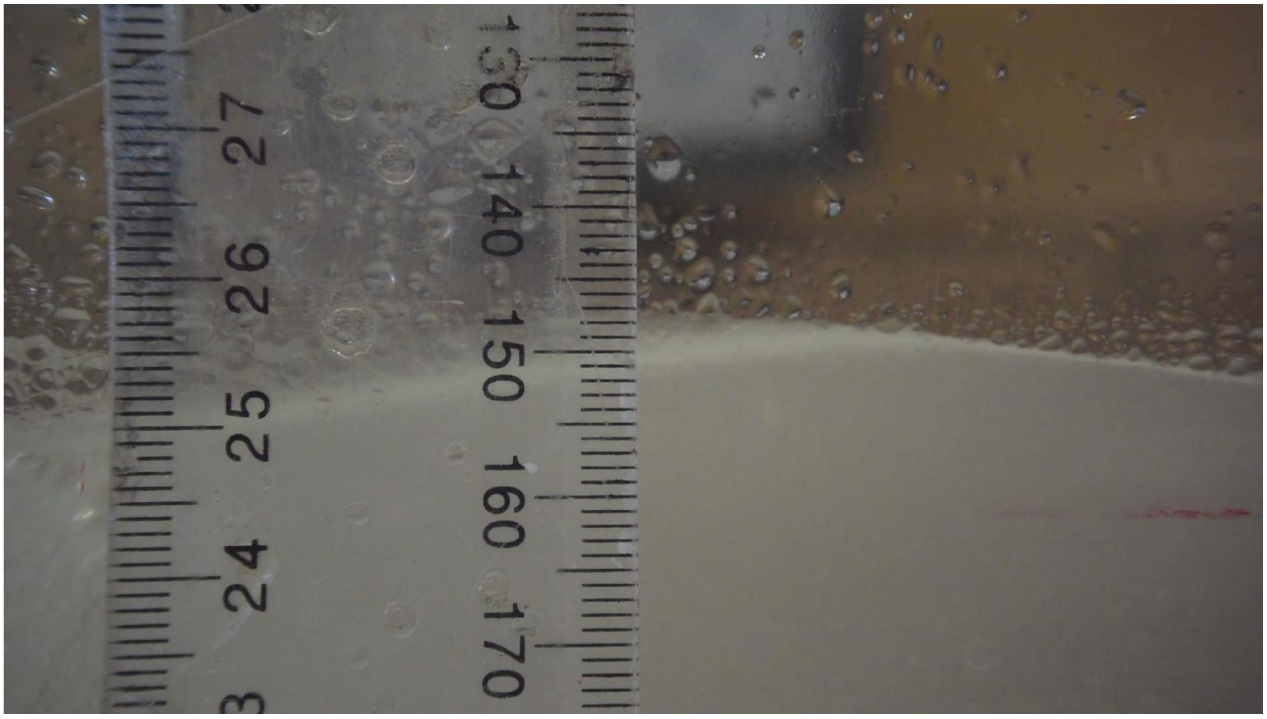

Figure 8-3 The measurement of longitudinal wave amplitude

8.3 Results and discussions

8.3.1 The trend of amplitude along furnace length

The trend of amplitude along furnace length shows the extent of bath surface deformation and energy dissipation of longitudinal wave while transmitting in the settlement zone. As the settlement zone of furnace is considerably long, the transmission of wave can be influenced by many factors. As a result, the trend of wave along the length of settlement zone changes remarkably under different conditions. There are three different trends observed in this study.

1) Amplitude increasing with flowrate in the same trend

The Figure 8-4 shows the simplest situation of amplitude trend with gas flowrate: the amplitude is decreasing along furnace length under each gas flowrate, which is under the lowest water and oil level. This trend is easy understanding as the energy is consumed in transmission and the amplitude is decreasing. Meanwhile, the greater gas flowrate creates greater initial amplitude of wave, so the amplitude measured at each point is greater.

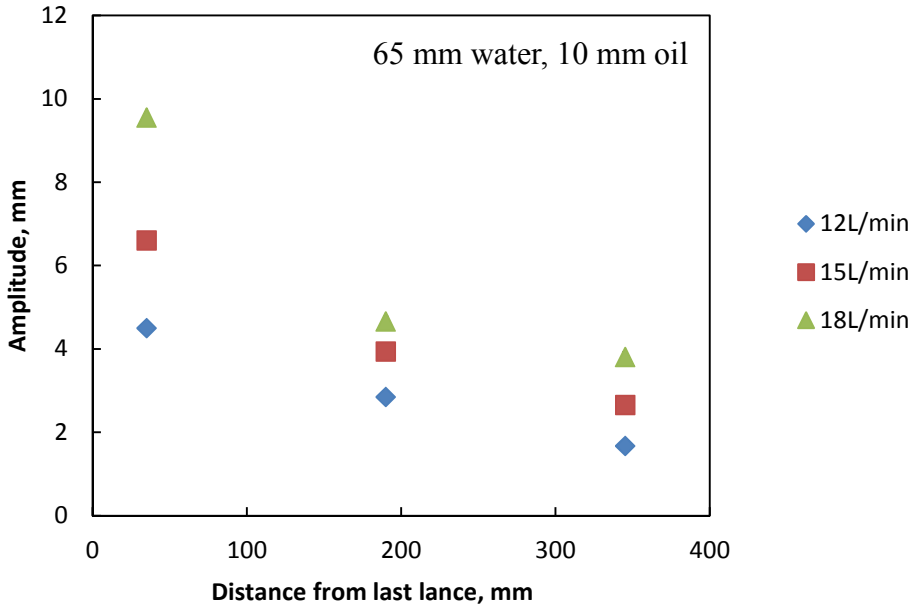

Figure 8-4 Amplitude of wave along settlement zone under different gas flowrates, 65 mm water, 10 mm oil, 50cSt oil

2) Amplitude trends becoming different at different flowrates

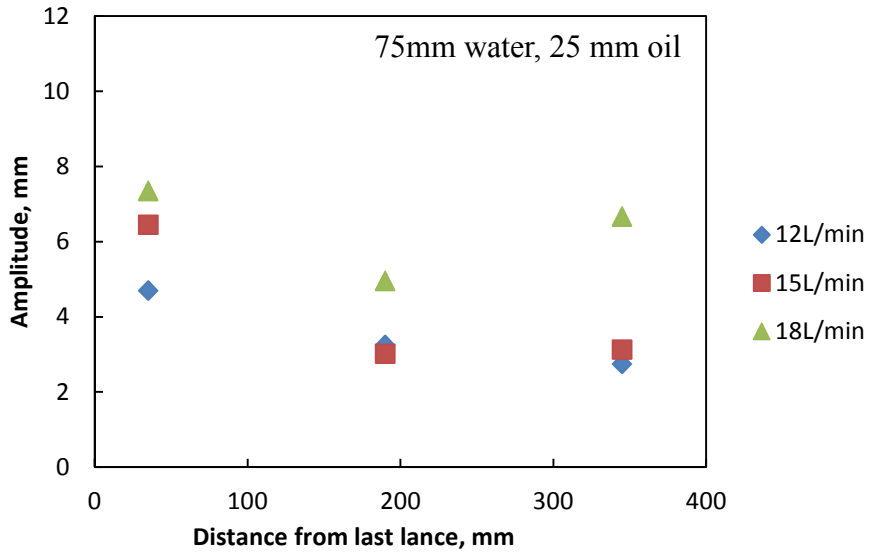

Figure 8-5 Amplitude of wave along settlement zone under different gas flowrates, 75mm water, 25 mm oil, 50cSt oil

When the total bath level is increased, the trend of amplitude is changed. As shown in Figure 8-5, at a low gas flowrate 12L/min, the amplitude is decreasing along furnace length. When the flowrate is increased to 15L/min, the amplitude at 345 mm is increased to a level almost equal to that of 190 mm. When the gas flowrate reaches 18L/min, the trend of amplitude from the second point to the

third becomes increasing, which make the amplitude trend along furnace length becomes decreasing at first and increasing later. Additionally, the absolute value is also increased and higher than the former two. This trend changing is probably caused by the reflection of waves near the tapping end. At a low gas flowrate, the energy of wave is relatively low and the vibration of surface is consequently not able to reach the tapping end wall. As a result, the amplitude shows a decreasing trend along the length as energy keeps dissipating in transmission. However, at a higher gas flowrate, the wave has enough energy to reach the tapping end wall and reflects against it. The reflected wave transmits in the opposite direction and overlaps with incoming new wave near the tapping end so the vibration of surface is promoted and amplitude is increased. Greater gas flowrate leads to more intensive reflected wave, and the overlap of wave results in greater amplitude at the third measuring point, which makes the increasing trend from the second point to the third more significant. Therefore, at a relatively great flowrate with high total bath level, the amplitude at the third measuring point is significantly influenced by the wave reflection.

3) Standing wave involved

When the total bath depth is further increased, the trend of amplitude becomes more complicated. As shown in Figure 8-6, the water level is 75mm and oil level is increased to 35 mm. Under such condition, the amplitude trend of 12 L/min still is decreasing and that of 15 L/min is still decreasing at first and increasing later. Whereas the amplitude of 18 L/min is far more increased than the situation of 75mm water and 25 mm oil. This great increasing of amplitude is because the 1st asymmetric standing wave is occurring under the combination of 75 mm water, 35 mm oil and 18 L/min, as shown in Figure 8-7. The occurrence condition and the features of the 1st asymmetric wave has been discussed in previous study under the condition of single lance and single phase. It is interesting that in the present study this standing wave is still able to occur while the top oil layer is in presence and all the nine lances are used for blowing. In its presence, the plumes of nine lances are rotating uniformly in the same direction, which drives the entire bath to swing synchronically. As a result, the amplitude is significantly increased.

It is also noticeable that the occurrence of the 1st asymmetric standing wave is probably relevant to the reflection of longitudinal wave at the tapping end wall. As discussed in the previous section, the reflection is increased with increasing gas flowrate. When the gas flowrate is increased to an even

greater value, the reflected wave is powerful enough to transmit back close to reaction zone. As a result, the reflected wave is able to interact with incoming new wave in the almost whole settlement zone. Under certain bath total level, the interaction between two opposite waves reaches resonance, and thus a standing wave is formed. However, detailed mechanism of this formation still needs further investigation as the too many factors are involved such as oil level, water level and lance configuration.

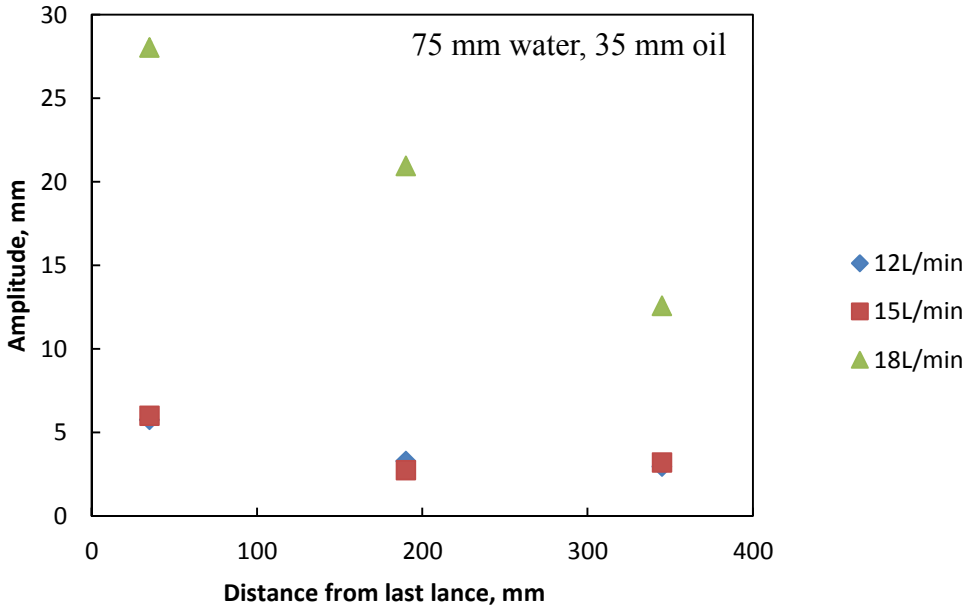

Figure 8-6 Amplitude of wave along settlement zone under different gas flowrates, 75mm water, 35 mm oil, 50cSt oil

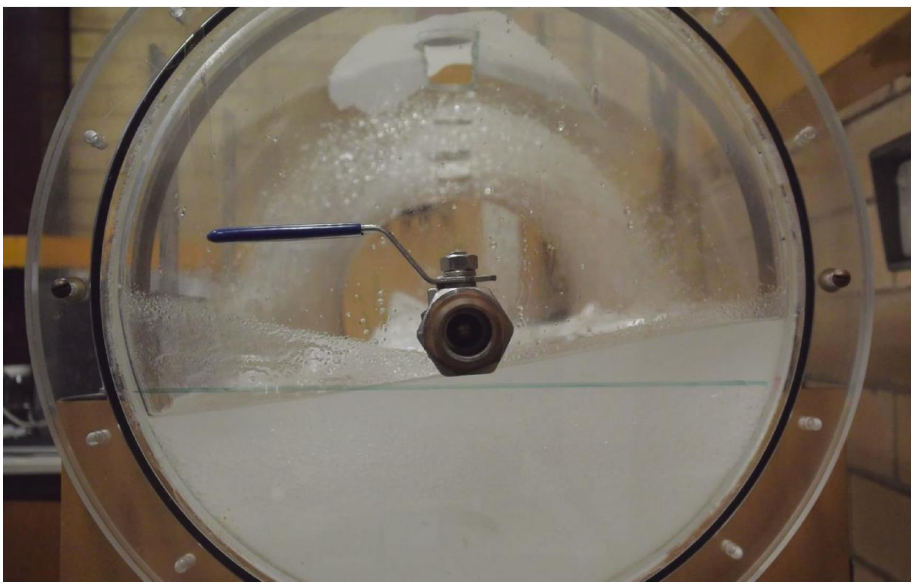

Figure 8-7 The 1st asymmetric standing wave takes place even in the presence of top oil layer, 75 mm water, 35 mm oil, 50cSt oil

8.3.2 Effect of oil level

As the trend of longitudinal wave can be affected by many factors, it is essential to make the other factors as stable as possible while investigating the effect of oil level. The fixed gas flowrate 12L/min is selected as it is corresponding to the industrial average gas flowrate according to principles of similarity. The two fixed water level 65 mm and 75 mm is selected because these two heights are also corresponding to the minimum and maximum matte height in industry, respectively. The three oil heights 10, 25 and 35 mm are corresponding to the extreme slag height, minimum and maximum slag height in normal operation, respectively. The results are shown in the Figure 8-8. The longitudinal wave is created by the gas blowing in the reaction zone, and its amplitude is decreasing with distance at this low gas flowrate, because the energy is dissipating in transmission under such gas flowrate. On the other hand, it is shown in the two figures that the change of oil levels has little effect on the amplitude of longitudinal wave under such condition. This means the amplitude of longitudinal wave is not sensitive to the slag height variation. In industrial practice, the slag is periodically tapped via tapping hole, so the slag level is varying from time to time. This conclusion indicates that the surface wave is not affected by slag level variation due to normal slag tapping operation. It is supposed that the surface vibration caused by longitudinal wave is a potential factor to help the settling of matte droplets in slag layer. Accordingly, as the surface wave is not affected normal slag tapping operation, the settling of matte droplets is not sensitive to slag tapping, either.

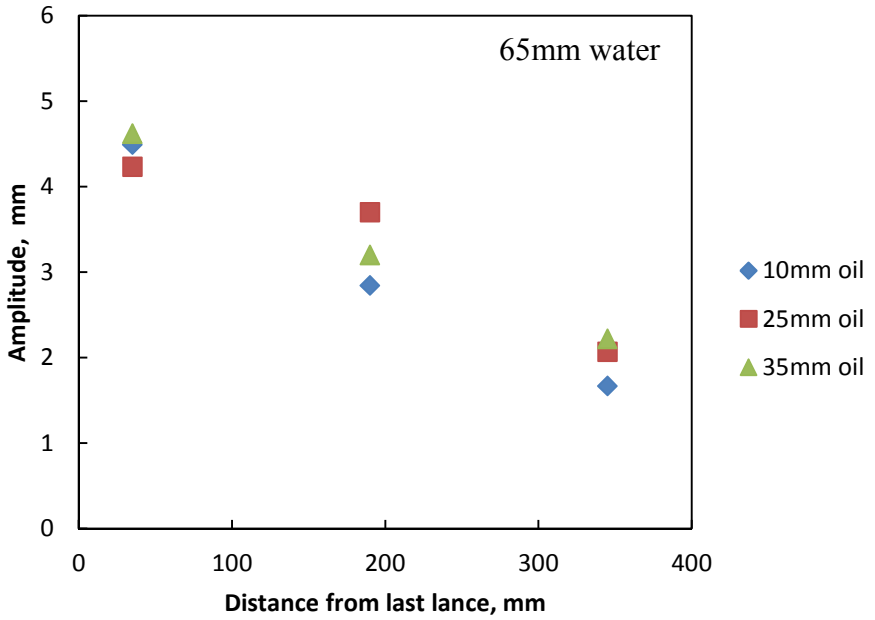

(a)

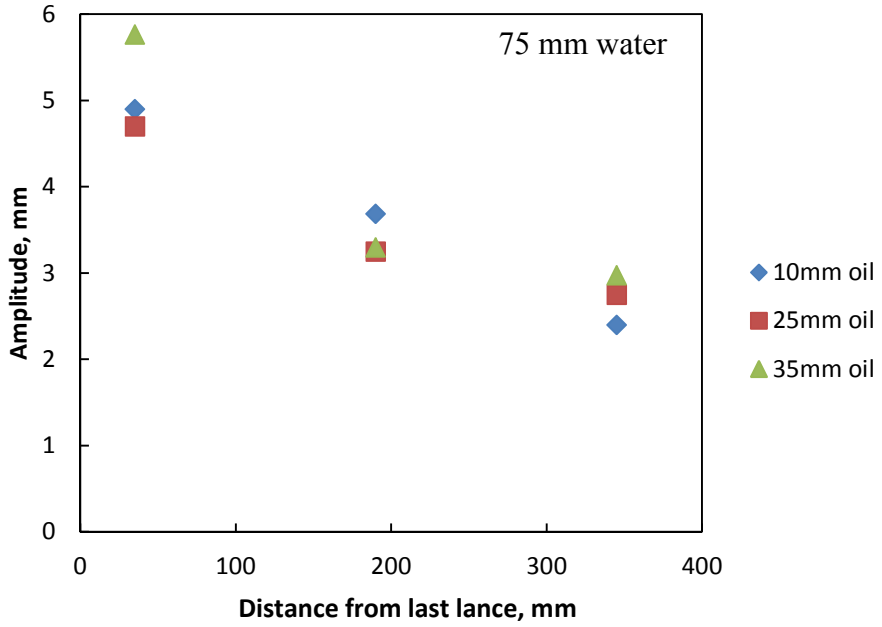

(b)

Figure 8-8 Amplitude of wave along settlement zone under different oil levels, 12L/min gas flowrate, 50cSt oil

8.3.3 Effect of water level

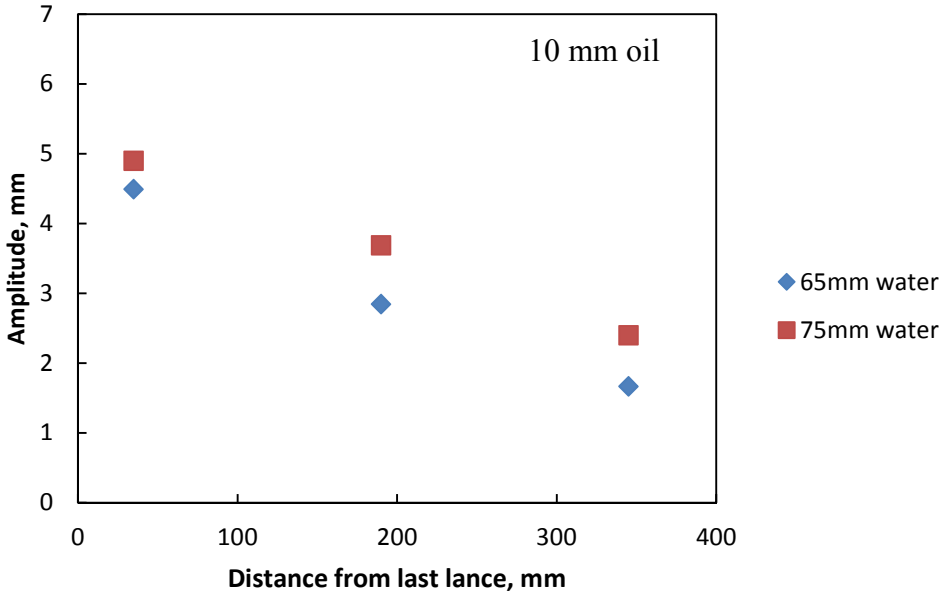

(a)

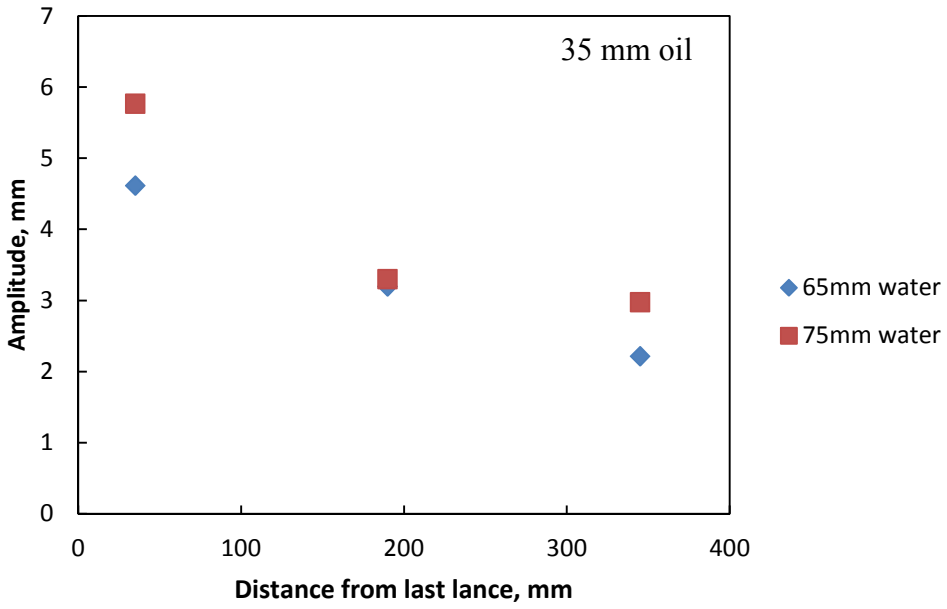

(b)

Figure 8-9 Amplitude of wave along settlement zone under different water levels, 12L/min gas flowrate, 50cSt oil

Figure 8-9 shows the effect of water level on the amplitude of longitudinal wave. As discussed above, the gas flowrate is fixed at 12L/min corresponding to industrial average flowrate, and the 10 and 35 mm oil which represent the minimum and maximum slag level are selected. It is found that higher water depth leads to higher amplitude of wave at each three measuring point. In industrial

practice, the matte is tapped via tapping hole periodically, and the new feeds are charged from feed mouth continuously, so the matte level is varying from time to time. This conclusion suggests that when the matte depth is at high level, for example right before matte tapping, the wave amplitude in settlement zone is also at high level. On the contrary, when the matte tapping is just finished and the matte depth is at low level, the amplitude is consequently becoming lower.

8.3.4 Effect of oil viscosity

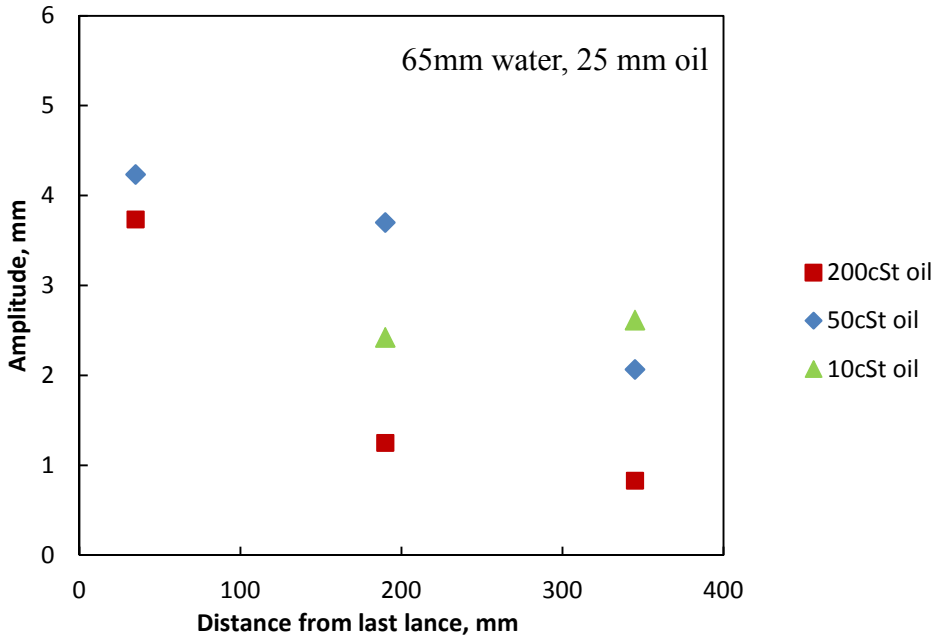

Figure 8-10 Amplitude of wave along settlement zone under different oil viscosities, 65mm water, 25 mm oil, 12L/min gas flowrate

To investigate the effect of oil viscosity, the 65 mm water level and 25 mm oil level are selected, and 12 L/min gas flowrate is used. These parameters are all corresponding to the parameters of the normal industrial operation as discussed above. With those parameters fixed, the viscosity of oil is varied to show the effect of slag viscosity on the amplitude of longitudinal wave and the result is shown in Figure 8-10. As shown in the figure, the 200 cSt oil has the lowest amplitude among the three. In addition, the amplitude of 200 cSt oil along the distance shows a fast decreasing trend, and the amplitude at the third measuring point is less than 1 mm, which means the surface is almost calm near the tapping end. The amplitude trend of 50 cSt is also decreasing with distance, but the absolute amplitude value is higher than that of 200 cSt. This indicates the slag viscosity has remarkable effect on the amplitude of surface wave as the high viscosity oil layer leads to more

energy dissipation in wave transmission which then results in fast amplitude attenuation. The trend of 10 cSt oil is, however, different from the former two. Firstly, the data of the first measuring point of 10 cSt oil layer is missing due to the intensified emulsification near the reaction zone. The surface at the measuring point is covered with froth of gas, oil and water due to the low viscosity of oil, which makes the measurement of surface vibration impossible. Secondly, the trend from the second to the third point is increasing, which is close to the situation in Figure 8-5 discussed in previous section. It is interesting that the increasing amplitude trend in Figure 8-5 takes place at higher gas flowrate such as 18L/min for 50 cSt oil, while the it takes place at low gas flowrate of 12L/min for 10 cSt oil. It suggests that the reflection of wave is able to occur at a lower gas flowrate when the viscosity of upper layer is lower. In industrial practice, it means low viscosity slag means more intensive surface vibration near the tapping end.

8.3.5 Amplitude comparison at tapping end wall

The amplitude of wave is also monitored at tapping end wall. Rulers are set up at the edge of tapping end wall as well as at the centre to monitor the amplitude. The results are shown in Figure 8-12. It is found that under the same water level, oil level and oil viscosity, the wave amplitude at the edge is always higher than at the centre, and it is also true at different gas flowrates. In Figure 8-12(b), where the oil viscosity is the maximum in this study, the absolute values of amplitude are relatively low, but the amplitude at the edge is still higher than at centre. As a result, one can expect that the amplitude of surface vibration at the edge is always higher than the centre. One explanation is that the edge of tapping end is a corner where waves from all directions overlap, so the amplitude is accordingly promoted. It is also found that in the Figure 8-12 (b) the amplitude of both centre and edge are increasing with gas flowrate, but this trend is not found in Figure 8-12 (a). As discussed in above section, it is possible that there is not much wave reflection due to large energy dissipation caused by high viscosity in the presence of 200 cSt, so the amplitude is simply increasing with input gas. Whereas in the presence of 10 cSt oil, the reflection is extensively taking place as energy dissipation is low in transmission, so the amplitude is not simply increasing with gas input.

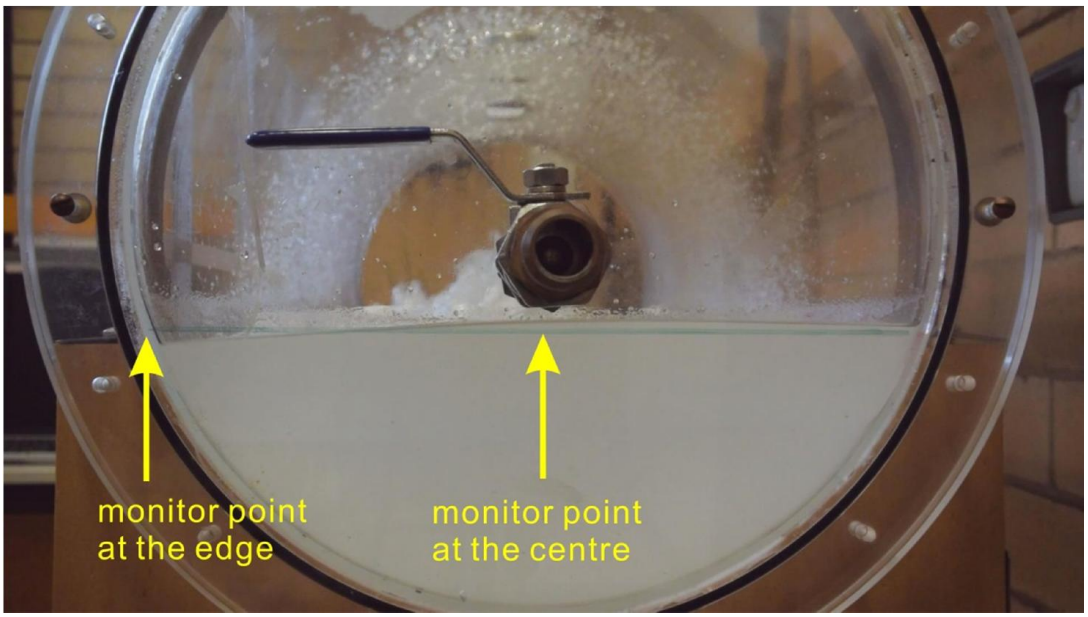

Figure 8-11 tapping end wall monitor points positioning

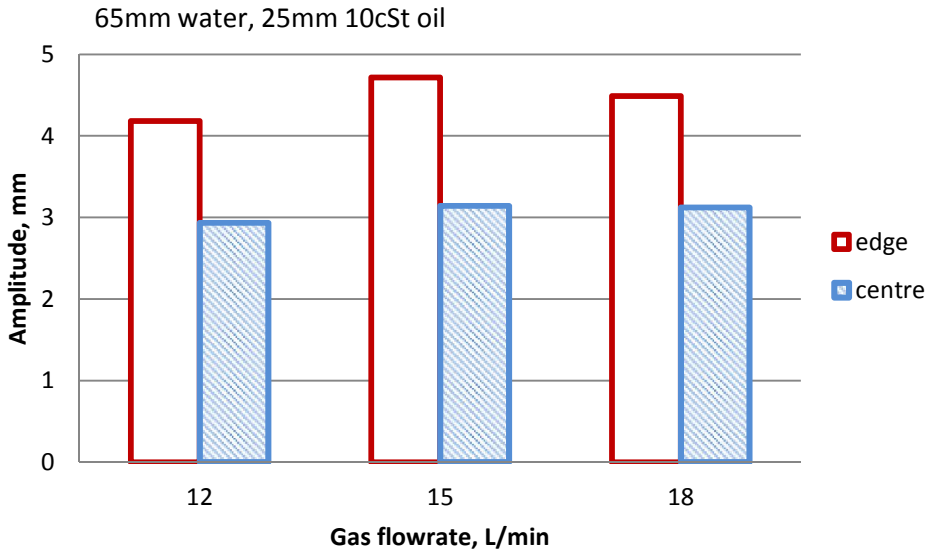

(a)

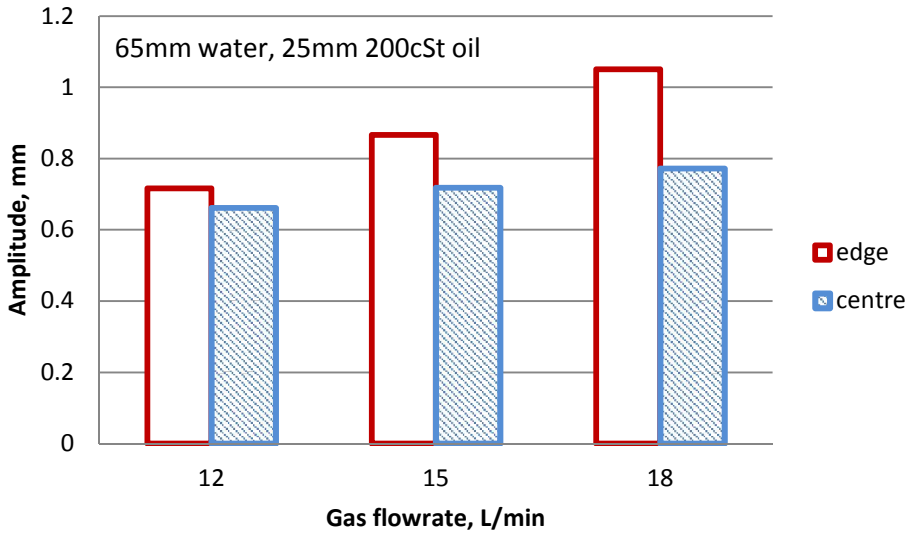

(b)

Figure 8-12 Amplitude comparison between edge and centre of tapping end

8.3.6 Wave frequency

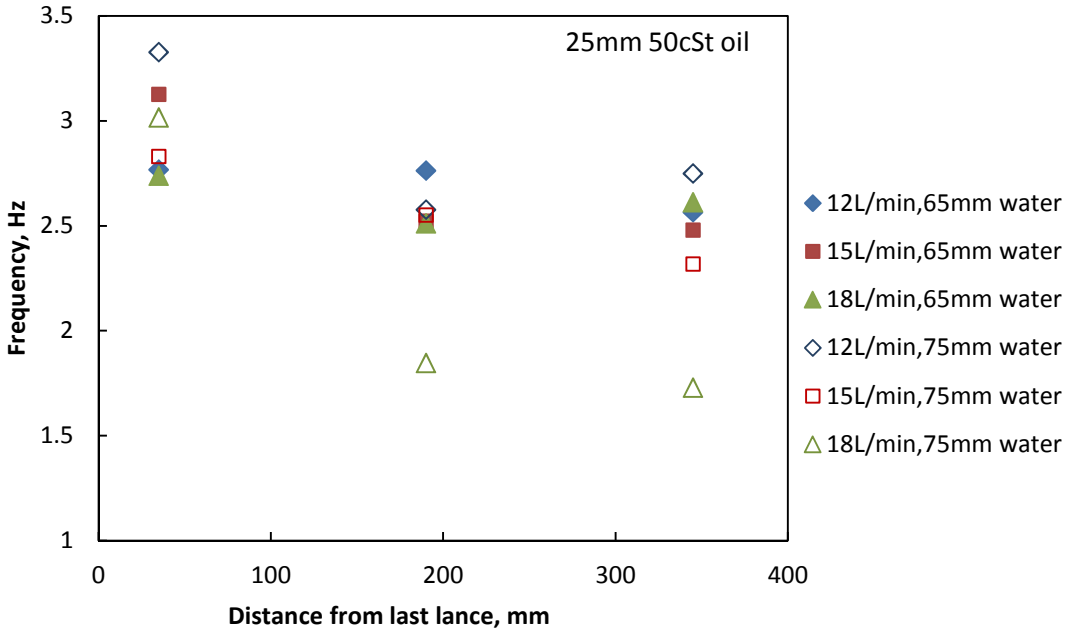

Figure 8-13 The effect of gas flowrate and water height on wave frequency trend

Figure 8-13 shows the frequency of wave measured at each ruler under different conditions. It is found that the frequency along furnace settlement zone shows a slightly decreasing trend except the 18L/min and 75 mm water scenario. The slightly decreasing trend of the majority of points is probably caused by energy dissipation in transmission, while the 18L/min and 75 mm water scenario is because the 1st asymmetric standing wave is involved under such condition. As the 1st

asymmetric standing wave is discussed in previous study, it is not repeated here. Under the other conditions, the amplitude of wave is close to each other, without any distinct variation against gas flowrate or water level. Furthermore, the result in Figure 8-13 is done with oil level fixed at 25 mm, and the results under other oil levels such as 10 and 35 mm, which are not shown here for simplicity, are the similar to Figure 8-13. The absolute values of frequency measured at different points under different conditions are within a range from 2.5-3.2 Hz. This means that the vibration frequency of bath surface is not sensitive to the gas flowrate, matte or slag level change. Therefore, the industrial normal operations like input gas flowrate change, matte and slag tapping do not affect the vibration frequency of surface.

To investigate the effect of slag viscosity on frequency, the other parameters are fixed and only viscosity of oil is changed from 10, 50 to 200 cSt. As shown in Figure 8-14, the frequency is still within the range of 2.5-3.2 Hz with the first points slightly higher. This result means that the frequency of longitudinal wave is not sensitive to the oil viscosity, either.

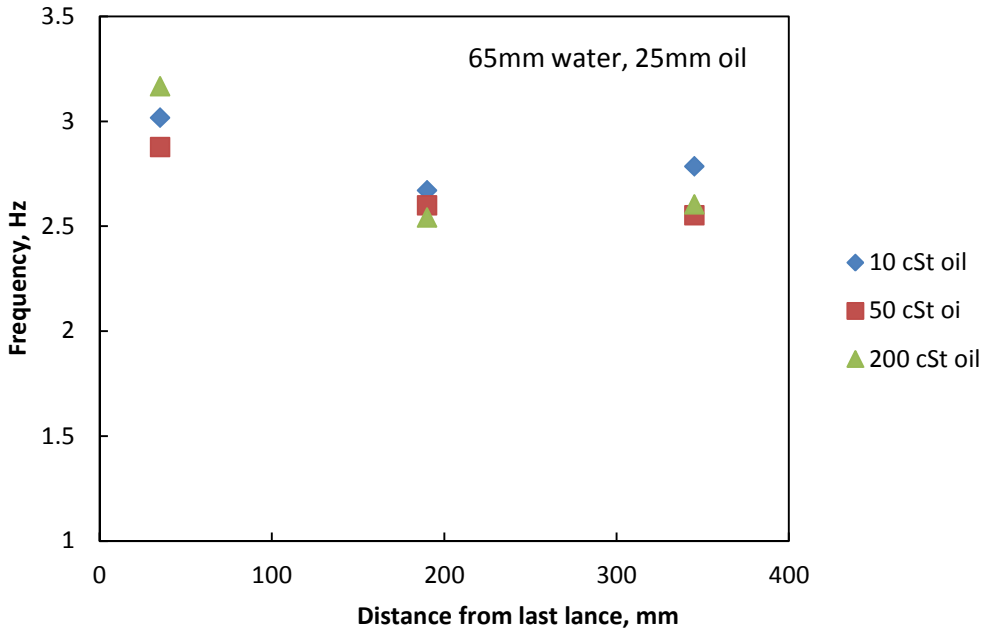

Figure 8-14 Effect of oil viscosity on longitudinal wave frequency trend

In summary, it is found that the frequency of longitudinal wave is not affected by operational parameters such as bath level, gas input or slag viscosity. It is contently starts at around 3 Hz near the reaction zone and deceases slightly along the length of settlement zone to a value around 2.5 Hz

near the tapping end. This trend is steady under most of the conditions except when the combination of bath level and flowrate reaches a special value and enables the 1st asymmetric standing wave to take place. When the standing wave is in presence, the vibration of surface is dominated by it and the longitudinal wave becomes difficult to observe, so the recorded frequency is the frequency of the standing wave which is much lower than the others as shown in Figure 8-13. It is found that the occurrence gas flowrate of the 1st asymmetric standing wave is higher than the gas flowrate corresponding to industrial normal operation, but the detailed occurrence condition with nine lances blowing and the top oil layer still requires further study.

8.4 Industrial application

The experimental results indicate that under normal gas flowrate of industrial practice (corresponding to 12L/min in experiment), the longitudinal wave on bath surface shows a decreasing trend from the last lance to the tapping end. At such gas flowrate, the overall amplitude will be increased if the matte layer height is increased, but it almost remain constant if the slag layer height is changed. This means that the surface vibration of molten bath is getting greater as smelting proceeds and matte level accumulates, but it falls back after matte is tapped and matte level returns to a lower level. On the other hand, the amplitude is not sensitive to the slag level variation, which means the slag tapping does cause significant influence on the surface vibration. Whereas the amplitude of surface wave is more sensitive to the viscosity of slag. The high viscosity slag reduces the amplitude of slag to a very low level at the tapping end, while the low viscosity slag leads to more reflection of wave and results in amplitude rising at the tapping end.

In industrial practice, it was found that the wave at the tapping end is helping the viscous slag tapping by pushing the slag out in gushes. Such phenomenon improves the slag tapping efficiency remarkably, especially the viscosity of slag is high. Considering the amplitude at the edge of tapping end is higher than at the centre, it could be an option to open a tapping hole at the edge of end wall when dealing with slag of even higher viscosity.

The amplitude trend of longitudinal wave can be changed if the gas flowrate and total bath level are increased. Higher gas flowrate leads to more wave reflection near the tapping end, which results in

amplitude rising near the tapping end. At a certain combination of bath level and gas flowrate, the reflected wave is able to reach resonance with incoming wave, and the 1st asymmetric wave is created. This means the standing wave is also able to occur in the presence of a top layer with all nine lances blowing together, which is closer to industrial condition. However, the detailed occurrence boundary under such condition still requires further study.

8.5 Conclusions

(1) The amplitude trend of longitudinal wave along furnace length is depended on the combination of gas flowrate and bath total height. There are three different trends observed in the present study: 1) amplitude increasing with flowrate in the same trend; 2) reflection of wave causing amplitude rising near the tapping end; 3) standing wave involved

(2) At the gas flowrate corresponding to industrial flowrate, the amplitude of wave is increasing with water level, but remains almost constant with oil level. At such gas flowrate, the higher viscosity oil leads to lower amplitude of wave, while the lower viscosity oil leads to more reflection of wave which results in amplitude rising near the tapping end.

(3) At the gas flowrate corresponding to industrial flowrate, the amplitude of wave at the edge of tapping end is always higher than at the centre.

(4) The frequency of longitudinal shows a slightly decreasing trend along the length of furnace due to the energy dissipation in transmission. Furthermore, the frequency of longitudinal wave is not affected by the water level, oil level or oil viscosity. When the combination of gas flowrate and bath level reaches a certain critical condition, the 1st asymmetric standing wave is able to take place, and the frequency of wave is dominated by this standing wave.

8.6 References

[1] L. Shui, Z. Cui, X. Ma, M. A. Rhamdhani, A. Nguyen, and B. Zhao: *Metall. Mater. Trans. B*, 2015, In Press.

[2] J. L. Liow and N. B. Gray: *Metall. Trans. B,* 1990, vol. 21B, pp. 987-996.

[3] E. Godoy, A. Osses, J. H. Ortega, and A. Valencia: *Applied Mathematical Modelling*, 2008, Vol.

32, pp. 1696-1710.

[4] J. Gonzalez, C. Real, M. Palomar-Pardave, L. Hoyos, M. Gutierrez, and R. Miranda: *International Journal of Chemical Reactor Engineering*, 2008, Vol. 6, Article A54.

[5] B. Zhao, Z. Cui, and Z. Wang: *Int. Symp. High-Temp. Metall. Process*., 4th, 2013, pp. 1-10.

[6] L. Shui, Z. Cui, X. Ma, M. A. Rhamdhani, A. Nguyen, and B. Zhao: *Metall. Mater. Trans. B*, 2015, Vol. 46B, pp. 1218-1225

[7] M. Chen and B. Zhao: *Proceeding of Copper-Cobre 2013*, Santiago, Chile, 2013, pp. 799-812.

[8] J. Szekely: Fluid Flow Phenomena in Metals Processing, 1979, Academic Press INC, New York, NY, USA, pp.392-418.

[9] D. Gupta and A. K. Lahiri: *Metall. Mater. Trans. B*, 1994, Vol. 25B, pp. 227-233.

[10] P. Liovic, M. Rudman, and J. L. Liow: *Applied Mathematical Modelling*, 2002, Vol. 26, pp. 113-140

9 Summary

In the present study, in order to investigate the behaviour of molten bath in the newly established bottom blown copper smelting furnace, a 1/12 lab scale cold physical model of the furnace has been built. This model has been used to carried out a series of fluid dynamic studies related to bath mass transfer and surface wave formation.

In the first stage of the study, the mass transfer efficiency of single phase bath blown with a single lance was investigated. Mixing time was used as the index of mass transfer in this cold model and was measured to examine the characteristics of the fluid dynamics in the furnace. It was found that there was an effective stirring range adjacent to the blowing lance, within which mixing time changed little with horizontal or vertical distance, while outside of this range, mixing time increased with increasing horizontal distance and the increment was much greater on the surface of the bath. Mixing time decreased with increasing bath height and gas flowrate within the effective stirring range. However, the effective stirring range can be reduced with increasing the bath height. An empirical prediction of mixing time from gas flowrate and bath height was established first time for horizontal bottom blown furnace:

$$\tau = 37.5Q^{-0.39}H^{-1.08}$$

Building on the basis of the single phase mixing behaviour study, multiphase bath mixing behaviour was also studied to further investigate the mass transfer in the presence of a slag layer. Single lance blowing was used and experimental variables including water height, gas flowrate, oil layer height and oil viscosity were adjusted to investigate the impact of each on mixing time. It was found that the mixing time decreased with increasing water height and gas flowrate at a greater rate than in the single phase bath, while it increased with increasing oil layer height and, to a lesser extent, oil viscosity. An overall empirical relationship with these variables was developed giving a good prediction of mixing time under different conditions.

$$\tau = 0.21H^{-1.53}Q^{-1.73}h^{2.21}{\nu_s}^{0.24}$$

The prediction of mixing time was generalized to model-independent format, which provides wider use for industrial operation of bottom blown copper smelting furnaces

Secondly, the wave formation on the surface of a single phase bath surface with single lance blowing was investigated. Three different types of surface waves were observed in the lab scale model of the bottom blown copper smelting furnace. The 1st asymmetric standing wave was the most significant type among the three because it led to the entire bath swinging laterally, even at the tapping end. The 1st asymmetric standing wave only occurred at certain combinations of bath height and gas flowrate, which can be represented in two sub-boundaries. Additionally, as the lance angle was increased, the critical bath height and flowrate for the occurrence of the 1st asymmetric standing wave also increased. Empirical correlations were obtained as follows:

Sub-boundary 1

$$\frac{H}{D} = 0.036 Fr_{mD}^{-0.1} \alpha^{0.084}$$

Sub-boundary 2

$$\frac{H}{D} = 0.63 We^{0.44} \alpha^{-0.39}$$

When the blowing angle was increased to 25º, the 1st asymmetric standing wave was substituted by the 1st symmetric standing wave. The combination of conditions governing the occurrence of the 1st symmetric standing wave were not as clear. The measured amplitude under a range of conditions showed that the wave amplitude at the tapping end increased with increasing flowrate and bath height, with a step-change increase in amplitude when the 1st symmetric standing wave occurred. The frequency of the 1st asymmetric standing wave did not change with flowrate or blowing angle, but slightly increased with increasing bath height.

When the combination of bath height and gas flowrate was outside of the critical occurrence boundaries for the standing wave, a longitudinal wave existed on the bath surface. To study the behaviour of the longitudinal wave, the model operation was altered to be closer to industrial practice. Nine lances were used for blowing and silicone oil was applied on the water surface to investigate the behaviour of longitudinal wave. It was found that the trend in the amplitude of longitudinal wave along the furnace length was dependent on the combination of gas flowrate and bath level, with three typical trends being observed: 1) increasing amplitude with increasing flowrate; 2) reflection of the wave causing an increase in amplitude near the tapping end; 3) occurrence of a standing wave. At the gas flowrate in the model corresponding to the industrial

flowrate, the amplitude of the wave increased with water level, but remained almost constant with oil level. A higher viscosity oil layer led to a lower amplitude, while lower viscosity oil led to an increase in amplitude near the tapping end. The amplitude of the wave at the edge of the tapping end was always found to be higher than at the centre. The frequency of the longitudinal wave was not affected by the water level, oil level or oil viscosity. The standing wave occurrence was also linked with the longitudinal wave reflection at a certain combination of gas flow rate and bath height.

This study focuses on the fluid dynamics of the molten bath in the novel bottom blown copper smelting furnace, and uses a physical model to simulate the behaviour of the gas stirred bath under various conditions. All of the experimental conditions are based on industrial data and the industrial operations of the furnace, so the results obtained in this study provide useful information for understanding this new technology as well as guidelines for optimization of operations, such as gas flowrate control, matte and slag height adjustment, and lance configuration. The present study is a first step in the investigation of the behaviour of the molten bath in this novel furnace. Following this methodology, the issues further related to bath splash, more complicated lance configuration, the effect of a separating dam between the reaction and settlement zone and so on are worth studying. Therefore, more research work relevant to this topic can be expected in the future, which will contribute to the improved understanding and optimisation of this technology.